Integrating Machine Learning and Optimization with Spatiotemporal Techniques to Develop a Methodology for Assessing Rural Resilience

A Technical Report Submitted to the Rural Safe Efficient Advanced Transportation (R-SEAT) Center and United States Department of Transportation

FINAL REPORT

Principal Investigator:
Eren Erman Ozguven, Ph.D.
Associate Professor
Director, Resilient Infrastructure & Disaster Response Center (RIDER)
Department of Civil & Environmental Engineering
Florida A&M University-Florida State University (FAMU-FSU) College of Engineering
2035 E Paul Dirac Dr., Sliger Building, Suite 207, Tallahassee, FL 32310, USA
Phone: +1(850) 410-6146
Email: eozguven@eng.famu.fsu.edu

Co-Principal Investigator:
Ren Moses, Ph.D.
Professor
Department of Civil & Environmental Engineering
Florida A&M University-Florida State University (FAMU-FSU) College of Engineering
2525 Pottsdamer Street, Building B, Room B222F, Tallahassee, FL 32310, USA
Phone: +1(850) 410-6191
Email: moses@eng.famu.fsu.edu

Research Assistant:
Samuel Takyi
Doctoral Candidate
Department of Civil & Environmental Engineering
Florida A&M University-Florida State University (FAMU-FSU) College of Engineering
2035 E Paul Dirac Dr., Sliger Building,
Tallahassee, FL 32310, USA
E-mail: syt20g@fsu.edu

Research Assistant:
Richard Antwi
Doctoral Candidate
Department of Civil & Environmental Engineering
Florida A&M University-Florida State University (FAMU-FSU) College of Engineering
2035 E Paul Dirac Dr., Sliger Building,
Tallahassee, FL 32310, USA
E-mail: rantwi@eng.famu.fsu.edu

April 2025

DISCLAIMER

The contents of this report reflect the views of the authors, who are responsible for the facts and accuracy of the information presented herein. This document is disseminated in the interest of information exchange. The report is funded, partially or entirely, under the grant 69A3552348321 from the U.S. Department of Transportation's University Transportation Centers Program. The U.S. Government assumes no liability for the contents or use thereof.

METRIC CONVERSION CHART

When You Know	Multiply by	To Find
Length		
inches (in)	25.4	millimeters (mm)
feet (ft)	0.305	meters (m)
yards (yd)	0.914	meters (m)
miles (mi)	1.61	kilometers (km)
Volume		
fluid ounces (fl oz)	29.57	milliliters (mL)
gallons (gal)	3.785	liters (L)
cubic feet (ft^3)	0.028	meters cubed (m^3)
cubic yards (yd^3)	0.765	meters cubed (m^3)
Area		
square inches (in^2)	645.1	millimeters squared (mm^2)
square feet (ft^2)	0.093	meters squared (m^2)
square yards (yd^2)	0.836	meters squared (m^2)
acres	0.405	hectares (ha)
square miles (mi^2)	2.59	kilometers squared (km^2)

TECHNICAL REPORT DOCUMENTATION PAGE

1. Report No.	2. Government Accession No.	3. Recipient's Catalog No.

4. Title and Subtitle	5. Report Date
Integrating Machine Learning and Optimization with Spatiotemporal Techniques to Develop a Methodology for Assessing Rural Resilience	04/05/2025
	6. Performing Organization Code 59-0977035

7. Author(s)	8. Performing Organization Report No.
Eren Erman Ozguven https://orcid.org/0000-0001-6006-7635 Ren Moses https://orcid.org/0000-0003-2988-5220 Samuel Takyi https://orcid.org/0009-0000-5419-3002 Richard Antwi https://orcid.org/0000-0002-2853-2856	

9. Performing Organization Name and Address	10. Work Unit No. (TRAIS)
Florida A&M University-Florida State University College of Engineering 2035 E Paul Dirac Dr., Sliger Building, Suite 275 Tallahassee, FL 32310, USA	11. Contract or Grant No. 69A3552348321

12. Sponsoring Agency Name and Address	13. Type of Report and Period Covered
Rural Safe Efficient Advanced Transportation (R-SEAT) 2525 Pottsdamer Street Tallahassee, FL 32310	Final Report Period Covered: 06/01/2023 – 04/05/2025
	14. Sponsoring Agency Code

15. Supplementary Notes

16. Abstract

This project develops an integrated methodology to assess and enhance the resilience of rural communities against natural disasters, with a focus on hurricanes and tornadoes in Florida. By combining Geographical Information Systems (GIS)-based spatiotemporal analysis, machine learning, and optimization techniques, the project addresses the unique challenges faced by rural areas, which are often underserved and disproportionately affected by extreme weather events. The methodology leverages high-resolution satellite imagery, remote sensing, and geospatial data to evaluate the impacts of disasters on transportation infrastructure and impacted populations, such as the elderly. The project builds on three key components: (1) a machine learning-based framework for assessing roadway closures and accessibility using satellite imagery, as demonstrated in the analysis of Hurricanes Ian and Idalia, which achieved 89% accuracy in classifying roadway conditions; (2) the development of indices such as the Road Closure Impact Index (RCII) and Roadway Vulnerability Index (RVI) to quantify infrastructure disruptions and vulnerabilities; and (3) an integrated GIS and image processing approach for post-tornado debris detection, utilizing spectral indices like the Normalized Difference Vegetation Index (NDVI) to identify high-impact areas and inform recovery efforts. The outcomes of this project provide actionable insights for prioritizing infrastructure restoration, improving situational awareness, and guiding resource allocation during disaster response. By focusing on Florida's Panhandle as a test bed, the project extends knowledge on rural resilience and informs strategic adaptation plans. Aligned with USDOT priorities, this work supports advanced asset management by leveraging cutting-edge technologies to enhance the resilience of transportation systems in disaster-prone regions.

17. Key Words	18. Distribution Statement
Machine Learning, Roadway Closures, Geospatial Analysis, Disaster Resilience, Satellite Imagery	No restrictions

19. Security Classif. (of this report)	20. Security Classif. (of this page)	21. No. of Pages	22. Price
Unclassified	Unclassified	118	

ACKNOWLEDGEMENTS

This project was sponsored by the Rural Safe Efficient Advanced Transportation (R-SEAT) Center and United States Department of Transportation. The Principal Investigators would like to thank the representatives of the REAT Center for their valuable feedback throughout the project activities.

EXECUTIVE SUMMARY

This project seeks to address the critical gap in disaster resilience research for rural communities, which are often underserved and disproportionately affected by natural disasters such as hurricanes and tornadoes. While urban resilience has been extensively studied, rural areas face unique challenges due to their distinct characteristics, limited infrastructure, and underserved populations, such as the elderly Focusing on Florida's Panhandle as a test bed, this project develops an integrated methodology to assess and enhance the resilience of rural communities by combining Geographical Information Systems (GIS)-based spatiotemporal analysis, machine learning, and optimization techniques.

The project is structured around three core components, each contributing to a comprehensive understanding of disaster impacts and resilience strategies:

i. **Machine Learning-Based Roadway Closure Assessment:**
Using high-resolution satellite imagery and machine learning models, the project evaluates the impacts of hurricanes on roadway closures and accessibility. For instance, the analysis of Hurricanes Ian and Idalia achieved 89% accuracy in classifying roadway conditions into fully closed, partially closed, and open categories. This approach identifies heavily impacted coastal regions and provides actionable insights for post-disaster recovery, enabling government agencies to prioritize resource allocation effectively.

ii. **Development of Resilience Indices**:
The project also introduces two novel metrics, the Road Closure Impact Index (RCII) and the Roadway Vulnerability Index (RVI), to quantify the severity and consistency of infrastructure disruptions. These indices leverage remote sensing, geospatial analysis, and machine learning to assess the impacts of wind, storm surge, and flooding on transportation systems. For example, these metrics were derived from Hurricanes Idalia and Debby in Taylor County, Florida, revealing distinct patterns of damage and vulnerability.

iii. **Post-Tornado Debris Detection and Analysis:**
An integrated GIS and image processing approach is used in the project to assess tornado-induced debris impacts on roadways and communities. By analyzing spectral indices such as the Normalized Difference Vegetation Index (NDVI) from pre- and post-tornado satellite imagery, the project identifies high debris concentrations in densely populated areas. This methodology, tested in Leon County, Florida, after EF-2 and EF-1 tornadoes, provides critical information for disaster response and recovery operations.

The project's methodology is designed to assess vulnerability at multiple levels, enabling:

- Identification of the most impacted rural communities based on the frequency and duration of service disruptions.
- Characterization of spatial and temporal patterns in infrastructure and environmental disruptions.

- Hierarchical prioritization of transportation system restoration to ensure efficient recovery for impacted populations.

Outcomes and Impacts:

The project extends knowledge on rural community resilience, offering critical insights into risks, constraints, and barriers to recovery. By testing and validating the methodology in Florida's Panhandle, the project:

- Provides decision-support tools for situational awareness and resource allocation during disaster preparedness, response, and recovery.
- Informs governments and communities in developing strategic adaptation plans and improving disaster resilience.
- Highlights the differential impacts of disasters on impacted groups, ensuring efficient recovery and resource distribution.

Alignment with USDOT Priorities:

This project aligns with the USDOT priorities, particularly under the themes of Advanced Asset Management. By leveraging cutting-edge technologies such as machine learning, remote sensing, and geospatial analysis, the project enhances the resilience of infrastructure assets. It also embodies the USDOT's innovation principles by enabling adaptability and resilience in transportation systems for the digital age.

In summary, this project not only advances the scientific understanding of rural disaster resilience but also provides practical tools and strategies for governments and communities to mitigate risks, improve preparedness, and ensure efficient recovery in the face of increasing disaster-related challenges.

.

TABLE OF CONTENTS

LIST OF FIGURES

LIST OF TABLES

Chapter 1 Introduction

Natural disasters such as hurricanes and tornadoes pose significant challenges to transportation infrastructure, leading to roadway closures, debris accumulation, and disruptions in accessibility. The increasing frequency and intensity of these extreme weather events, particularly in hurricane-prone regions like Florida's Panhandle, underscore the urgent need for improved methodologies to assess and mitigate their impacts. Traditional damage assessment approaches often rely on manual inspections, historical data, and static models, which are time-consuming, resource-intensive, and ineffective for real-time decision-making. However, recent advancements in remote sensing, machine learning, and geospatial analysis provide new opportunities for dynamic, data-driven disaster impact assessments.

This project integrates high-resolution aerial imagery, machine learning models, and GIS-based spatial analysis to develop innovative methodologies for assessing roadway vulnerability, disaster-induced accessibility constraints, and post-event recovery needs. The research is structured around three key studies, each addressing a critical aspect of disaster impact assessment and response:

i. **Machine Learning-Based Roadway Vulnerability and Impact Assessment (Chapter 2):** This study a) utilizes aerial imagery and machine learning models to detect and classify roadway disruptions caused by hurricanes, b) introduces two novel indices—the Road Closure Impact Index (RCII) and the Roadway Vulnerability Index (RVI)—to quantify hurricane-induced transportation network disruptions, and c) is applied to Hurricanes Idalia and Debby in Taylor County, Florida, demonstrating the ability to identify heavily impacted roadway segments for prioritization in disaster response.
ii. **Hurricane-Induced Roadway Closures and Accessibility Analysis (Chapter 3):** This study a) assesses the impact of Hurricanes Ian and Idalia on roadway closures and transportation accessibility, b) develops a machine learning framework to classify roadway conditions (Open, Partially Closed, Fully Closed) based on post-hurricane satellite imagery, and c) integrates GIS datasets, including evacuation routes, land use, and hydrological features, to examine how different environmental and infrastructural factors contribute to hurricane-related roadway disruptions.
iii. **Post-Tornado Debris Detection and Analysis Using Satellite Imagery (Chapter 4):** This study a) focuses on post-disaster debris detection and its impact on transportation networks using Normalized Difference Vegetation Index (NDVI) analysis, b) evaluates tornado-induced vegetative debris along roadways in Leon County, Florida, following severe EF-2 and EF-1 tornadoes, and c) uses an integrated GIS and image processing approach to assess debris accumulation, identifying critical roadway segments requiring immediate clearance for emergency response operations.

By combining machine learning, remote sensing, and GIS-based methodologies, this project contributes to a comprehensive framework for disaster impact assessment and infrastructure resilience planning. The findings offer actionable insights for policymakers, emergency

responders, and transportation agencies, ensuring more efficient disaster preparedness, response, and recovery efforts in regions affected by extreme weather events.

Chapter 2 Assessing The Impact of Hurricanes on Roadway Closures and Accessibility: A Machine Learning-Based Case Study of Hurricanes Ian and Idalia in Florida

2.1 Introduction

Hurricanes have been responsible for a great number of fatalities and property damage in the U.S. history. Between 1980 and 2021, the approximate total hurricane-induced cost of damages in the U.S. was more than $2 trillion (National Oceanic and Atmospheric Administration (NOAA), n.d.). A significant portion of this adverse impact was on the critical infrastructure such as roadways, bridges, and tunnels, which are necessary for our society's operations and functionality. (Jeffrey 2009). Similarly, Hurricane Ian severely impacted southeast Florida's transportation network in 2022, and Hurricane Idalia crippled northwest Florida's roadways, both causing extensive damage. Assessing this damage following the hurricanes is essential for post-event reconstruction and humanitarian aid (Sijia Hu 2022). Specifically, determining the magnitude and duration of these impacts in the context of roadway disruptions and transportation accessibility has the utmost importance for efficient response and recovery operations and has thus become a significant topic of interest in literature.

Traditional approaches of assessing post-hurricane roadway conditions and accessibility rely on manual observations and reports, which can be challenging and prone to error. While it is possible to manually analyze remotely sensed images using skilled human analysis and image annotation tools, this would also be very labor-intensive and slow down the ability to respond quickly to natural disasters like hurricanes. Although several automated techniques for damage mapping using imagery from satellites have been proposed, practical damage mapping is still based on labor- and time-intensive manual analysis of satellite images (Vetrivel et al. 2016). However, current developments in machine learning methods that utilize satellite imagery offer innovative and efficient solutions to evaluate how hurricanes impact roadways. High-resolution satellite images, which are typically made accessible shortly after a disaster event like a hurricane, are an ideal data source for faster damage assessment over broad areas for rapid response activities (Kerle and Hoffman 2013). This provides the opportunity for the complex patterns of hurricane-induced destruction and disruption caused to be analyzed and understood with the use of machine learning tools, allowing for more efficient emergency response and preparation in the future.

Although satellite images have been increasingly available lately, their complexity and limited spatial resolution have been two reasons why automated approaches have not been developed(Vetrivel et al. 2016)In addition, the development of reliable methodologies to assess the impact of hurricanes on roadways depends on a substantial amount of training samples on roadway closures from past hurricanes, which are typically not easily accessible (Dong and Shan 2013). The transferability of a pre-trained supervised model that was previously created for a different geographic region is also limited(Dong and Shan 2013). However, the pre-trained model can be fine-tuned using a modest number of training samples that reflect the area of interest.

Therefore, a sizable number of training samples are needed for each study region, either for building a new model or calibrating an existing model.

In the literature, several studies have used machine learning and other remote sensing techniques to assess the impact of natural disasters on the infrastructure. For example, bi-temporal remote sensing images have been used in several studies (Peng et al. 2019; Mauricio Sánchez-Silva and Libardo García 2001) to create a near real-time and precise map of earthquake damage. In another study, the performance of a random forest classifier was used to identify collapsed buildings and assess building damage by comparing the performance of convolutional neural network (CNN) features and the grey-level co-occurrence matrix texture together with a high-resolution post-earthquake imagery (Ji et al. 2019).

Decision trees (Spekkers et al. 2014), random forests (Tavus, Kocaman, and Gokceoglu 2022), and neural networks (Zapico, González, and Worden 2003; Kourehli 2015) are a few examples of machine learning techniques that have been successful in other domains and can be applied to hurricane damage assessment. These algorithms have the potential to gain knowledge from historical data on roadway closures and accessibility, wind speeds, rainfall amounts, storm surge heights, and the geographic characteristics of the impacted areas. Debris field detection, ingress route blockage detection, building damage detection and assessments, and remote sensing in tactical support of rescue plans are some potential applications for using machine learning with satellite images (Barnes, Fritz, and Yoo 2007). However, there is still a need for tools that can readily be trained and used to process massive volumes of imagery from disaster zones, as well as tools that can adapt to disaster-related features. For image processing, algorithms like support vector machine (Cortes, Vapnik, and Saitta 1995), and K-nearest neighbor (Cover and Hart 1952) have frequently been used compared to conventional computer vision techniques like scale-invariant feature transform (SIFT) (Lowe 2004), and Histogram of Oriented Gradient (HOG) (Dalal and Triggs 2005).

Machine learning models with remotely sensed images can provide reliable projections about the state of the roadways during and in the aftermath of hurricanes by examining these variables and finding patterns and connections. In addition, to capture the dynamic nature of hurricane impacts, machine learning models can manage huge volumes of data, such as real-time sensor data, satellite imagery, social media feeds, and official reports (Wang et al. 2019; Pourebrahim et al. 2019; Kim, Bae, and Hastak 2018; Martín et al. 2020). They can also help forecast more accurately and raise decision-makers' situational awareness. To prioritize response efforts, machine learning models can also identify crucial roadway segments. Emergency response teams can successfully plan for evacuation routing, resource deployment, and pre-positioning of supplies by anticipating which roadways would likely be affected by closures or restricted accessibility. In the wake of a hurricane, this preventive approach can help save lives, reduce property damage, and speed up the recovery process.

This study developed a machine learning- and high-resolution satellite imagery-based methodology to assess the impact of hurricanes Ian and Idalia on roadways with a specific focus on roadway closures and transportation accessibility. To fully understand the relationship between the hurricanes' impact and the physical characteristics of the affected areas, this study incorporated Geographic Information System (GIS) data layers such as evacuation routes and boundary shapefiles, land use, elevation, hydrological features, and population density. A novel machine learning model was developed to classify roadway conditions (Open, Partially Closed, Fully Closed) based on post-hurricane imagery. A comprehensive dataset of roadway conditions in Lee and Taylor counties, Florida, after being impacted by Hurricane Ian and Idalia, respectively, was curated and labeled, serving as a valuable resource for future research. This information could help in identifying vulnerable locations and evaluating the accessibility of the roadways at those locations. The proposed technique can be used by engineers and urban planners to assess the resilience of the roadway infrastructure to hurricanes and identify areas that are vulnerable to significant damage.

2.2 Study Area, Data, Hurricanes Ian and Idalia

A Category 4 hurricane, Hurricane Ian, made landfall in Southwest Florida on September 28, 2022, as the fifth-strongest tropical cyclone in the U.S. history (Pavur, Lakshmi, and Lambert 2023) with maximum sustained winds of 150 miles per hour (Sodders et al. 2023). It was the strongest hurricane to hit Florida since Hurricane Michael in 2018 and the first Category 4 hurricane to impact Southwest Florida since Hurricane Charley in 2004. Lee County, located on the southwest coast of Florida, covers an area of approximately 1,212 square miles. It includes several cities and towns such as Fort Myers, Cape Coral, and Bonita Springs, along with numerous barrier islands and a diverse range of landscapes. The region is characterized by its coastal and inland environments, featuring urban areas, agricultural lands, wetlands, and water bodies. The county lies between 26.3°N to 26.8°N latitude and 81.5°W to 82.3°W longitude. The elevation varies from sea level along the coast to about 30 feet inland. The roadway network in Lee County consists of major highways, arterial roads, and local streets. Key highways include Interstate 75 (I-75) and U.S. Route 41, which are vital for transportation and evacuation during emergencies. The county has several critical bridges and causeways connecting the mainland to barrier islands, such as the Sanibel Causeway and the Matlacha Pass Bridge. The county has a mix of densely populated urban centers and sparsely populated rural areas. Urbanization is concentrated in cities like Fort Myers and Cape Coral. Lee County is highly vulnerable to hurricanes due to its coastal location. Hurricane Ian, which struck the region, caused widespread damage, including flooding, wind damage, and debris accumulation on roadways.

Taylor County, Florida, serves as another significant study area for assessing the impact of hurricanes on roadway infrastructure. In 2023, the region was notably affected by Hurricane Idalia, a Category 4 hurricane, which brought extensive damage to its roadway networks and other critical infrastructure. The proposed detection model was applied to this hurricane to test applicability of the model to other hurricanes and affected areas other than Hurricane Ian and Lee County, which

was used to train the model. Taylor County covers approximately 1,232 square miles (3,191 square kilometers), making it one of the larger counties in Florida by land area. The county is bordered by the Gulf of Mexico to the southwest and includes several rivers, creeks, and the extensive Econfina River State Park. The county's roadway network includes state highways, county roads, and local streets. Key highways include U.S. Route 98, which runs along the coast, and U.S. Route 221, which traverses the county from north to south. Taylor County has a population of approximately 21,000 residents. The population is concentrated in the county seat, Perry, with smaller communities and rural areas spread throughout the county. The impact on transportation infrastructure necessitated a detailed analysis of roadway conditions to support disaster response and recovery efforts. The impact on transportation infrastructure necessitated a detailed analysis of roadway conditions to support disaster response and recovery efforts.

The National Oceanic and Atmospheric Administration (NOAA) projected that Ian's insured and uninsured losses were more than $50 billion. As seen in Figure 2.1, it moved inland after the landfall and swiftly intensified into a tropical storm before returning to the Atlantic Ocean (Karimiziarani and Moradkhani 2022). It had a drastic impact on the Gulf coast of southwest Florida where several coastal areas of Lee and Collier counties experienced storm surges that were approximately 12 to18 feet (3.6 to5.5 meters) above the sea level (National Environmental Satellite Data and Information Service 2022). This paper will focus on one of these impacted counties, namely Lee County.

High-resolution aerial imagery of the affected areas was acquired shortly after the hurricane's passage. The post hurricane imagery was acquired through the National Hurricane Center and the National Oceanic and Atmospheric Administration from September 9, 2022, to October 3, 2022, after hurricane Ian made landfall. The pre-hurricane imagery was acquired from the Florida Aerial Photo Look-Up System (APLUS) through the Florida Department of Transportation (FDOT). The imagery was collected using advanced aerial surveying techniques to ensure detailed and accurate representations of the road conditions. This timely collection was critical for assessing the immediate impacts of the hurricane and for providing actionable insights for emergency response teams. This information indicated whether roadways were blocked or impassable as well as any accessibility problems. Existing road network shapefiles for Lee County were obtained from local government GIS databases. These shapefiles provided a detailed layout of the road infrastructure, including major highways, arterial roads, and local streets. The road network data was essential for delineating the areas of interest and for applying the classification model to assess road conditions.

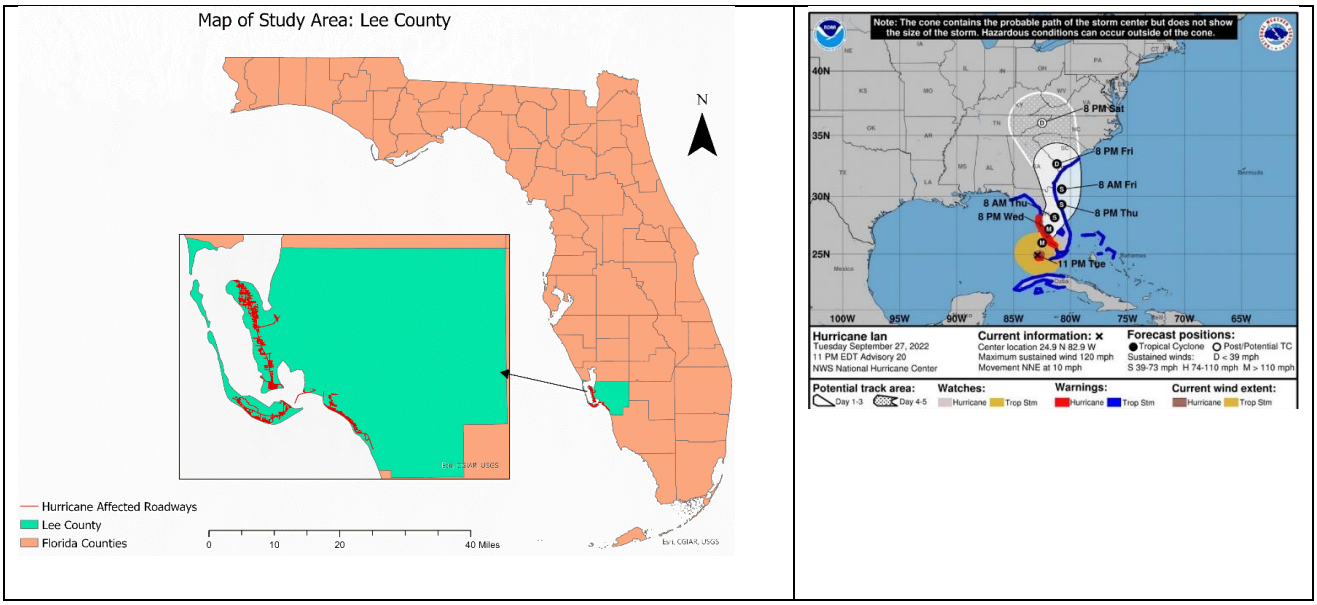

Figure 2:1 Map of Study Area, Hurricane Ian's Track, and Path over the State of Florida (Lu et al. 2019)

Figure 2:2 Images of Damages Caused by Hurricane Ian on Roadway Infrastructure (27)

Several examples of damage caused by Hurricane Ian on the roadways can be seen in Figure 2.2. To fully understand the relationship between the hurricane's impact and the physical characteristics of the affected areas, this study incorporated GIS data layers such as evacuation routes and boundary shapefiles, land use, elevation, hydrological features, and population density. Additionally, emergency response reports and documentation that include roadway closures,

evacuation routes, and other response actions were available from emergency management agencies, transportation departments, and other relevant organizations. These reports helped with model training and validation and offered other insights.

2.3 Methodology

The proposed methodology shown in Figure 2.3 involves the following steps:

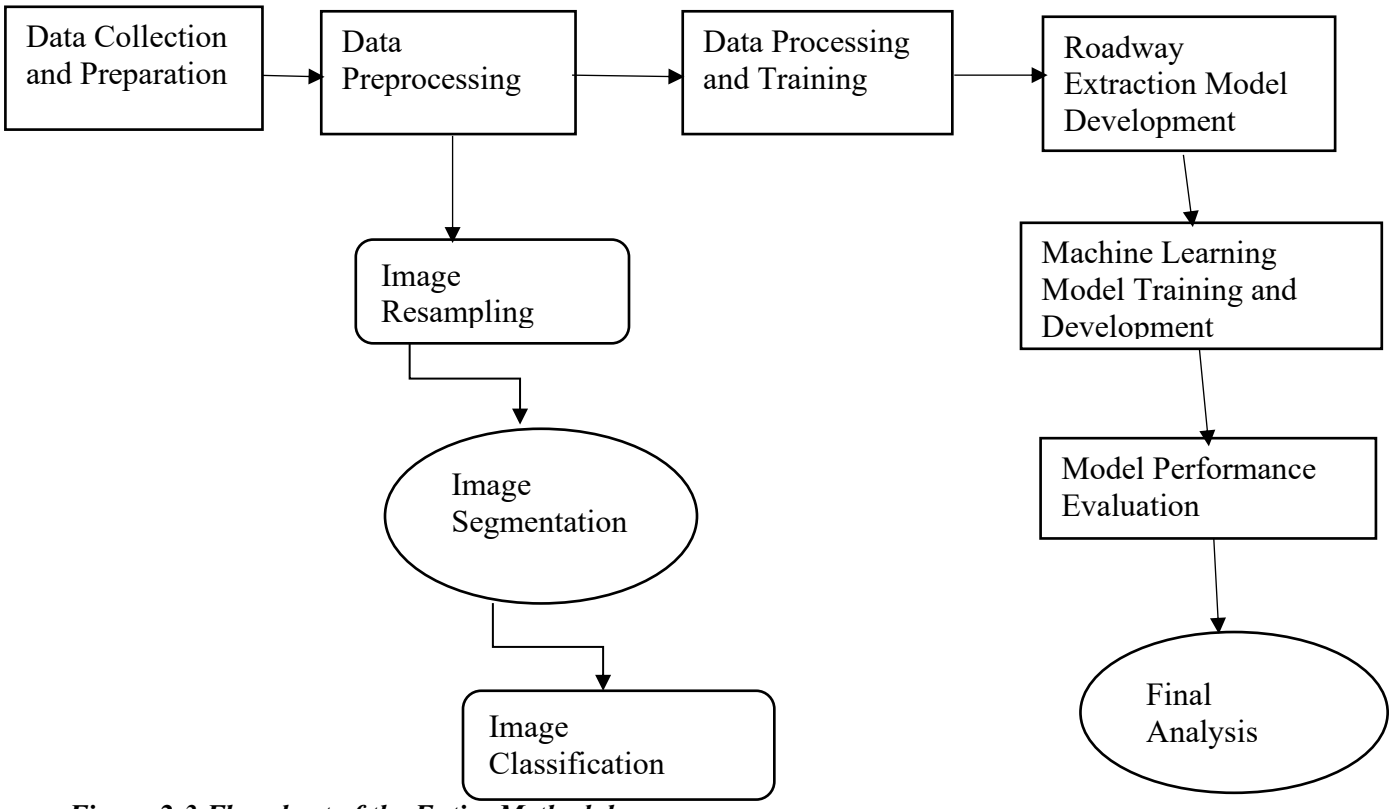

Figure 2:3 Flowchart of the Entire Methodology

2.3.1 Data Collection and Preparation

High-resolution satellite images of the study area, captured before and after Hurricane Ian and Idalia, were obtained covering both the roadway network and surrounding areas from Florida Department of Transportation's Surveying Office ("Florida Department of Transportation. Https://Fdotewp1.Dot.State.Fl.Us/AerialPhotoLookUpSystem/" 2023). Roadway closure and transportation accessibility information was also obtained before, during, and after Hurricane Ian and Idalia ("Florida Department of Transportation. Https://Fdotewp1.Dot.State.Fl.Us/AerialPhotoLookUpSystem/" 2023). A buffer of 6 meters was applied to the roadway network shapefiles to define the areas of interest for assessing roadway conditions. This buffer ensured that the analysis captured the full extent of roadway impacts, including debris and partial closures that extended beyond the immediate roadway surface.

2.3.2 Data Preprocessing

2.3.2.1 Image Registration

Pre-hurricane and post-hurricane satellite imageries were registered and aligned to allow for precise comparison and analysis. The process of aligning two or more images spatially to improve comparison or integration is known as image registration. When working with images taken from several sensors at different times or from different angles, this has been known to be helpful, with the objective of bringing images into a common coordinate system. The fundamental steps in image registration are shown in Figure 2.4.

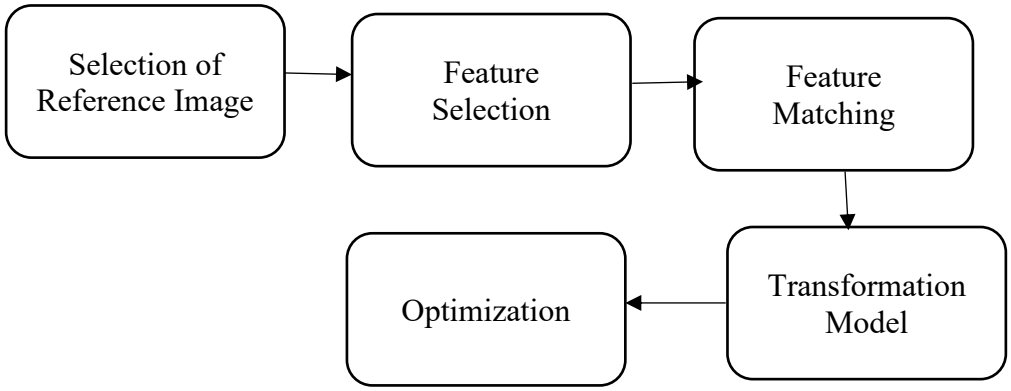

Figure 2:4 Flowchart of Image Registration Processing

2.3.2.2 Image resampling

The images for the pre-hurricane were resampled to match the coordinate system and pixel resolution of the post-hurricane imagery (Figure 2.5). When resampling an image, the spatial extent is preserved but the pixel resolution is changed. In this study, the nearest neighbor method was used to resample the imagery.

c

Figure 2:5 Images before and after Resampling: (a) Pre-hurricane Satellite Imagery before Resampling, (b) Pre-hurricane Imagery after Resampling, and (c) Post-hurricane Imagery, the Reference for Resampling

2.3.2.3 Image segmentation

An image is divided into numerous different areas or segments using this computer vision technique centered on features like color, texture, or shape (Richard Szeliski 2022). Image segmentation is the process of dividing the imagery into semantically significant sections, each of which stands for a particular object or portion of the image. It is an essential stage in many computer vision applications (Minaee et al. 2022), such as scene analysis, object recognition, and understanding imagery. We can extract useful information from an image by segmenting it, which will make it easier to process or analyze.

Although there are several methods for segmenting images, a Convolutional neural networks (CNN)-based deep learning methodology was used in this study. CNNs have been frequently employed for image segmentation (Hina Ajmal et al. 2018) since the emergence of deep learning. Neural networks were also used by models like U-Net, Mask R-CNN (He et al. 2017), and FCN (Fully Convolutional Networks) (IEEE Computer Society., n.d.) to learn complex features and forecast pixel-level segmentation masks. In this study, samples were trained based on significant features required for this study, such as roadways and buildings. Segmentation was based on these relevant features and satellite imageries were segmented to extract relevant roadway information.

This process helped in separating individual roadway segments for analysis as shown in Figure 2.6.

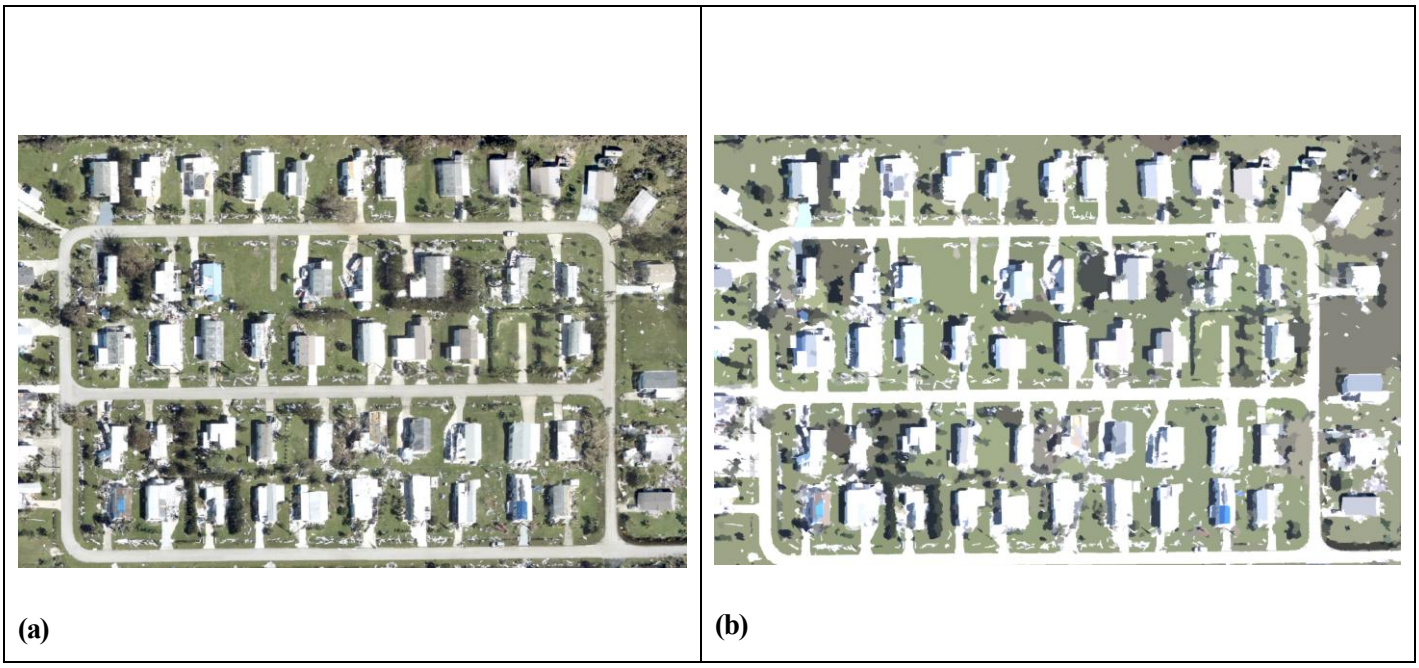

Figure 2:6 (a) Original Post-Hurricane Image, and (b) Segmented Post-Hurricane Image

2.3.2.4 Image Classification

The classification process in this study is an object-based supervised classification where several classifiers exist for supervised classification such as random forest, support vector machine, and maximum likelihood classifiers. In this paper, a support vector machine classifier was used in the image classification process supported by segmentation, training of sample collection, and editing. Figure 2.7 shows the workflow of the entire image classification process.

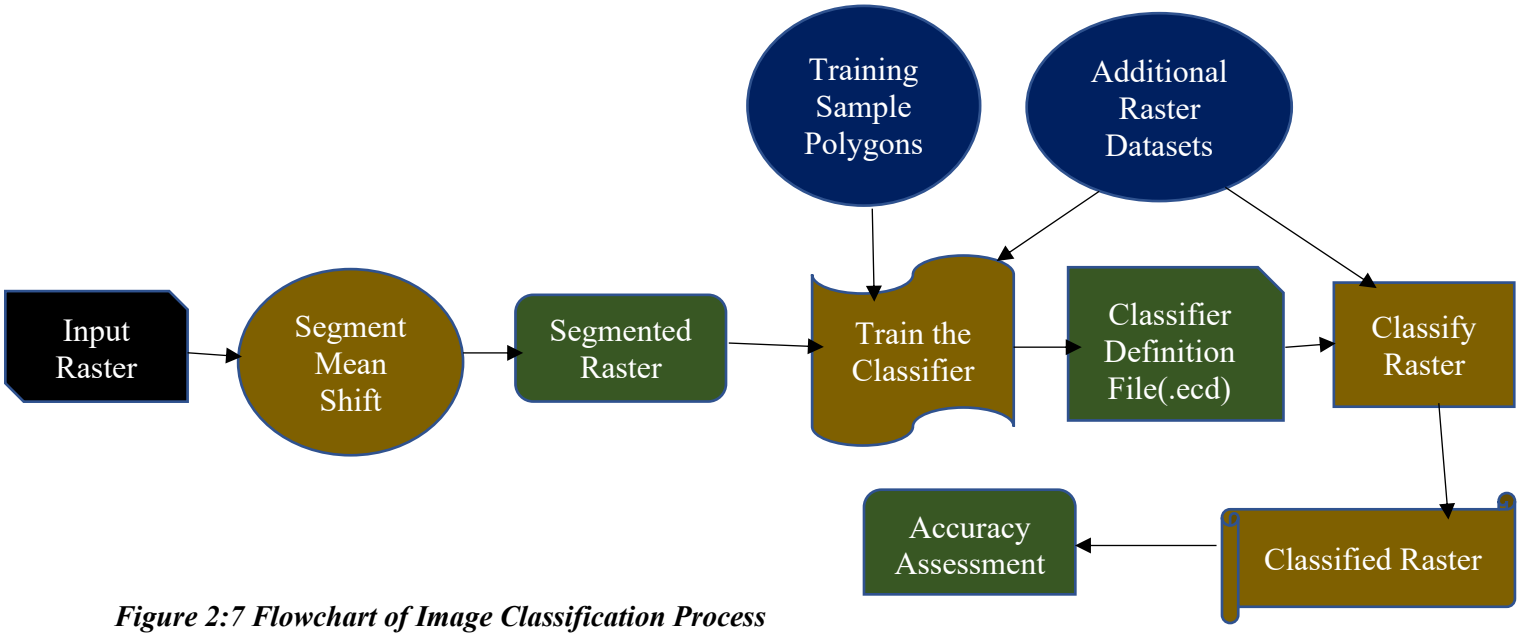

Figure 2:7 Flowchart of Image Classification Process

During the image classification process, segmented images were generated from the original images. An ISO Cluster classification was applied initially with random colors to classify all features into five classes. Support vector machine classifier was used to classify the images into several features as shown below in Figure 2.8 with manually labelled training samples. The final classification was performed based on the manually labelled training data. The result of the classification is shown in Figure 2.8.

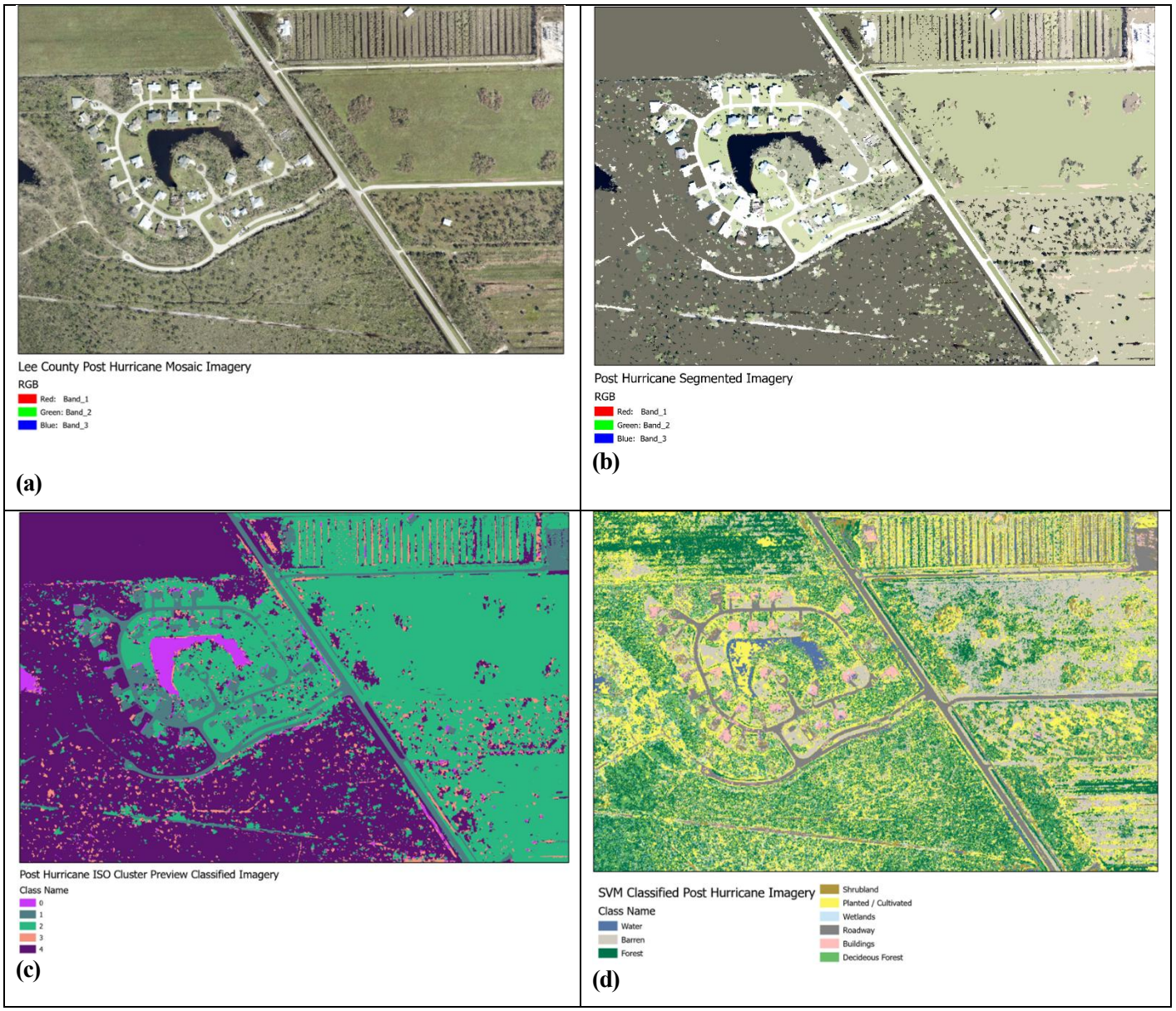

Figure 2:8 (a) Post Hurricane Imagery (b) Segmented Post hurricane Imagery (c) ISO Cluster Classification, and (d) SVM Classified Post Hurricane Imagery

2.3.3 Data Processing and Training Procedure

2.3.3.1 Manual Labeling

The collected aerial imagery underwent a meticulous manual labeling process to prepare it for training the machine learning model. The labeling process involved the following steps:

i. Identification of Roadway Segments**:** Roadway segments within the imagery were identified and extracted based on their visibility and accessibility.
ii. Drawing Bounding Boxes**:** Rectangular bounding boxes were drawn around roadway segments to demarcate areas of interest. Each bounding box encompassed a roadway section, capturing both the roadway surface and the adjacent areas that might contain debris or obstructions.
iii. Classification Criteria**:** Each bounding box was labeled according to the observed conditions within the enclosed area. The classification criteria were based on the presence and extent of debris and damage:
    - Open**:** Roadway segments with no visible obstructions or debris, indicating fully passable conditions.
    - Partially Closed**:** Roadway segments with partial obstructions or debris that hindered traffic flow but did not completely block the road.
    - Fully Closed: Roadway segments completely obstructed by debris or damage, rendering them impassable.
iv. Ensuring Consistency**:** The labeling process was carried out by trained personnel to ensure consistency and accuracy. Each labeled segment was cross-checked and validated to minimize errors and ensure reliable training data.

2.3.3.2 Training Procedure

Training includes the following steps:

i. Data Splitting: The labeled data was divided into three subsets: training, validation, and testing.
ii. Training Set: This set was used to train the machine learning model; this set contained 80% of the labeled data.
iii. Validation Set: This set was used to tune the model parameters and avoid overfitting, this set allowed for model performance evaluation during training and 10% was used.
iv. Testing Set**:** This set was used to assess the final model's performance; this set provided an unbiased evaluation of the model's ability to classify road conditions accurately and contained 10% of the entire labeled data.

The creation of training data is a key step in developing a reliable model to detect roadway closures from satellite images. The reliability and accuracy of the model's predictions will be considerably impacted by well-developed and annotated data. The essential phases in data preparation are shown in Figure 2.9. First, pre- and post-hurricane aerial images were obtained. These images cover the entire county area affected by the hurricane. Also, data including buildings, roadblocks, construction zones, accidents, floods, and other types of roadway closures were obtained. The collected images were manually labelled using rectangular bounding boxes to identify areas of roadway closures in three main classes: 1) open, 2) partially closed, and 3) fully closed roadways.

To boost the data set's diversity and strengthen the generalization of the model, data augmentation techniques including rotation and scaling were applied to the annotated images. Three subsets of the dataset were created: the training set, the validation set, and the test set. The validation set was created to fine-tune hyperparameters and avoid overfitting, and the test set was used to assess the performance of the final model. The annotated data was converted into a YOLO format suitable for the chosen deep learning architecture. To effectively handle the data sets, data loading techniques like batching were utilized to give data to the model in digestible chunks.

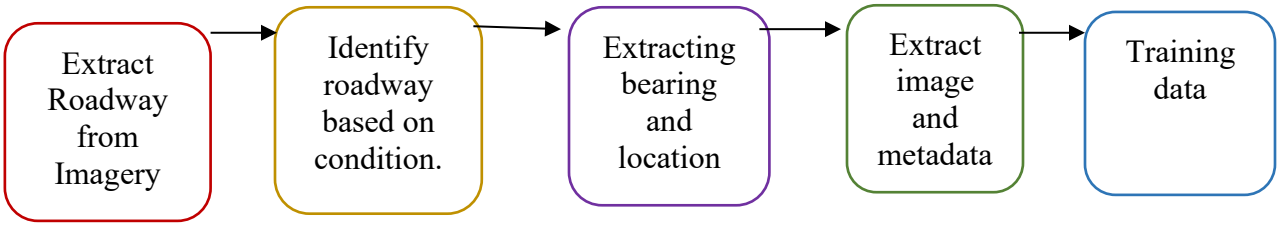

Figure 2:9 Framework for Training Data for the Model

2.3.4 Machine Learning Model Development for Roadway Extraction from Aerial Imagery

Multitask Roadway Extraction Model (X. Lu et al. 2019) was used in this study to extract roadway features from the aerial imagery as seen in Figure 2.10. The model uses the centerline extraction network which runs in parallel during training. The multilevel conceptual characteristics were taken out of the roadway detection network and convolved to create the roadway centerline extraction network (X. Lu et al. 2019). Resnet 34 is used as the fundamental multi-task learning network here. Unlike U-Net, ResNet-34, a Residual Network (ResNet) architecture variant, is not a multi-task learning network. ResNet is mostly applied to deep convolutional neural networks (CNNs) intended for feature extraction and image categorization. Unlike U-Net, it has a different kind of architecture, and its main function is not multi-task learning or producing finer details. The deep designs of ResNet with skip connections or residual blocks are well-known. The vanishing gradient issue was partially resolved by these connections, enabling the training of extremely deep networks. Through the ability to extract hierarchical characteristics from input images, ResNet, with 34 layers, can recognize and depict intricate patterns and structures found in images. Model metrics and loss graph can be seen in Figure 2.11. On the other hand, Figure 2.12 shows the ground truth results whereas Figure 2.13 presents the extracted roadways.

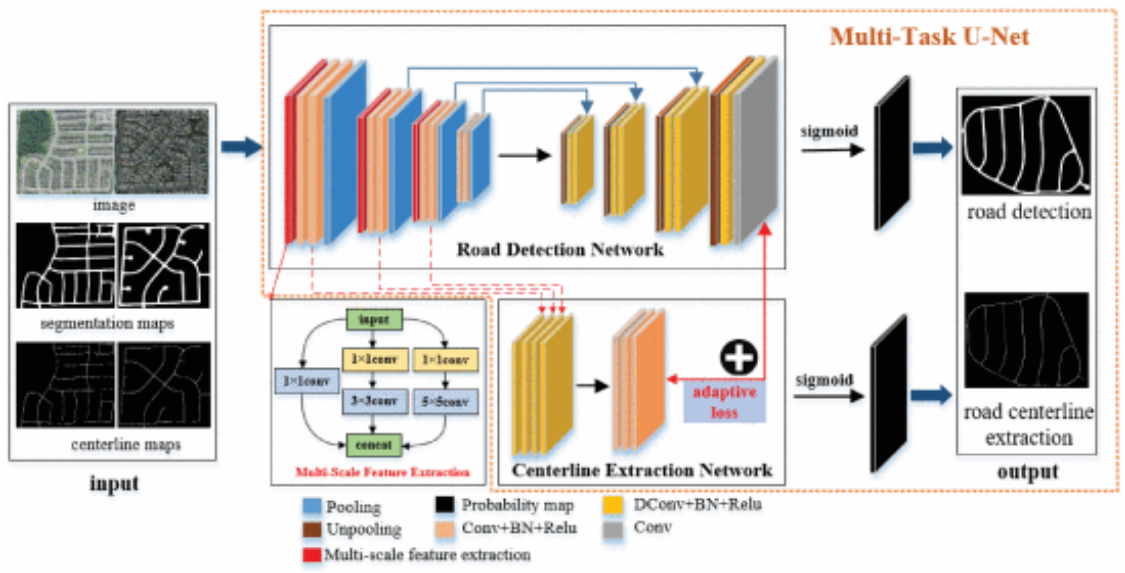

Figure 2:10 Framework of the Multi-Scale and Multi-Task Automatic Roadway Extraction Model (X. Lu et al. 2019)

MultiTaskRoadExtractor

Backbone: resnet34

Learning Rate: 1.2023e-03

Training and Validation loss

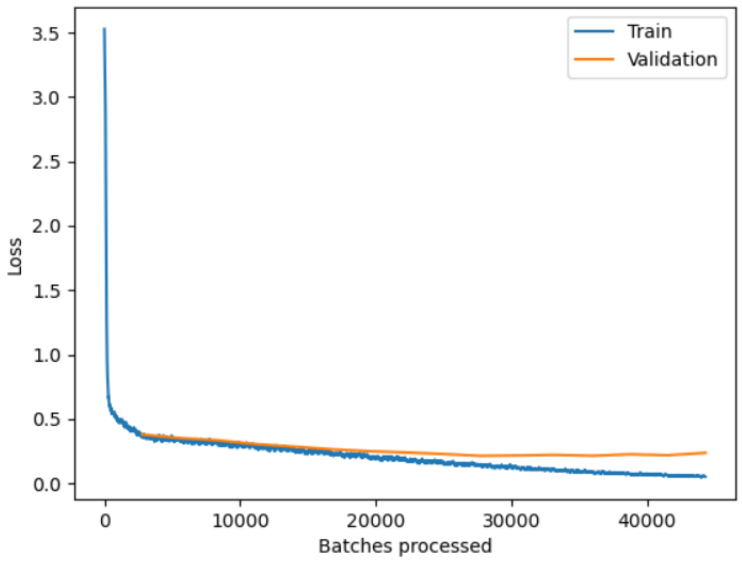

Analysis of the model

mIoU: 0.8760746660186743

Figure 2:11 Roadway Extractor Model Metrics and Loss Graph

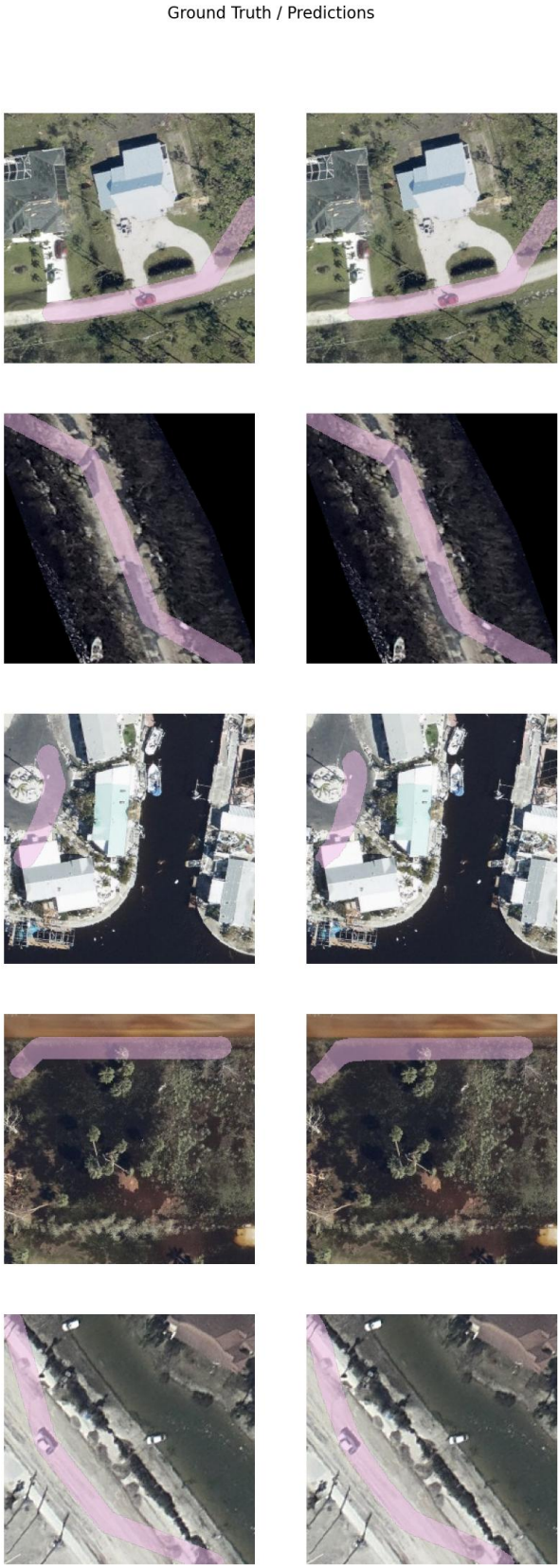

Figure 2:12 Ground Truth/Prediction Results for Roadway Extraction Model

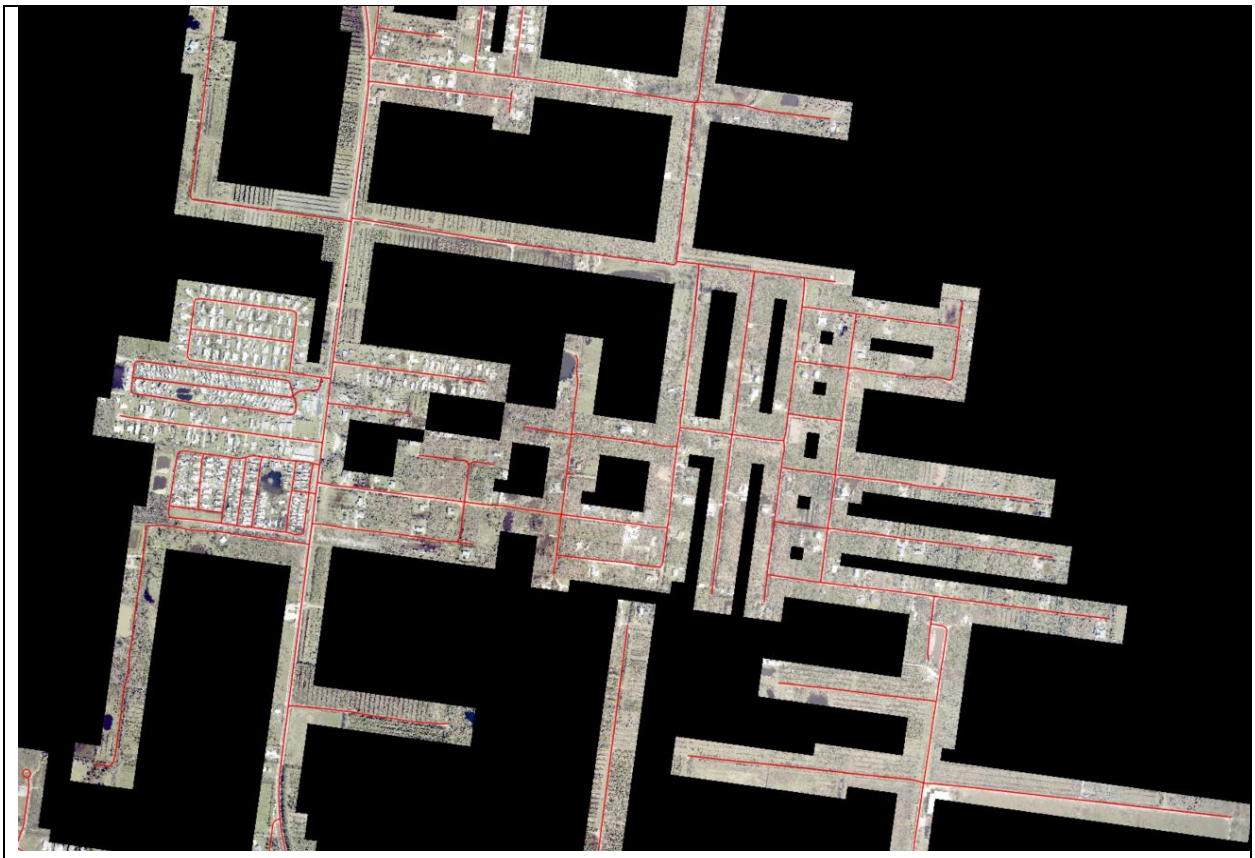

Figure 2:13 Results of the Extracted Roadways

2.3.5 Machine Learning Model Training and Development for Detection

We used a convolutional neural network (CNN) model to classify roadway conditions. The model was trained on labeled data, with features including roadway surface condition, debris presence, and closure extent. The training process involved specific hyperparameters such as Model Architecture: YOLO V3, Learning Rate: 0.001, Number of Epochs: 20, batch size = 4, Image Size: 256x256, Training Split: 80%, Test split: 10%, Validation Split: 100% of the dataset, Non-Max Suppression Threshold: 0.3, Augmentation Techniques: Horizontal and Vertical Flips, Random Rotation.

The model was trained using 600 manually labelled bounding boxes based on the three classes of roadways (i.e., open, partially closed, and fully closed) using the deep learning toolbox in ArcGIS Pro. 40% of the training dataset contained open classes, 30% contained partially closed, and the remaining 30% contained fully closed classes. The partially closed and fully closed data sets were roadway areas that were closed due to a variety of factors such as debris from damage of buildings, trees, and flooding. The learning rate, input image size, number of epochs, batch size, anchor box size and ratios, training and test data percentages are among the configurable parameters and hyperparameters of the object detection model. The validation and training loss graph was used to illustrate the ML model evaluation metrics. Using a suitable loss function, the YOLO v3 model

was trained on the provided dataset. On the validation set, which comprises 10% of the input training dataset, the validation loss and mean average precision were calculated. The batch size, learning rate, and training epoch are the object detection parameters that have the most influence on object detection. To get the best results, the model's hyperparameters were adjusted based on how well it performed on the validation set. The performance of the trained model was assessed on the test set to calculate its accuracy, precision, recall, and F1-score in identifying roadway closures. The data preparation processes were iterated, changing the model design, or gathering new data based on the adequacy of the model's performance. This action helped in improving the outcomes.

2.3.5.1 Yolo v3 Architecture.

One of the fastest object detection methods available is called "You only look once," or YOLO. YOLO acquires universal representations of items and performs noticeably better than top detection techniques like DPM and R-CNN when trained on actual images. When compared to Fast R-CNN, its background errors are reduced by more than half(Redmon et al. 2016). YOLOv2 uses the Darknet-19 classification network to extract features whereas YOLOv3 uses the far more advanced Darknet-53 network (Tsang 2018). Even though it is no longer the most accurate object detection algorithm, it is still a great option when real-time detection is required without sacrificing too much precision. Therefore, it was employed in this study.

Initially, YOLO v3 was based on Darknet, a network with 53 layers originally trained on ImageNet. To enhance its detection capabilities, an additional 53 convolutional layers were added, resulting in a total of 106 layers for the YOLO v3 fully convolutional architecture (Kathuria 2019). This extension contributes to the slower performance of YOLO v3 when compared to YOLO v2. In terms of measured floating-point operations per second, Darknet-53 also performs the best (Redmon, J., & Farhadi 2018). This indicates that the network structure makes better use of the GPU, making evaluation more efficient and faster. The current architecture of YOLO v3 can be seen in Figure 2.14 whereas ground truth/prediction results are shown in Figure 2.15 and loss graph is shown in Figure 2.16.

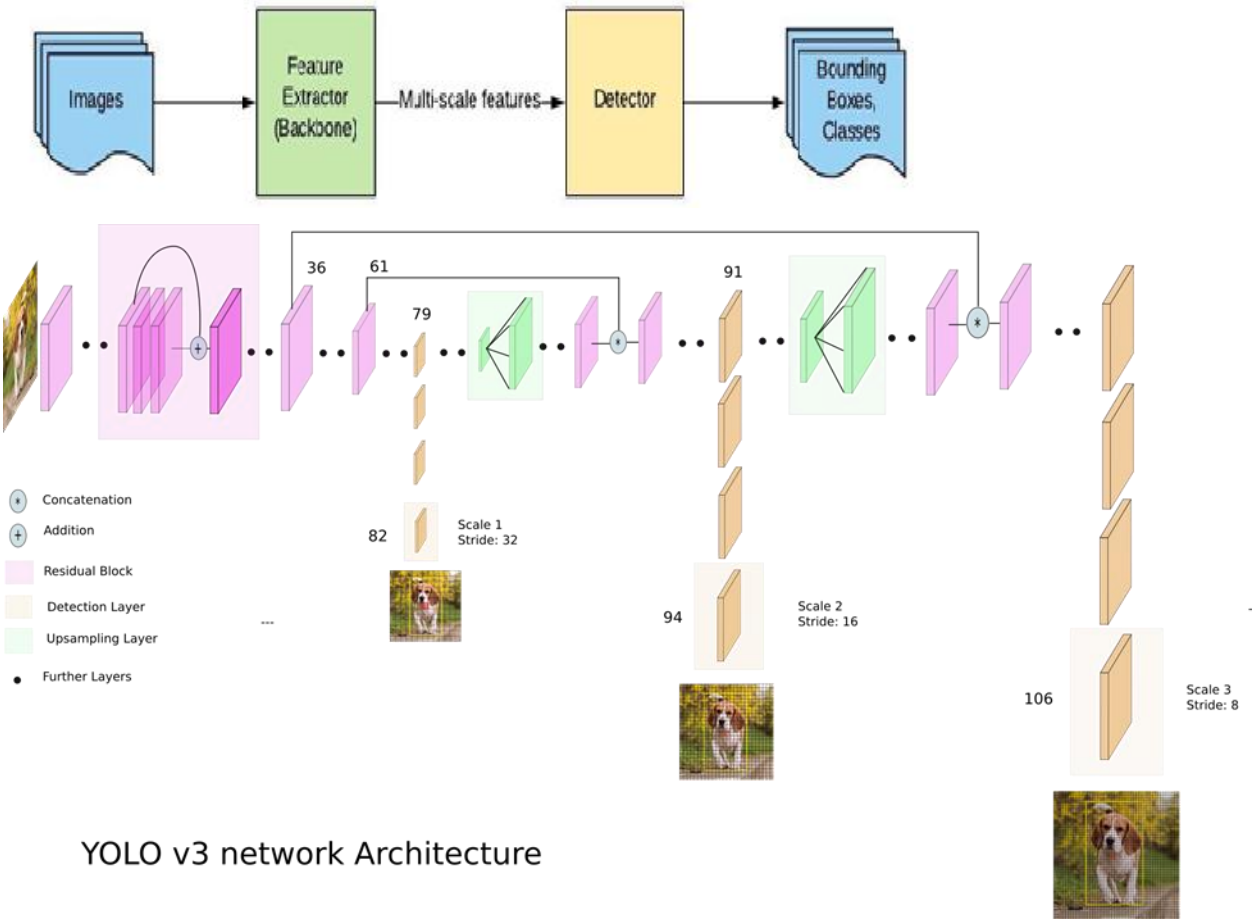

Figure 2:14 YOLO v3 Network Architecture (Kathuria 2019)

Figure 2:15 Ground Truth/Prediction Results for Detection Model

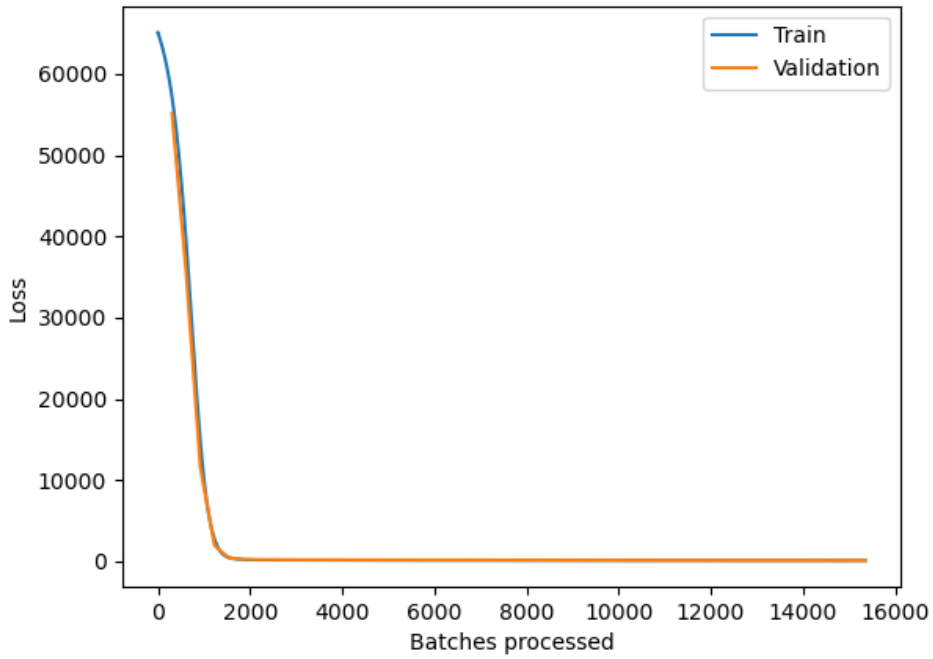

Figure 2:16 Loss Graph for Detection Model

2.4 Model Results on Hurricane Ian Impacts

Quantitative findings of the study are presented here, with a focus on how Hurricane Ian affected roadways and based on a data set of high-resolution images taken before and after Hurricane Ian. Note that we classified roadways into three groups, namely open, totally closed, and partially closed, as part of the study. Bounding boxes were used as part of the process to identify and classify roadway segments according to these conditions along with georeferencing and resolution standardization as preprocessing techniques. Findings indicate that roadway conditions were properly identified by the classification model, which showed good accuracy. According to the results, roadway segments were classified as fully closed, partially closed, and open classifications with an average confidence level of 92% by the model. Table 1 presents a summary of the outcomes for each class.

Table 2-1 Numbers According to the Roadway Classification

Roadway Classification	Count
Open Roadways	110
Fully Closed Roadways	55
Partially Closed Roadways	96

In addition, visualizations were created to supplement the numerical results. These included confusion matrices and sample images that showed the bounding boxes that were detected. A

representative confusion matrix for the three classes is shown in Table 2, giving a summary of true positives, true negatives, false positives, and false negatives. Figure 2.17 shows several images presenting the performance of the model whereas Figure 2.18 shows some images where the model failed in detection.

Table 2-2 A Representative Confusion Matrix Providing an Overview of True Positives, True Negatives, False Positives, and False Negatives across the Three Classes.

	Predicted Class		
Actual Class	Open	Fully Closed	Partially Closed
Open	104	9	48
Fully Closed	6	38	3
Partially Closed	1	5	47

i. The diagonal parts show accurate predictions, going from top-left to bottom-right.

ii. Misclassifications are represented by off-diagonal elements.

iii. As an example, the number in the "Open" row and "Fully Closed" column denotes the number of cases that were actually open but were anticipated to be fully closed.

Figure 2:17 Sample Images with Superimposed Bounding Boxes Offering a Visual Depiction of the Model's Ability to Identify Different Roadway Conditions

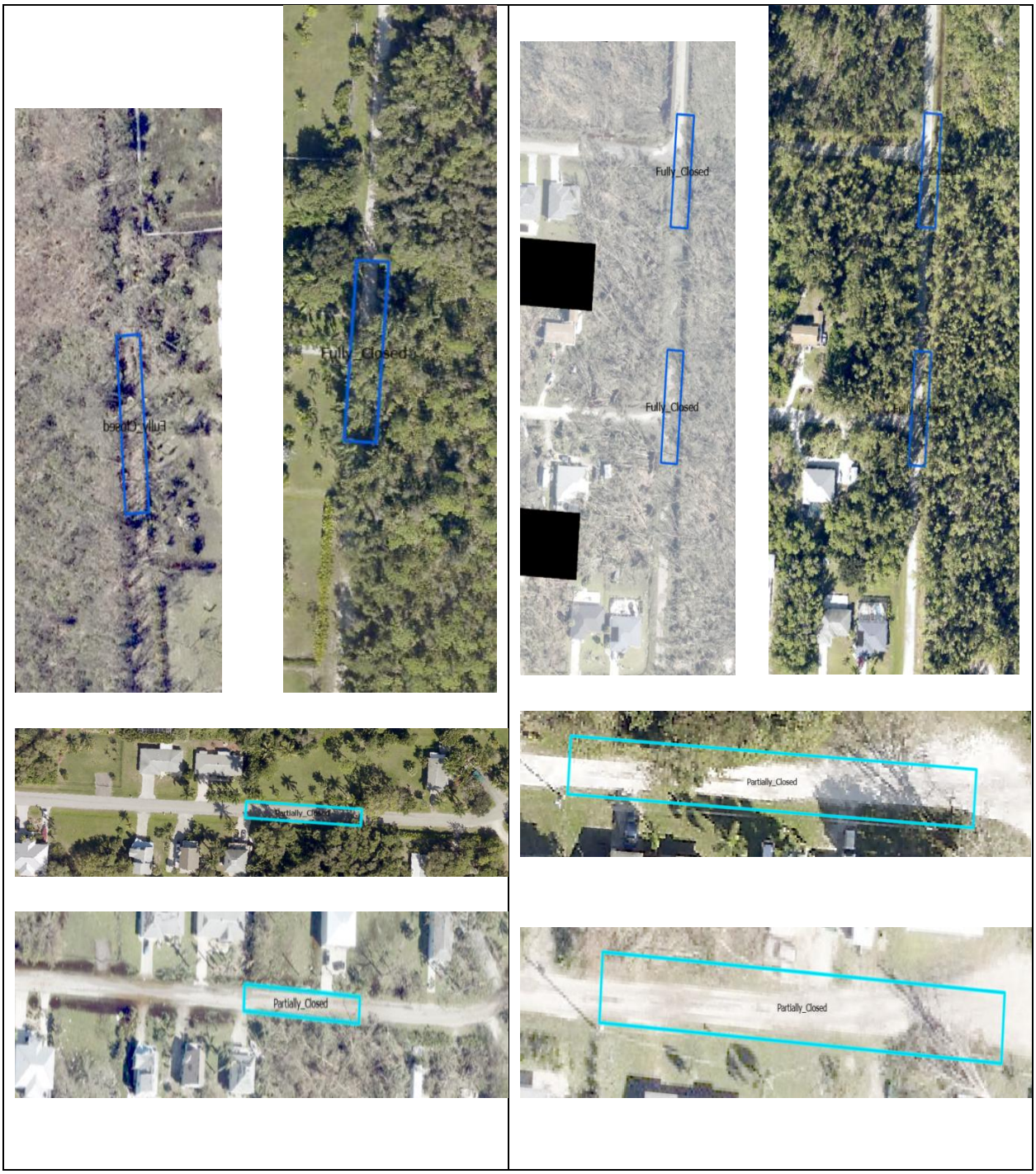

Figure 2:18 Areas that were Falsely Detected Due to Occlusion

Finally, we used precision, recall, and F1-score to evaluate the model's performance. The conventional formulas shown below were utilized to calculate these measures for every class. Recall measures the ability to identify every positive occurrence, precision expresses the accuracy of positive predictions, and the F1-score offers a fair evaluation that takes both precision and recall into account.

The ratio of accurately predicted positive observations to the total number of predicted positives is known as precision. It measures how well positive predictions were accurate.

$$P = \frac{TP}{TP+FP}$$

where

TP (True Positives) is the number of instances correctly predicted as positive.

FP (False Positives) is the number of instances incorrectly predicted as positive.

Recall is the ratio of correctly predicted positive observations to the total actual positives. It measures the model's ability to capture all positive instances.

$$R = \frac{TP}{TP+FN}$$

where

TP (True Positives) is the number of instances correctly predicted as positive.

FN (False Negatives) is the number of instances incorrectly predicted as negative.

The ratio of the harmonic means of recall and precision is known as the F1-score. It offers a fair evaluation, particularly in cases where the proportion of positive to bad occurrences is imbalanced.

$$F1 = \frac{\mathbf{2}.(\boldsymbol{P}.\boldsymbol{R})}{\boldsymbol{P}+\boldsymbol{R}}$$

Table 2-3 Model Performance Evaluations

	True Positive (TP)	**False Positive (FP)**	**False Negative (FN)**
Open	104	57	7
Fully Closed	38	9	14
Partially Closed	47	6	51

	Precision (%)	Recall (%)	F1-Score (%)
Open	65	94	77
Fully Closed	81	73	77
Partially Closed	89	48	62

Computed metrics provide insightful information about how well the model performed. In addition to confirming the correctness of our classification, precision, recall, and F1-score provided insight into the ability of the model to accurately detect and differentiate between different roadway conditions impacted by Hurricane Ian.

2.5 Discussions on Findings

Findings indicate that the impacts of Hurricane Ian were most noticeable in coastal regions, which suggests that there were more roadway closures. However, the interaction of debris and storm surge made precise detection more difficult. The Sanibel area was impacted as shown in Figure 2.19 and the model identified many closures. The Fort Myers area had 24 fully closed detections, and the St. James area had 14 fully closed road detections out of the overall 55 fully closed roadway detections. Bokeelia and Pine Island area were affected moderately per the model detection and Sanibel had many flooded roadways where the model had a minimum number of fully closed detections but had several partially closed roadway detections. However, when analyzed from aerial imagery, most of the closures in these regions were due to sea debris, and flooding. The map shown in Figure 2.19 also shows how seriously affected the roadways were in the Fort Myers beach region and San Carlos Island. Many roadways in these locations were totally blocked due to debris from buildings and trees, as well as debris from the seawater. The roadway debris from mobile homes and other buildings were found in regions that were not near beaches, resulting in both partial and full closures. Among these, the areas of St. James City and the Flamingo Bay Area were severely impacted. Compared to other areas of the county, Bokeelia and Pine Island's roadways were less severely impacted according to the model.

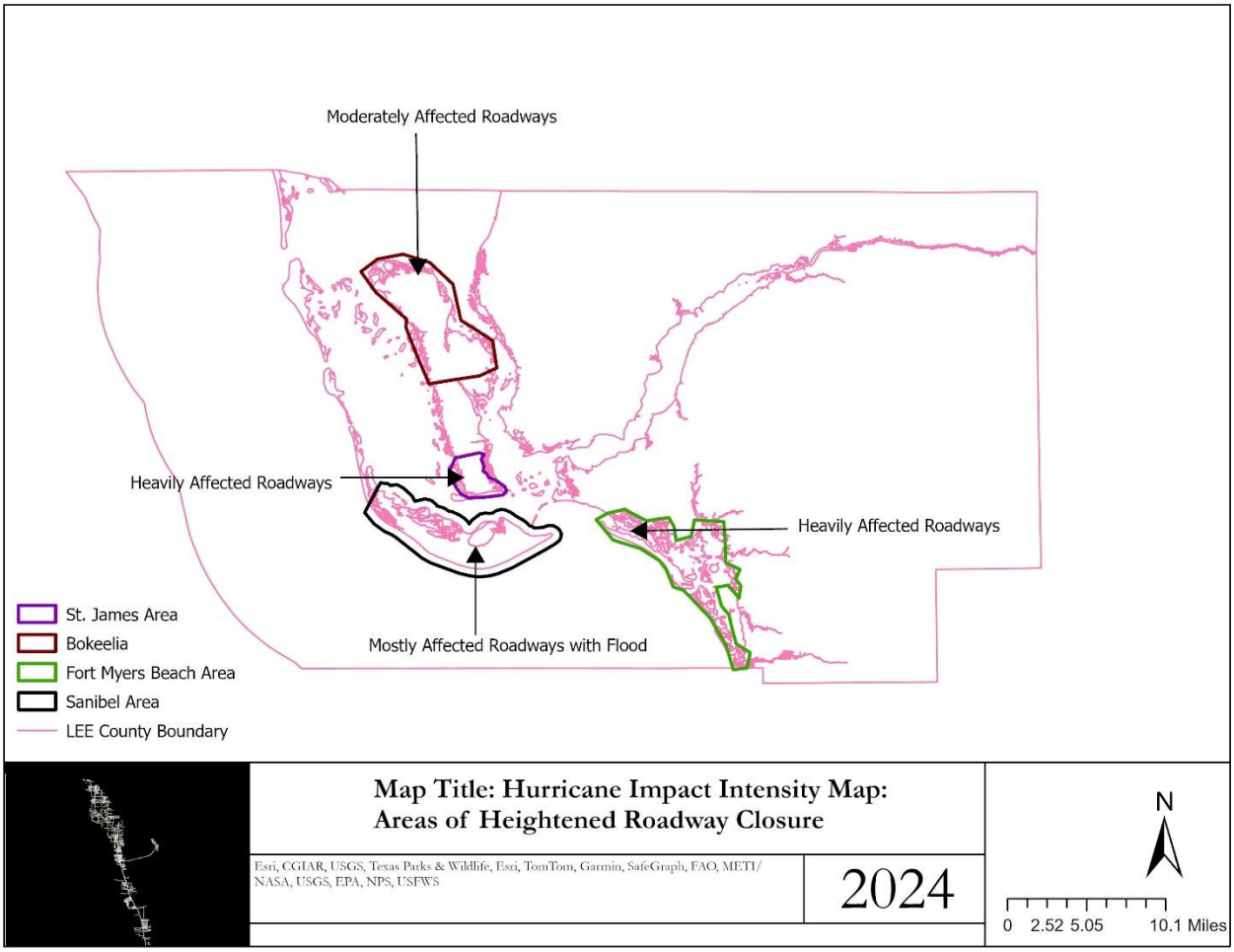

Figure 2:19 Affected Areas Impacted by Hurricane Ian and Roadway Closures

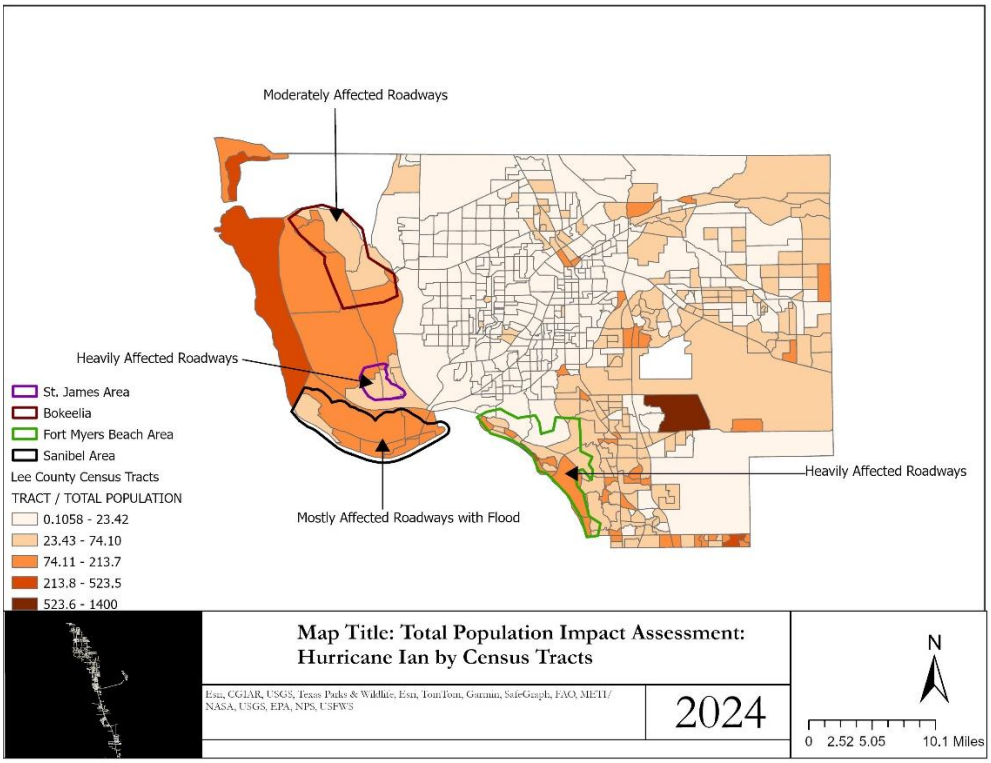

Figure 2:20 Total Population Impact Assessment by Census Tracts

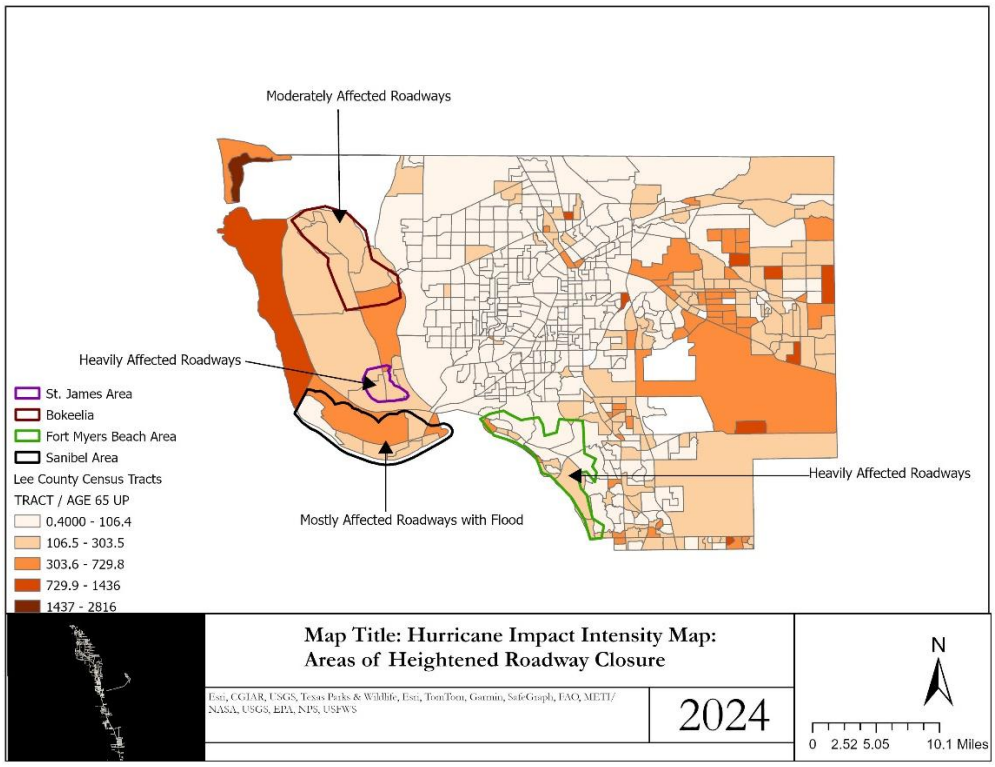

Figure 2:21 Aged Population Impact Assessment by Census Tracts

We also focused on the demographics of the impacted region and tried to provide some insights into the vulnerability of the populations with respect to the findings of the model related to roadway closures. U.S. Census tract data on total population and aged (65+) population have been used for this purpose. Figure 2.20 illustrates how an in-depth assessment of the overall population distribution across affected and unaffected areas is made possible by the study's use of census tract data.

Figure 2.20 indicates that there have been a higher number of populations, both total and aged, in heavily affected areas, which are probably the ones experiencing the greatest impact of hurricane-related damage. On the other hand, places that were relatively spared from the hurricane's impacts have lower total population. The correlation between the number of older people in Figure 2.21 and the intensity of the hurricane effect is also a significant observation. Elderly people make up a larger percentage of the population in heavily impacted areas, which are marked by their heightened vulnerability. This realization emphasizes possible difficulties older populations may encounter during and after hurricanes such as those related to their health conditions, highlighting the need for providing better accessibility in these catastrophic situations. Understanding the population patterns in both affected and unaffected areas has major implications for emergency response strategies. Areas that are severely affected and have higher total and older population numbers need to receive more attention and resources. Using this information on roadway closures, emergency responders can prioritize help, develop better evacuation strategies, and provide better access to healthcare services where the most urgent need exists. Local government agencies, nonprofits, and community organizations can also create customized resilience-building initiatives by identifying high-risk locations and those that are living in that region.

The model's effectiveness in these domains is essential for understanding accessibility issues, particularly for senior citizens living in coastal areas. The results of the detection indicate that there might be challenges in accurately predicting roadway accessibility for this group of people. It is essential to understand how Hurricane Ian affected roadway accessibility when developing emergency response plans with a focus on the elderly. Also, the rapid decision-making of emergency responders is facilitated by the correct identification of roadway conditions, which enables effective resource allocation and prioritizes help for older populations who may have mobility issues.

2.5.1 Application of the Model to Hurricane Idalia

To validate the robustness and generalizability of our model, we applied it to the aftermath of Hurricane Idalia, which impacted Northeast Florida, specifically in Taylor County. Aerial images were obtained from the National Hurricane Center and National Oceanic and Atmospheric Administration (National Oceanic and Atmospheric Administration 2023). The timestamp for these images is from August 8, 2023, to September 2, 2023, after hurricane Idalia made landfall. The classification results demonstrated that our model effectively identifies roadway conditions in different geographic areas and for different hurricane events.

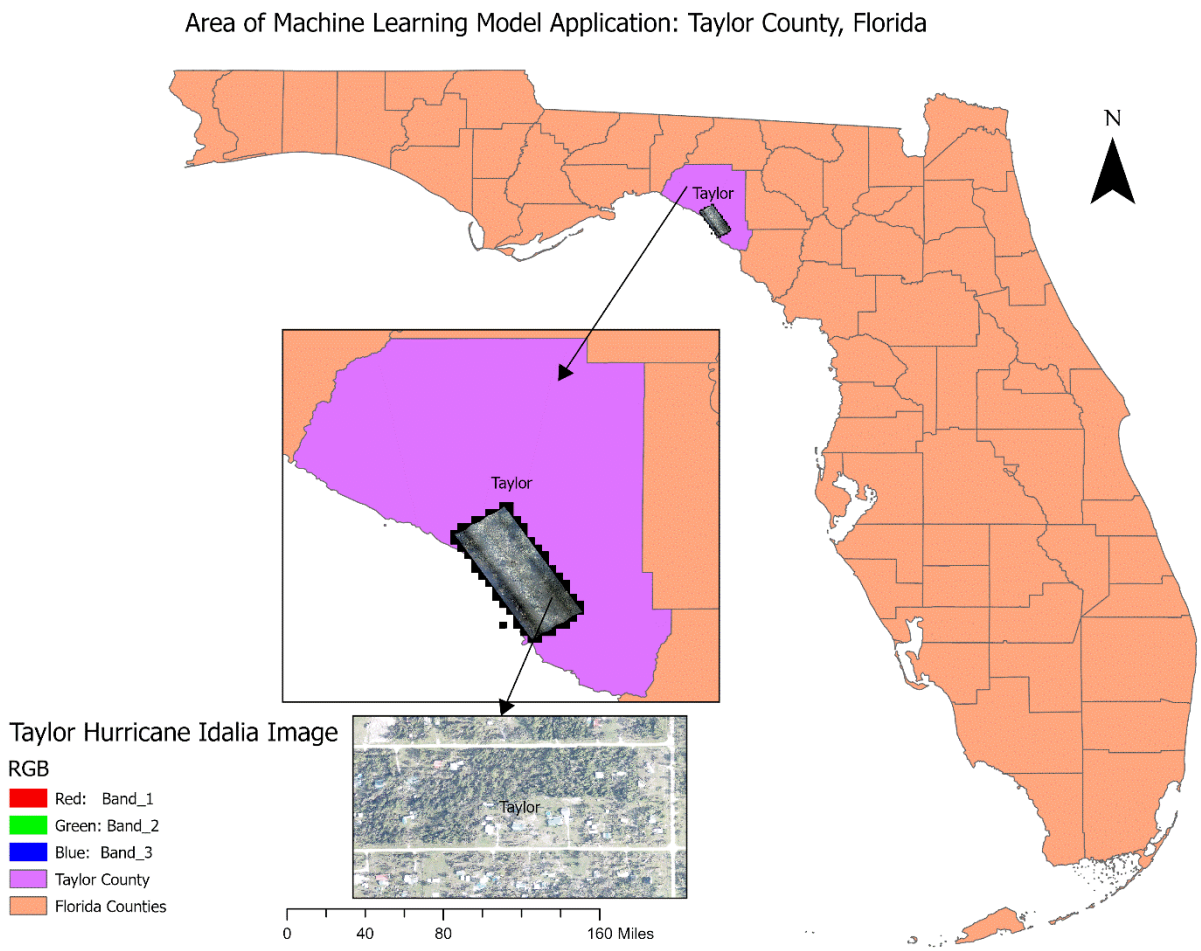

Figure 2:22 Area of Machine Learning Model Application in Taylor County, Florida

2.5.2 Results

The model categorized roadways into three classes as before: Open, Partially Closed, and Fully Closed. The detection results were encouraging, showing a high level of accuracy across all categories at an average confidence of 85%. The precision rates for each class—Open, Partially Closed, and Fully Closed—were notably high, indicating that the model is reliable in differentiating between various roadway conditions.

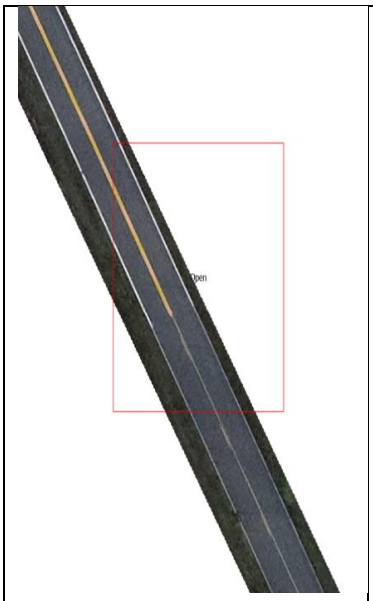
Open


Document was last saved: Just now
Open

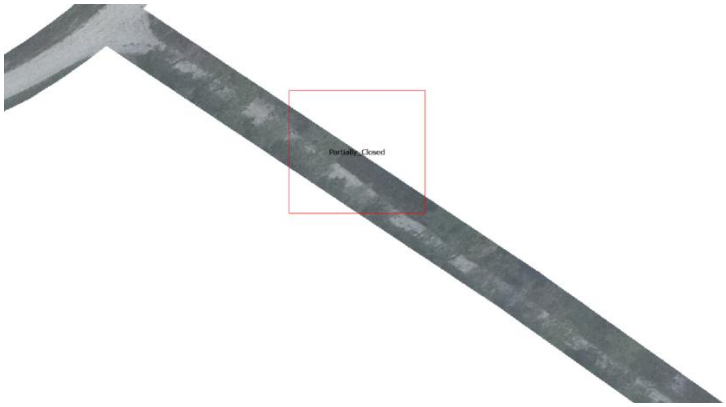
Partially_Closed

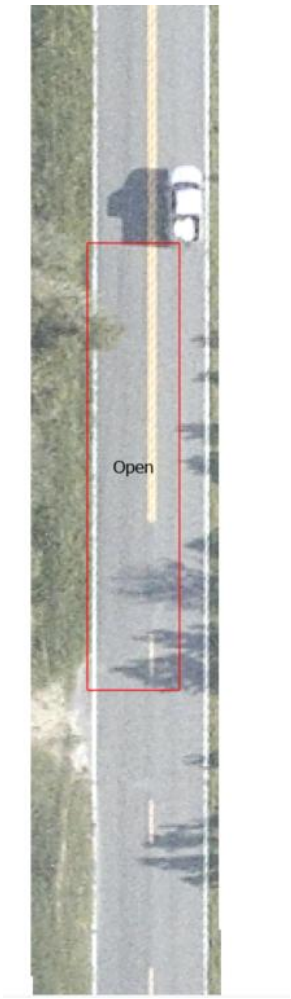
Open

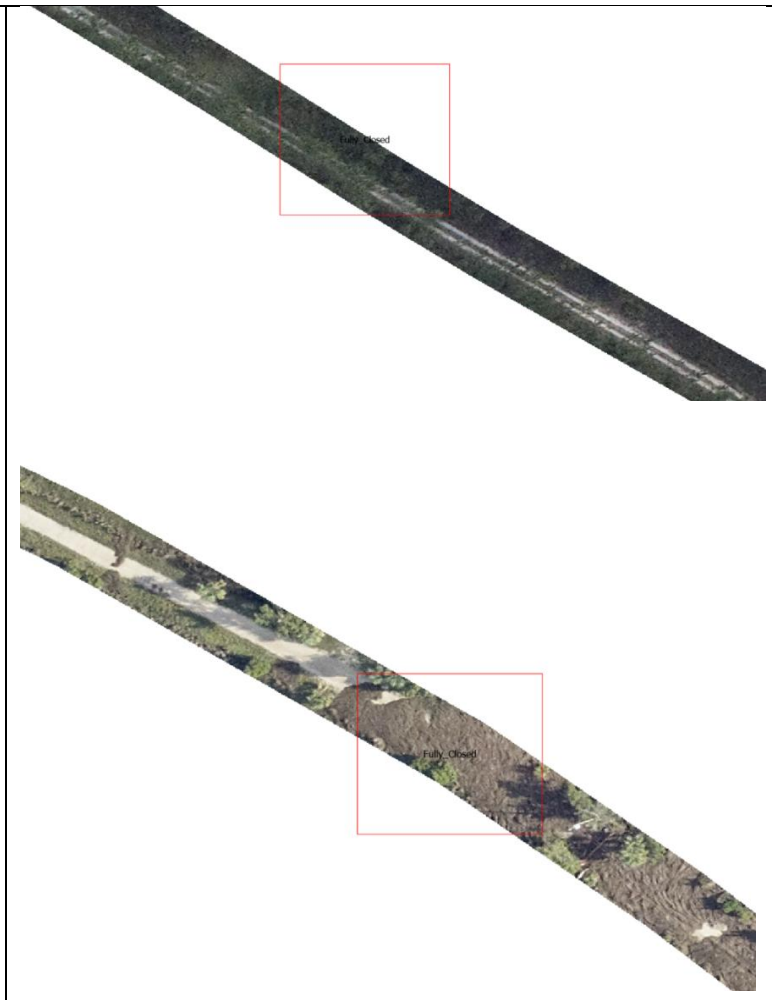

Figure 2:23 Sample Detection Images Hurricane Idalia and the Model's Ability to Identify Different Roadway Conditions

Table 2-4 Model Performance Evaluations of Hurricane Idalia

Class	Open	Partially Closed	Fully Closed	Total
Number of Detections	115	16	38	**169**

	True Positive (TP)	False Positive (FP)	False Negative (FN)
Open	93	22	
Fully Closed	36	2	7
Partially Closed	15	1	17

	Precision (%)	Recall (%)	F1-Score (%)
Open	81	100	90
Fully Closed	95	84	89
Partially Closed	94	47	63

These findings support the applicability of our model beyond the initial study area in Lee County, Florida. The high precision rates across different classifications suggest that the model is capable of accurately assessing roadway conditions in the wake of different hurricanes, thereby offering a valuable tool for disaster response and recovery efforts in various regions. By successfully applying the model to Hurricane Idalia, we have demonstrated its effectiveness in identifying the extent of roadway closures and debris presence under different circumstances. This validation highlights the model's potential for broader use in emergency management and urban planning.

2.6 Conclusions, Limitations, And Future Work

This study provided a machine learning-based methodology to study the impact of Hurricane Ian and Idalia on roadways in the context of roadway closures and accessibility. We classified the condition of the roadways following these hurricanes into three categories: open, totally closed, and partially closed. We accomplished this by utilizing both machine learning techniques and high-resolution satellite images. The results show how the proposed methodology can offer accurate and timely data on roadway closures, which would be helpful for disaster response and planning.

Findings have significant implications for improving the resilience of infrastructure and directing emergency management plans. The proposed technique can be used by emergency responders and disaster management organizations to evaluate roadway conditions immediately following hurricanes. Planning optimal routes for emergency vehicles and resource allocation could depend heavily on this information. This methodology can also be used by engineers and urban planners to assess the resilience of the roadway infrastructure to hurricanes and identify areas that are vulnerable to significant damage. Future improvements and investments in infrastructure can be guided by this information as well as educating the public in making decisions about the timing and route of evacuations. The model can be used by government agencies engaged in post-disaster recovery efforts to select areas that need immediate attention, which could help in facilitating the effective distribution of resources needed for reconstruction and restoration.

However, it is imperative to acknowledge specific constraints that impacted on the analysis and application of our findings. The presence of debris, vegetation, or other obstructions (occlusion) on roadways interferes with visibility in aerial imagery, making it difficult to accurately identify the condition of the roadways. This is one drawback of the study. Furthermore, the categorization of roadway conditions, specifically differentiating between fully closed and partially closed roadways, was susceptible to uncertainty brought on by a significant accumulation of debris. One major obstacle is the variation in debris distribution between different areas. While some partially closed roadways may have minimal debris and are mistakenly classified as open, others may have a lot of debris and are mistakenly classified as entirely closed. Our classification model's accuracy is complicated by the dynamic nature of this debris distribution. Environmental factors like shadows, reflections, and terrain variations also have an impact on the assessment of roadway conditions, leading to false positives. These factors can introduce noise into the imagery, leading to potential misinterpretations of roadway conditions. While important, the temporal dynamics of roadway conditions such as variations in debris accumulation over time are difficult to adequately depict in static imagery. Also, our ability to depict the dynamic nature of post-hurricane roadway conditions is limited by the absence of timestamped data such as the number of these taken to flying over the area and changes in roadway conditions with time.

Further research is still needed to solve aforementioned issues and improve the proposed methodology. Incorporating dynamic temporal data sources, exploring cutting-edge techniques to reduce occlusion effects, and improving the model to better handle shading in roadway conditions could all be steps toward addressing these limitations. Further studies could concentrate on improving the technique to tackle issues more effectively in coastal regions, enhancing the precision of identification when debris and flooding are present, and customizing the model to the unique vulnerabilities of the public. Enhancing machine learning algorithms and integrating temporal data in real-time will also help increase the accuracy of accessibility assessments.

2.7 References

Barnes, Christopher F., Hermann Fritz, and Jeseon Yoo. 2007. "Hurricane Disaster Assessments with Image-Driven Data Mining in High-Resolution Satellite Imagery." *IEEE Transactions on Geoscience and Remote Sensing* 45 (6): 1631–40. https://doi.org/10.1109/TGRS.2007.890808.

Buslaev, Alexander, Selim Seferbekov, Vladimir Iglovikov, and Alexey Shvets. 2018. *Fully Convolutional Network for Automatic Road Extraction from Satellite Imagery*. https://doi.org/10.1109/CVPRW.2018.00035.

Cortes, Corinna, Vladimir Vapnik, and Lorenza Saitta. 1995. "Support-Vector Networks Editor." *Machine Learning* 20:273–97.

Cover, T M, and P E Hart. 1952. "Approximate Formulas for the Information Transmitted Bv a Discrete Communication Channel." *IEEE TRANSACTIONS ON INFORMATION THEORY* 24 (1): 335–42.

Cristian, Alexandru. 2024. "Post-Disaster Recovery and Environmental Monitoring Using GIS and GeoAI: Building Damage Assessment Insights from McDonough County." https://doi.org/10.13140/RG.2.2.25657.17760.

Dalal, Navneet, and Bill Triggs. 2005. "Histograms of Oriented Gradients for Human Detection." In *IEEE Computer Society Conference on Computer Vision and Pattern Recognition (CVPR'05), San Diego, CA, USA,* 886–93. https://doi.org/10.1109/CVPR.2005.177.

Dong, Laigen, and Jie Shan. 2013. "A Comprehensive Review of Earthquake-Induced Building Damage Detection with Remote Sensing Techniques." *ISPRS Journal of Photogrammetry and Remote Sensing*. Elsevier B.V. https://doi.org/10.1016/j.isprsjprs.2013.06.011.

Drejza, Susan, Pascal Bernatchez, Guillaume Marie, and Stéphanie Friesinger. 2019. "Quantifying Road Vulnerability to Coastal Hazards: Development of a Synthetic Index." *Ocean and Coastal Management* 181 (November). https://doi.org/10.1016/j.ocecoaman.2019.104894.

Ferguson, Neil, Georgia Boura, Ander Gray, Edoardo Patelli, and Enrico Tubaldi. 2023. "Vulnerability of the Scottish Road Network to Flooding."

"Florida Department of Transportation. Https://Fdotewp1.Dot.State.Fl.Us/AerialPhotoLookUpSystem/." 2023. 2023.

Goodfellow, Ian, Yoshua Bengio, and Aaron Courville. 2017. "Deep Learning: The MIT Press, 2016, 800 Pp, ISBN: 0262035618." *Genetic Programming and Evolvable Machines* 19 (October). https://doi.org/10.1007/s10710-017-9314-z.

Hassan, Sitti Asmah, Hamizah Amalina Amlan, Nor Eliza Alias, Mariyana Aida Ab-Kadir, and Nur Sabahiah Abdul Sukor. 2022. "Vulnerability of Road Transportation Networks under Natural Hazards: A Bibliometric Analysis and Review." *International Journal of Disaster Risk Reduction* 83 (December). https://doi.org/10.1016/j.ijdrr.2022.103393.

Hauptman, Leanne, Diana Mitsova, and Tiffany Roberts Briggs. 2024. "Hurricane Ian Damage Assessment Using Aerial Imagery and LiDAR: A Case Study of Estero Island, Florida." *Journal of Marine Science and Engineering* 12 (4). https://doi.org/10.3390/jmse12040668.

He, Kaiming, Georgia Gkioxari, Piotr Dollar, and Ross Girshick. 2017. "Mask R-CNN." *Proceedings of the IEEE International Conference on Computer Vision* 2017-October (December):2980–88. https://doi.org/10.1109/ICCV.2017.322.

He, Kaiming, Xiangyu Zhang, Shaoqing Ren, and Jian Sun. 2016. "Deep Residual Learning for Image Recognition." In *Proceedings of the IEEE Conference on Computer Vision and Pattern Recognition (CVPR)*, 770–78. http://image-net.org/challenges/LSVRC/2015/.

Hina Ajmal, Saad Rehman, Umar Farooq, Qurrat U. Ain, Farhan Riaz, and Ali Hassan. 2018. "Convolutional Neural Network Based Image Segmentation: A Review." *Proc.SPIE* 10649 (April). https://doi.org/10.1117/12.2304711.

"Https://Www.Bing.Com/Images/Search?Q=hurricane+ian&qpvt=Hurricane+Ian&form=IGRE&first=1&cw=1473&ch=823." 2023. 2023.

"Https://Www.Tampafp.Com/Hurricane-Debby-Leaves-Severe-Damage-in-Florida-Sen-Rubio-and-Rep-Cammack-Urge-Full-Federal-Assistance/#google_vignette." 2024. 2024.

IEEE Computer Society. n.d. “2015 IEEE Conference on Computer Vision and Pattern Recognition (CVPR) : Date, 7-12 June 2015.”

Jeffrey, E. F. 2009. “What-in-the-World-Is-Infrastructure.” Infrastructure Investor. 2009. https://corenergy.reit/wp-content/uploads/2018/03/what-in-the-world-is-infrastructure.pdf.

Jena, Ratiranjan, Biswajeet Pradhan, and Ghassan Beydoun. 2020. “Earthquake Vulnerability Assessment in Northern Sumatra Province by Using a Multi-Criteria Decision-Making Model.” *International Journal of Disaster Risk Reduction* 46 (June). https://doi.org/10.1016/j.ijdrr.2020.101518.

Ji, Min, Lanfa Liu, Runlin Du, and Manfred F. Buchroithner. 2019. “A Comparative Study of Texture and Convolutional Neural Network Features for Detecting Collapsed Buildings after Earthquakes Using Pre- and Post-Event Satellite Imagery.” *Remote Sensing* 11 (10). https://doi.org/10.3390/rs11101202.

Karaer, Alican, Mingyang Chen, Michele Gazzea, Mahyar Ghorbanzadeh, Tarek Abichou, Reza Arghandeh, and Eren Erman Ozguven. 2022. “Remote Sensing-Based Comparative Damage Assessment of Historical Storms and Hurricanes in Northwestern Florida.” *International Journal of Disaster Risk Reduction* 72:102857. https://doi.org/https://doi.org/10.1016/j.ijdrr.2022.102857.

Karimiziarani, Mohammadsepehr, and Hamid Moradkhani. 2022. “Social Response and Disaster Management: Insights from Twitter Data Assimilation on Hurricane Ian.,” December. https://doi.org/http://dx.doi.org/10.2139/ssrn.4292734.

Kathuria, A. 2019. “What’s New in YOLO v3? 2018. Https://Towardsdatascience.Com/Yolo-v3-Object-Detection-53fb7d3bfe6b.” https://towardsdatascience.com/yolo-v3-object-detection-53fb7d3bfe6b.

Kerle, N., and R. R. Hoffman. 2013. “Collaborative Damage Mapping for Emergency Response: The Role of Cognitive Systems Engineering.” *Natural Hazards and Earth System Science* 13 (1): 97–113. https://doi.org/10.5194/nhess-13-97-2013.

Kim, Jooho, Juhee Bae, and Makarand Hastak. 2018. “Emergency Information Diffusion on Online Social Media during Storm Cindy in U.S.” *International Journal of Information Management* 40 (June):153–65. https://doi.org/10.1016/j.ijinfomgt.2018.02.003.

Kourehli, Seyed Sina. 2015. “Damage Assessment in Structures Using Incomplete Modal Data and Artificial Neural Network.” *International Journal of Structural Stability and Dynamics* 15 (6). https://doi.org/10.1142/S0219455414500874.

Linardos, Vasileios, Maria Drakaki, Panagiotis Tzionas, and Yannis L. Karnavas. 2022. “Machine Learning in Disaster Management: Recent Developments in Methods and Applications.” *Machine Learning and Knowledge Extraction*. MDPI. https://doi.org/10.3390/make4020020.

Loggins, Ryan, and William Wallace. 2015. “Rapid Assessment of Hurricane Damage and Disruption to Interdependent Civil Infrastructure Systems.” *Journal of Infrastructure Systems* 21 (October):4015005. https://doi.org/10.1061/(ASCE)IS.1943-555X.0000249.

Lowe, David G. 2004. “Distinctive Image Features from Scale-Invariant Keypoints.” *International Journal of Computer Vision* 60 (2): 91–110.

Lu, Qing-Chang, and Zhong-Ren Peng. 2011. “Vulnerability Analysis of Transportation Network Under Scenarios of Sea Level Rise.” *Transportation Research Record* 2263 (November). https://doi.org/10.3141/2263-19.

Lu, Xiaoyan, Yanfei Zhong, Zhuo Zheng, Yanfei Liu, Ji Zhao, Ailong Ma, and Jie Yang. 2019. “Multi-Scale and Multi-Task Deep Learning Framework for Automatic Road Extraction.” *IEEE Transactions on Geoscience and Remote Sensing* 57 (11): 9362–77. https://doi.org/10.1109/TGRS.2019.2926397.

Ma, Haijian, Nan Lu, Linlin Ge, Qiang Li, Xinzhao You, and Xiaoxuan Li. 2013. “Automatic Road Damage Detection Using High-Resolution Satellite Images and Road Maps.” In *International Geoscience and Remote Sensing Symposium (IGARSS)*, 3718–21. https://doi.org/10.1109/IGARSS.2013.6723638.

Martín, Yago, Susan L. Cutter, Zhenlong Li, Christopher T. Emrich, and Jerry T. Mitchell. 2020. “Using Geotagged Tweets to Track Population Movements to and from Puerto Rico after Hurricane Maria.” *Population and Environment* 42 (1): 4–27. https://doi.org/10.1007/s11111-020-00338-6.

Mathias, Jean Denis, Susan Spierre Clark, Nuri Onat, and Thomas P. Seager. 2018. “An Integrated Dynamical Modeling Perspective for Infrastructure Resilience.” *Infrastructures* 3 (2). https://doi.org/10.3390/infrastructures3020011.

Mauricio Sánchez-Silva, and Libardo García. 2001. “Earthquake Damage Assessment Based on Fuzzy Logic and Neural Networks.” *Earthquake Spectra* 17 (1): 89–112. https://doi.org/https://doi.org/10.1193/1.1586168.

Minaee, Shervin, Yuri Boykov, Fatih Porikli, Antonio Plaza, Nasser Kehtarnavaz, and Demetri Terzopoulos. 2022. “Image Segmentation Using Deep Learning: A Survey.” *IEEE Transactions on Pattern Analysis and Machine Intelligence* 44 (7): 3523–42. https://doi.org/10.1109/TPAMI.2021.3059968.

Mitsova, Diana, Monica Escaleras, Alka Sapat, Ann Margaret Esnard, and Alberto J. Lamadrid. 2019. “The Effects of Infrastructure Service Disruptions and Socio-Economic Vulnerability on Hurricane Recovery.” *Sustainability (Switzerland)* 11 (2). https://doi.org/10.3390/su11020516.

Mostafavi, Ali, Jamie Padgett, Leonardo Dueñas-Osorio, Elaina Sutley, Terri Norton, Henry Lester, Haizhong Wang, et al. 2022. *Hurricane Harvey Infrastructure Resilience Investigation Report*. https://doi.org/10.17603/ds2-gcrf-h607.

Mukherjee, Mahua, Kumar Abhinay, Md Munsur Rahman, Sonam Yangdhen, Subir Sen, Basanta Raj Adhikari, Rekha Nianthi, Sanya Sachdev, and Rajib Shaw. 2023a. “Extent and Evaluation of Critical Infrastructure, the Status of Resilience and Its Future Dimensions in South Asia.” *Progress in Disaster Science* 17 (January). https://doi.org/10.1016/j.pdisas.2023.100275.

———. 2023b. “Extent and Evaluation of Critical Infrastructure, the Status of Resilience and Its Future Dimensions in South Asia.” *Progress in Disaster Science* 17 (January). https://doi.org/10.1016/j.pdisas.2023.100275.

Mustakim, Md Mizanur. 2023. “Road Damage Detection Based on Deep Learning.” https://doi.org/10.13140/RG.2.2.22523.28967.

National Environmental Satellite Data and Information Service. 2022. “Hurricane Ian’s Path of Destruction.” Department of Commerce, National Oceanic and Atmospheric Administration. 2022. https://www.nesdis.noaa.gov/news/hurricane-ians-path-of-destruction.

National Oceanic and Atmospheric Administration. 2023. “Https://Noaa-Eri-Pds.S3.Amazonaws.Com/Index.Html#2023_Hurricane_Idalia/20230902a_RGB/.” 2023.

National Oceanic and Atmospheric Administration (NOAA). n.d. “‘Hurricane Costs.’” Accessed June 26, 2023. https://coast.noaa. gov/states/fast-facts/hurricane-costs.html.

Nguyen, Long, Alexis Slobodzian, Claude Villiers, and Seneshaw Tsegaye. 2022. “Interdependencies of Lifelines: A Case Study of Transportation Infrastructure Under Hurricane Impacts.” In , 1–10. https://doi.org/10.1007/978-981-19-1029-6_1.

Pavur, G., V. Lakshmi, and J.H. Lambert. 2023. “A Hydrological and Socioeconomic Risk Assessment of Tropic Cyclone Disasters by Leveraging Space-Based Earth Observation.” *EGU General Assembly*, April, EGU23-10474. https://doi.org/https://doi.org/10.5194/egusphere-egu23-10474,2023.

Peng, Bo, Zonglin Meng, Qunying Huang, and Caixia Wang. 2019. “Patch Similarity Convolutional Neural Network for Urban Flood Extent Mapping Using Bi-Temporal Satellite Multispectral Imagery.” *Remote Sensing* 11 (21). https://doi.org/10.3390/rs11212492.

Pourebrahim, Nastaran, Selima Sultana, John Edwards, Amanda Gochanour, and Somya Mohanty. 2019. “Understanding Communication Dynamics on Twitter during Natural Disasters: A Case Study of Hurricane Sandy Understanding Communication Dynamics on Twitter During.”

Pouryari, Maghsood, A Ardakani, and Nemat Hassani. 2021. “A Multi-Criteria Vulnerability of Urban Transportation Systems Analysis Against Earthquake Considering Topological and Geographical Method: A Case Study.” *Iranian Journal of Science and Technology, Transactions of Civil Engineering* 46 (July). https://doi.org/10.1007/s40996-021-00699-4.

Redmon, J., & Farhadi, A. 2018. “Yolov3: An Incremental Improvement. Https://Arxiv.Org/Abs/1804.02767. Accessed 12, 2023.”

Redmon, Joseph, Santosh Divvala, Ross Girshick, and Ali Farhadi. 2016. “You Only Look Once: Unified, Real-Time Object Detection.” In *Proc., IEEE Conference on Computer Vision and Pattern Recognition, Las Vegas, NV. IEEE, New York.*, 779–88. http://pjreddie.com/yolo/.

Richard Szeliski. 2022. *Computer Vision: Algorithms and Applications. 10.1007/978-3-030-34372-9*. *Springer*.

Robinson, Anthony C. 2020. *Geographic Information Systems (GIS) for Disaster Management: Second Edition*. https://doi.org/doi.org/10.4324/9781351034869.

Ruseruka, Cuthbert, Judith Mwakalonge, Gurcan Comert, Saidi Siuhi, and Judy Perkins. 2023. "Road Condition Monitoring Using Vehicle Built-in Cameras and GPS Sensors: A Deep Learning Approach." *Vehicles* 5 (3): 931–48. https://doi.org/10.3390/vehicles5030051.

Shafian, Sultan Al, and Da Hu. 2024. "Integrating Machine Learning and Remote Sensing in Disaster Management: A Decadal Review of Post-Disaster Building Damage Assessment." *Buildings*. Multidisciplinary Digital Publishing Institute (MDPI). https://doi.org/10.3390/buildings14082344.

Shafique, Ayesha, Guo Cao, Zia Khan, Muhammad Asad, and Muhammad Aslam. 2022. "Deep Learning-Based Change Detection in Remote Sensing Images: A Review." *Remote Sensing*. MDPI. https://doi.org/10.3390/rs14040871.

Sijia Hu. 2022. "Convolutional Neural Network Combined with Transfer Learning for Damage Assessment with Satellite Imagery." *CAIBDA 2022; 2nd International Conference on Artificial Intelligence, Big Data and Algorithms*, April, 1–7.

Singh, Prasoon, Vinay Shankar Prasad Sinha, Ayushi Vijhani, and Neha Pahuja. 2018. "Vulnerability Assessment of Urban Road Network from Urban Flood." *International Journal of Disaster Risk Reduction* 28:237–50. https://doi.org/https://doi.org/10.1016/j.ijdrr.2018.03.017.

Sodders, Nicole, Kimberly Stockdale, Kayla Baker, Arielle Ghanem, Benjamin Vieth, and Terri Harder. 2023. "Morbidity and Mortality Weekly Report Notes from the Field Vibriosis Cases Associated with Flood Waters During and After Hurricane Ian-Florida, September-October 2022" 72 (18). https://www.

Spekkers, M. H., M. Kok, F. H.L.R. Clemens, and J. A.E. Ten Veldhuis. 2014. "Decision-Tree Analysis of Factors Influencing Rainfall-Related Building Structure and Content Damage." *Natural Hazards and Earth System Sciences* 14 (9): 2531–47. https://doi.org/10.5194/nhess-14-2531-2014.

Tavus, Beste, Sultan Kocaman, and Candan Gokceoglu. 2022. "Flood Damage Assessment with Sentinel-1 and Sentinel-2 Data after Sardoba Dam Break with GLCM Features and Random Forest Method." *Science of the Total Environment* 816 (April). https://doi.org/10.1016/j.scitotenv.2021.151585.

Tsang, S. H. 2018. "Review: Yolov3—You Only Look Once (Object Detection). Https://Towardsdatascience.Com/ Review-Yolov3-You-Only-Look-Once-Object-Detection-Eab75d. Accessed June 25, 2023."

"United States Census Bureau." 2022. 2022. https://data.census.gov/profile/Taylor_County,_Florida?g=050XX00US12123.

Vetrivel, A, N Kerle, M Gerke, F Nex, and G Vosselman. 2016. "Towards Automated Satellite Image Segmentation and Classification for Assessing Disaster Damage Using Data-Specific Features with Incremental Learning." In *GEOBIA*. https://doi.org/10.3990/2.369.

Wang, Yandong, Shisi Ruan, Teng Wang, and Mengling Qiao. 2019. "Rapid Estimation of an Earthquake Impact Area Using a Spatial Logistic Growth Model Based on Social Media Data." *International Journal of Digital Earth* 12 (11): 1265–84. https://doi.org/10.1080/17538947.2018.1497100.

Westen, C. J. Van. 2013. "Remote Sensing and GIS for Natural Hazards Assessment and Disaster Risk Management." In *Treatise on Geomorphology: Volume 1-14*, 1–14:259–98. Elsevier. https://doi.org/10.1016/B978-0-12-374739-6.00051-8.

Yang, Liping, and Guido Cervone. 2019. "Analysis of Remote Sensing Imagery for Disaster Assessment Using Deep Learning: A Case Study of Flooding Event." *Soft Computing* 23 (24): 13393–408. https://doi.org/10.1007/s00500-019-03878-8.

Yuan, Faxi, William Mobley, Hamed Farahmand, and Yuanchang Xu. n.d. "Predicting Road Flooding Risk with Machine Learning Approaches Using Crowdsourced Reports and Fine-Grained Traffic Data." https://doi.org/10.48550/arXiv.2108.13265.

Zapico, J. L., M. P. González, and K. Worden. 2003. "Damage Assessment Using Neural Networks." *Mechanical Systems and Signal Processing* 17 (1): 119–25. https://doi.org/10.1006/mssp.2002.1547.

Zhang, Mingliang, Menghua Xu, Zhaoli Wang, and Chengguang Lai. 2021. “Assessment of the Vulnerability of Road Networks to Urban Waterlogging Based on a Coupled Hydrodynamic Model.” *Journal of Hydrology* 603:127105. https://doi.org/https://doi.org/10.1016/j.jhydrol.2021.127105.

Zhong, Hao, and Daan Liang. 2024. “A Study of Road Closure Due to Rainfall and Flood Zone Based on Logistic Regression.” *International Journal of Disaster Risk Reduction* 102:104291. https://doi.org/https://doi.org/10.1016/j.ijdrr.2024.104291.

Zhu, Yi Jie, Yujie Hu, and Jennifer M. Collins. 2020. “Estimating Road Network Accessibility during a Hurricane Evacuation: A Case Study of Hurricane Irma in Florida.” *Transportation Research Part D: Transport and Environment* 83 (June). https://doi.org/10.1016/j.trd.2020.102334.

Chapter 3 Developing A Machine Learning-Based Framework for Roadway Vulnerability and Impact Assessment Using Aerial Imagery

3.1 Introduction

Recent advancements in remote sensing technologies, especially the use of high-resolution aerial imagery, have opened new avenues for change detection and accurately detecting roadway disruptions in hurricane-prone areas(Shafique et al. 2022). The integration of aerial imagery with machine learning models offers a more comprehensive approach to roadway vulnerability assessments. The increasing frequency and intensity of hurricanes have posed significant challenges to transportation infrastructure, particularly in hurricane-prone areas such as the Gulf Coast of the U.S. Roadways, bridges, and other critical infrastructure are often severely impacted by these extreme weather events, leading to significant economic losses, disruption of essential services, and compromised public safety (Mukherjee et al. 2023a). The ability to assess roadway vulnerability and the impact of hurricanes is crucial for effective disaster preparedness, emergency response, and long-term infrastructure resilience planning (Loggins and Wallace 2015). However, traditional methods for evaluating roadway network vulnerability and damage assessment have often been static, relying on historical data and manual inspections, which can be time-consuming, resource-intensive, and less effective in real-time applications (Vetrivel et al. 2016). The advent of machine learning (ML) and remote sensing technologies offers new possibilities for dynamic, data-driven assessments of roadway conditions in the aftermath of a disaster, enabling more responsive and informed decision-making processes.

Remote sensing technologies, such as high-resolution aerial imagery and satellite data, provide a comprehensive view of the affected areas, enabling the detection and classification of damage to transportation networks(Dutta Roy et al., 2024). These technologies offer the advantage of capturing large-scale geospatial information that can be processed and analyzed using machine learning algorithms(Al Shafian and Hu 2024). This integration of remote sensing and machine learning allows for more accurate detection of roadway disruptions and the identification of vulnerable infrastructure, leading to more informed decision-making in disaster response and recovery efforts(Yang and Cervone 2019).

In recent studies, the use of aerial imagery and remote sensing techniques has proven effective in monitoring and assessing the impacts of hurricanes on transportation infrastructure(Hauptman, Mitsova, and Briggs 2024) For instance, imagery collected before and after hurricanes can be used to evaluate changes in road conditions, enabling the development of indices that measure the severity of roadway closures and the consistency of these closures across multiple events. This study introduces two such indices, the Road Closure Impact Index (RCII) and Roadway Vulnerability Index (RVI), which were developed as part of this research to offer a structured, quantitative approach to assessing the effects of natural disasters on critical infrastructure. By building on the growing body of literature that leverages remote sensing and machine learning for

disaster impact assessments, these indices contribute novel methodologies for quantifying roadway disruptions in hurricane-prone areas.

3.1.1 Challenges in Assessing Roadway Vulnerability and Impact

The vulnerability of roadway networks to hurricanes is a multi-dimensional problem that involves understanding both the physical characteristics of the roadways and the nature of the hurricanes themselves. Roadway vulnerability is influenced by several factors, including the geographic location of the roadway, its elevation, the quality of construction materials, and the level of maintenance (Hassan et al. 2022). Moreover, the impact of hurricanes on roadways can vary significantly based on wind speeds, storm surge levels, and rainfall intensity, leading to various types of damage such as flooding, debris accumulation, and structural failures (Nguyen et al. 2022). Traditional methods for assessing the vulnerability of roadway networks often rely on static models that use historical hurricane data and empirical damage functions to predict future risks. While these models provide a foundational understanding, they lack the ability to capture the dynamic and evolving nature of hurricane impacts, making them less effective for real-time applications (Mathias et al. 2018).

The immediate impact of hurricanes on roadways can be assessed through roadway closure data, which helps determine the accessibility of critical routes during and after a disaster. However, existing studies have primarily focused on post-event assessments and have not adequately captured the temporal dynamics of roadway closures, such as how quickly a roadway is restored or how frequently it experiences closures over time (Zhu, Hu, and Collins 2020). Furthermore, these studies often do not provide a comprehensive measure of roadway vulnerability that considers both the immediate impact and the consistency of roadway closures over multiple hurricane events. This gap highlights the need for a more integrated and dynamic framework that can assess both the impact and vulnerability of roadway networks in real time.

3.1.2 Role of Machine Learning in Disaster Management

Machine learning (ML) has emerged as a powerful tool in disaster management, offering new opportunities for predictive modeling, real-time monitoring, and automated decision support (Goodfellow, Bengio, and Courville 2017). In the context of roadway vulnerability and impact assessment, ML techniques can be used to analyze vast amounts of data from various sources, such as satellite imagery, aerial photography, weather forecasts, and traffic sensors, to detect patterns and predict potential roadway closures (Linardos et al. 2022). For example, convolutional neural networks (CNNs) have been widely used for image classification tasks, enabling the automatic detection of damaged or obstructed roads from aerial images (Buslaev et al. 2018). These models can classify roadway segments into several roadway conditions, providing a more granular understanding of road conditions and facilitating quicker response times for emergency services (Mustakim 2023).

Integrating machine learning with remote sensing data allows for a more dynamic assessment of roadway network vulnerabilities. Unlike traditional models, which often rely on pre-defined rules and thresholds, machine learning models can dynamically learn from data to improve their

accuracy over time in detecting roadway disruptions and classifying roadway conditions. In this study, machine learning models are trained to recognize patterns in aerial imagery that correspond to different roadway conditions such as open, partially closed, and fully closed, following a hurricane. This approach allows for more precise and adaptable assessments of road closures, enhancing the accuracy of impact metrics like the Road Closure Impact Index (RCII) and Roadway Vulnerability Index (RVI) over time. This capability is particularly useful in hurricane-prone areas, where the characteristics of each storm can differ significantly, and the impact on roadway networks can vary widely based on local conditions (Ferguson et al. 2023). Additionally, ML models can be retrained and fine-tuned as new data becomes available, providing a continuously evolving understanding of roadway vulnerabilities and enabling more adaptive infrastructure planning and disaster response strategies (Linardos et al. 2022).

3.1.3 Research Objectives and Framework Development

This study aims to develop a comprehensive framework for assessing roadway vulnerability and impact in hurricane-prone areas using machine learning-based detection models. The framework focuses on two primary, newly developed indices: the Road Closure Impact Index (RCII) and the Roadway Vulnerability Index (RVI). The RCII, created specifically for this study, measures the immediate impact of hurricanes on roadway closures by analyzing bounding boxes detected from aerial images. The RVI, also introduced in this research, assesses the consistency of roadway closure patterns across multiple hurricane events. Together, these indices provide a structured approach to quantify and compare the effects of hurricanes on transportation infrastructure, offering new insights into roadway vulnerability in disaster-prone areas. By integrating these indices, the proposed framework provides a more holistic understanding of roadway network vulnerabilities, accounting for both short-term impacts and long-term resilience. The case study area for this research is Taylor County, FL, a region significantly affected by Hurricanes Idalia and Debby. Using aerial images and a machine learning-based detection model, this study classifies road segments into three categories such as open, partially closed, and fully closed during both hurricanes.

The proposed framework contributes to the existing body of knowledge by integrating machine learning with remote sensing data to create dynamic, data-driven assessments of roadway vulnerabilities. It addresses the limitations of traditional models by providing real-time assessments and enabling more adaptive disaster preparedness and response strategies. Moreover, the development of RCII and RVI offers a novel approach to quantifying roadway network vulnerabilities, facilitating targeted investments in infrastructure resilience and enhancing community safety in hurricane-prone areas.

3.2 Literature Review

Roadway vulnerability and damage assessment in the context of natural disasters, especially hurricanes, has gained significant attention in recent years due to the increasing frequency and intensity of these events. As transportation networks are critical for evacuation, emergency response, and recovery, assessing their resilience and the impact of disruptions is crucial for

disaster preparedness and mitigation efforts. Various methodologies have been employed to study roadway networks post-hurricane, including remote sensing, machine learning, and vulnerability analysis, each contributing valuable insights into the effects of extreme weather on infrastructure. This literature review examines key approaches and frameworks that have been applied to detect roadway damage, assess roadway vulnerability, and develop indices for comparing hurricane impacts across affected regions.

3.2.1 Roadway Vulnerability and Risk Assessment in Hurricane-Prone Areas

Roadway vulnerability in regions prone to hurricanes has become an essential research focus for transportation and disaster resilience planning. Hurricanes frequently cause significant damage to transportation infrastructure, particularly roadway networks, due to high winds, flooding, and storm surges. Vulnerability assessments typically consider a range of factors such as geographic location, road quality, and storm intensity. According to (Zhang et al. 2021), factors such as proximity to water bodies, road condition, and drainage systems play critical roles in the vulnerability of transportation routes during hurricanes.

Several frameworks have been developed to quantify roadway vulnerability, often using multi-criteria decision-making approaches. Traditional static models, which assess pre-disaster conditions, can be improved through the integration of dynamic real-time data such as traffic flows, weather conditions, and rainfall (Jena, Pradhan, and Beydoun 2020; Pouryari, Ardakani, and Hassani 2021). As hurricanes can have varying impacts depending on local infrastructure and geographical features, region-specific vulnerability assessments are crucial. An example is a vulnerability index for coastal transportation networks, integrating factors such as infrastructure age, traffic volume, and proximity to flood-prone areas (Q.-C. Lu and Peng 2011). These assessments have proven valuable for guiding emergency response strategies and long-term resilience planning, especially in hurricane-prone areas like Taylor County, Florida, where infrastructure is vulnerable to both wind and water damage.

3.2.2 Impact of Hurricanes on Transportation Infrastructure: Road Closure and Damage Patterns

The impact of hurricanes on transportation infrastructure is well-documented, with roadway closures being one of the most immediate and disruptive effects. Hurricanes often cause roadways to close due to flooding, landslides, wind damage, and debris. It is observed that in many cases, roadway closures persist long after the hurricane has passed due to the time required for debris removal, water drainage, and infrastructure repair(Mukherjee et al. 2023b). The long-term closure of critical roadways can have profound economic and social consequences, particularly in rural areas like Taylor County, where transportation networks are less robust, and recovery efforts may be slower.

Research into the damage patterns of hurricanes highlights the importance of drainage and infrastructure quality in determining road network resilience. According to (Mostafavi et al. 2022), Hurricane Harvey caused widespread roadway closures due to flooding, especially in areas with inadequate drainage systems. Similarly, in the aftermath of Hurricane Katrina, poorly maintained roadways with insufficient drainage were among the most severely impacted. Studies show that hurricanes disproportionately affect low-income regions with older infrastructure, underscoring the need for targeted interventions in vulnerable areas (Mitsova et al. 2019). By comparing the impacts of Hurricanes Idalia and Debby, this research aims to deepen our understanding of how different storm characteristics contribute to varying levels of roadway disruptions.

3.2.3 Machine Learning Techniques for Roadway Damage Detection and Classification

In recent years, machine learning (ML) has emerged as a powerful tool for detecting and classifying roadway damage in the aftermath of hurricanes and other natural disasters. Machine learning models, such as Convolutional Neural Networks (CNNs), Random Forests, and Support Vector Machines (SVMs), have been successfully applied to the analysis of aerial and satellite imagery to detect roadway conditions. (Ruseruka et al. 2023) demonstrated the effectiveness of CNNs in classifying and detecting roadway conditions such as pavement damages by processing aerial images with built in camera in real time. The speed and accuracy of these models have proven invaluable in real-time disaster response scenarios, enabling rapid decision-making.

Machine learning offers several advantages over traditional assessment techniques, which rely heavily on manual inspections. (Goodfellow, Bengio, and Courville 2017) argue that the use of supervised learning techniques in disaster management allows for the development of predictive models based on historical data, improving both the speed and accuracy of post-hurricane damage assessments. Additional research by (Yuan et al., n.d.) shows how Random Forest models can be trained on pre-disaster data to predict which road segments are most likely to flood and close during a hurricane. Also, another study shows how machine learning and remote sensing can be integrated to assess building damage after natural disasters. This predictive capability is particularly valuable in regions like Taylor County, where rapid and accurate roadway assessments are critical to coordinating evacuation and recovery efforts.

3.2.4 Remote Sensing and GIS Applications in Post-Hurricane Infrastructure Monitoring

Remote sensing technologies, such as satellite imagery, LiDAR, and aerial photography, have become key tools for monitoring infrastructure, particularly roadway networks, following extreme events like hurricanes. Remote sensing allows for the rapid acquisition of high-resolution data over large geographic areas, making it ideal for real-time roadway condition assessments. (Ma et al. 2013; Karaer et al. 2022) highlights the effectiveness of remote sensing in detecting road damage caused by hurricanes, especially in regions prone to flooding and landslides. The ability to integrate real-time remote sensing data with Geographic Information Systems (GIS) allows for the

spatial visualization of damage, helping decision-makers prioritize roadway repairs and manage recovery efforts.

GIS plays a critical role in visualizing the spatial distribution of roadway damage and providing a comprehensive view of the hurricane's impact on transportation infrastructure. (Robinson 2020) discusses how GIS can be combined with pre-disaster and post-disaster imagery to map areas of damage, aiding in the identification of vulnerable roadway segments. Furthermore, (Van Westen 2013; Cristian 2024) demonstrated the use of GIS in post-hurricane recovery planning, highlighting its ability to overlay multiple data sources, including real-time traffic information and roadway damage assessments. The integration of GIS and remote sensing has been instrumental in disaster response efforts, allowing for a more efficient allocation of resources and quicker recovery times for affected roadways.

3.2.5 Development and Application of Vulnerability and Impact Indices for Roadway Networks

Developing vulnerability and impact indices for roadway networks is critical for quantifying the extent of damage caused by hurricanes and other disasters. A study by (Singh et al. 2018) examines the growing impact of floods on transportation networks, particularly in urban areas of India where heavy precipitation led to severe disruption. The study proposes an integrated framework that combines meteorological data, land use information, and hydrodynamic models to assess roadway network vulnerability. The framework develops critical maps and indices, showing percentage of the roadway network may become impassable during severe floods, highlighting the need for proactive measures to maintain transportation resilience in flood-prone areas. This index helps prioritize road repairs and allocate resources efficiently in post-disaster scenarios.

(Zhong and Liang 2024) explores the relationship between rainfall intensity and roadway closures, employing logistic regression analysis based on data from TxDOT and Harris County Flood Warning System (HCFWS). The study examined different flood zones, including FEMA-identified areas and regions affected during Hurricane Harvey. Their analysis highlights that rainfall intensity over a four-day window significantly influences road closure probability, especially when drainage systems are compromised. This methodology identifies critical routes to infrastructure, emphasizing its practical application in managing access to essential services during extreme weather events. (Drejza et al. 2019) provides a comprehensive framework for assessing the vulnerability of coastal roadway networks to erosion and flooding hazards. The study integrates parameters like roadway exposure, network characteristics, and adaptation measures, offering a scoring system that identifies critical infrastructure requiring immediate intervention.

Based on the reviewed literature, a significant research gap exists in quantifying and consistently assessing the impacts of weather and climate related events on transportation infrastructure. Given the complexity and variability of these events, there is a need for systematic, data-driven frameworks that can measure both the immediate severity and the recurring vulnerability of

roadway networks under extreme weather conditions. This study addresses this gap by proposing a comprehensive framework aimed at improving disaster preparedness and infrastructure resilience in hurricane-prone areas. RCII and RVI provide standardized measures to assess the extent of roadway vulnerability and impact based on historical data, disaster patterns, and flood zones. RCII quantifies the severity of roadway closures by considering frequency and duration, helping prioritize roadway maintenance and emergency response. Meanwhile, RVI assesses the overall risk levels of specific roadway segments, combining factors like flood-prone locations to identify critical vulnerabilities proactively. By combining the RCII and RVI with real-time data from machine learning models, it is possible to develop a comprehensive framework for assessing roadway network vulnerabilities and improving disaster preparedness in hurricane-prone regions like Taylor County in Florida.

3.3 Study Area and Data

3.3.1 Study Area: Hurricanes Idalia, Debby, and Taylor County, Florida

Taylor County is located in the Big Bend region along Florida's Gulf Coast, a predominantly rural area with a population of approximately 21,000 residents and known for its exposure to hurricanes and other tropical storms due to its proximity to the Gulf of Mexico. Approximately 20.4% of the population in Taylor County is 65 years or older. Given the county's total population of around 21,796 (as of 2020), this translates to about 4,450 older adults("United States Census Bureau" 2022). The county is characterized by a mixture of coastal lowlands, dense forest areas, which play a significant role in shaping the region's vulnerability to hurricanes and tropical storms. It lies in the path of many tropical systems that develop in the Gulf of Mexico, making it particularly susceptible to storm surges, high winds, and flooding. With a land area of approximately 1,232 square miles, Taylor County's roadway network is predominantly made up of state highways, local roadways, and evacuation routes. The most critical transportation routes include U.S. Route 98, which runs along the coast, and U.S. Route 221, which connects the inland regions of the county.

Historically, Taylor County has experienced significant hurricane activity. The combination of wind, rain, and storm surges during these hurricanes often leads to roadway closures and damage, especially in low-lying areas prone to flooding. The county's vulnerability to hurricanes makes it a suitable case study for analyzing roadway vulnerability and damage patterns using machine learning and high-resolution imagery. For instance, the region has been exposed to both major and minor hurricanes, most recently Hurricanes Idalia and Debby, which caused widespread damage to infrastructure, particularly to the roadway network.

In this study, the focus is on assessing the impact of these wo major hurricanes, which both made landfall near and directly impacted Taylor County. The aim is to compare their respective effects on the transportation infrastructure, particularly the roadway network, to understand how different storm characteristics result in varying levels of damage and accessibility issues. These comparisons are vital for improving resilience strategies and emergency response mechanisms in the region.

Hurricane Idalia, which made landfall in the late summer of 2023, was a powerful Category 3 hurricane that brought destructive winds, storm surges, and torrential rainfall to Taylor County. Idalia's impacts were felt across the county, with widespread power outages, downed trees, and significant roadway closures. The storm surge caused flooding in low-lying coastal areas, resulting in roadway washouts and debris accumulation on major and minor transportation routes. This hurricane serves as a recent example of the challenges Taylor County faces due to its geographic vulnerability and underlines the need for accurate damage detection and resilient infrastructure planning.

Hurricane Debby, on the other hand, made landfall in August 2024 as a strong Category 1 hurricane, bringing intense winds, torrential rainfall, and coastal flooding to Taylor County. Though not as powerful as Hurricane Idalia in terms of wind speed, Debby's extended duration and heavy rainfall resulted in significant inland flooding and roadway closures. The slow-moving nature of the storm, combined with its passage over the Apalachee Bay, contributed to severe impacts across the Big Bend region, including Taylor County. Debby brought significant flooding and storm surges between 3 to 5 feet above normal in areas already recovering from Hurricane Idalia, which hit the area less than a year prior.

Debby's impact on the roadway network was severe, with many roadways submerged or blocked by debris. Floodwater inundated both major and minor routes, restricting access for emergency responders and disrupting transportation for days after the storm. Taylor County's infrastructure that was already under pressure, following the impacts of Hurricane Idalia in 2023, faced further strain due to back-to-back flooding and storm surge events. The slow-moving nature of the storm contributed to higher rainfall accumulation in coastal communities, underscoring the need for improved flood mitigation and drainage infrastructure in Taylor County.

In this study, we focus on the coastal region of Taylor County as seen in Figure 3.1. Figure 3.2, on the other hand, shows some examples of damage to the roadway infrastructure caused by the hurricanes.

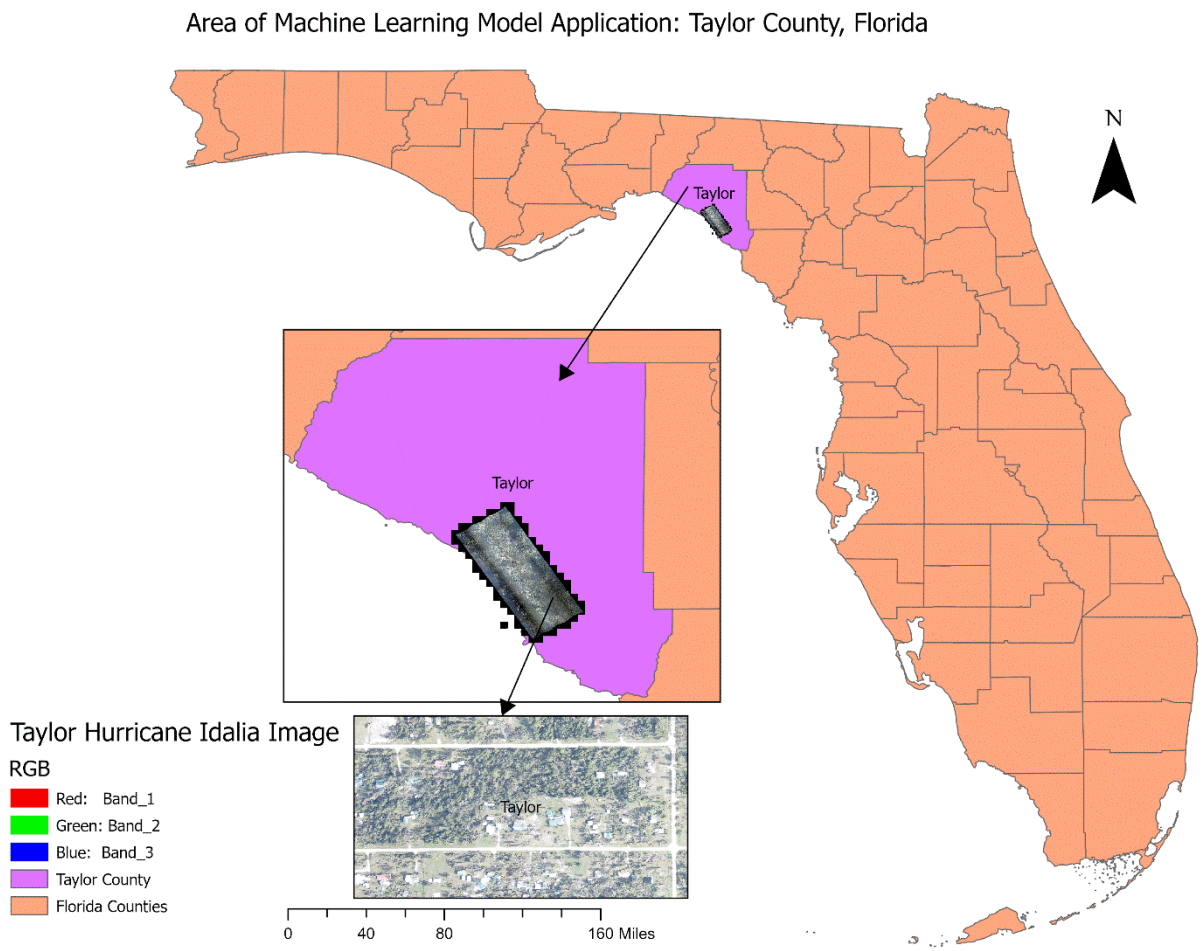

Figure 3:1 Area of Machine Learning Model Application in Taylor County, Florida

Figure 3:2 Images of Damage Caused by Hurricanes Idalia and Debby on Roadway Infrastructure ("Https://Www.Tampafp.Com/Hurricane-Debby-Leaves-Severe-Damage-in-Florida-Sen-Rubio-and-Rep-Cammack-Urge-Full-Federal-Assistance/#google_vignette" 2024)

3.3.2 Data Collection

3.3.2.1 Aerial Imagery

The primary data source for this study consists of high-resolution post-hurricane aerial imagery. The aerial images were obtained from the National Hurricane Center (NHC), a reliable and authoritative source of post-disaster imagery. These images provide crucial information about the state of the roadway network after the landfall of Hurricanes Idalia and Debby (Figure 3.3). The imagery used for this research captures Taylor County's roadway conditions following both hurricanes, providing a basis for damage detection and classification. The resolution of the imagery is sufficient to detect subtle changes in roadway conditions, including minor damage, debris, and flood-affected areas.

Figure 3:3 Sample of Aerial Imagery from Hurricane Idalia (National Oceanic and Atmospheric Administration 2023)

3.3.2.2 Roadway Shapefiles

The shapefiles for Taylor County's roadway network were acquired from the Florida Department of Transportation (FDOT) database. These shapefiles offer comprehensive spatial information about the roadways, including the classification of roadways (e.g., highways, local roadways), road widths, and connectivity to evacuation routes. This data is critical for overlaying the detected roadway damages with actual roadway infrastructure. The shapefiles allow for the mapping and quantification of roadway closures and damage patterns, as well as their integration into the machine learning model used for classification.

3.3.2.3 Evacuation Routes

In addition to the general roadway network data, evacuation route information was obtained from FDOT's emergency management and transportation databases. These routes are vital for understanding which roadways are most critical during hurricane evacuations and how they are impacted by roadway closures and damage. Taylor County's evacuation routes are typically coastal or lead inland, making them particularly vulnerable to storm surges and flooding during

hurricanes. The data on evacuation routes is integrated with the aerial imagery and roadway shapefiles to prioritize recovery efforts and assess roadway vulnerabilities.

3.4 Methodology

The methodology involved the acquisition of high-resolution aerial imagery collected before and after two hurricane events in Taylor County, FL. The imagery was pre-processed to remove distortions and noise, followed by segmentation to classify road segments into categories such as fully accessible, partially closed, and fully closed. A machine learning model was then trained on these segmented images to detect vulnerable roadways, defined in this study as roads with a high likelihood of closure or restricted access due to severe storm impacts, such as flooding, erosion, or structural damage. This classification captures roads that are either fully or partially closed, providing an indicator of susceptibility to disruption during hurricane events.

The proposed methodology shown in Figure 3.4 involves the following steps:

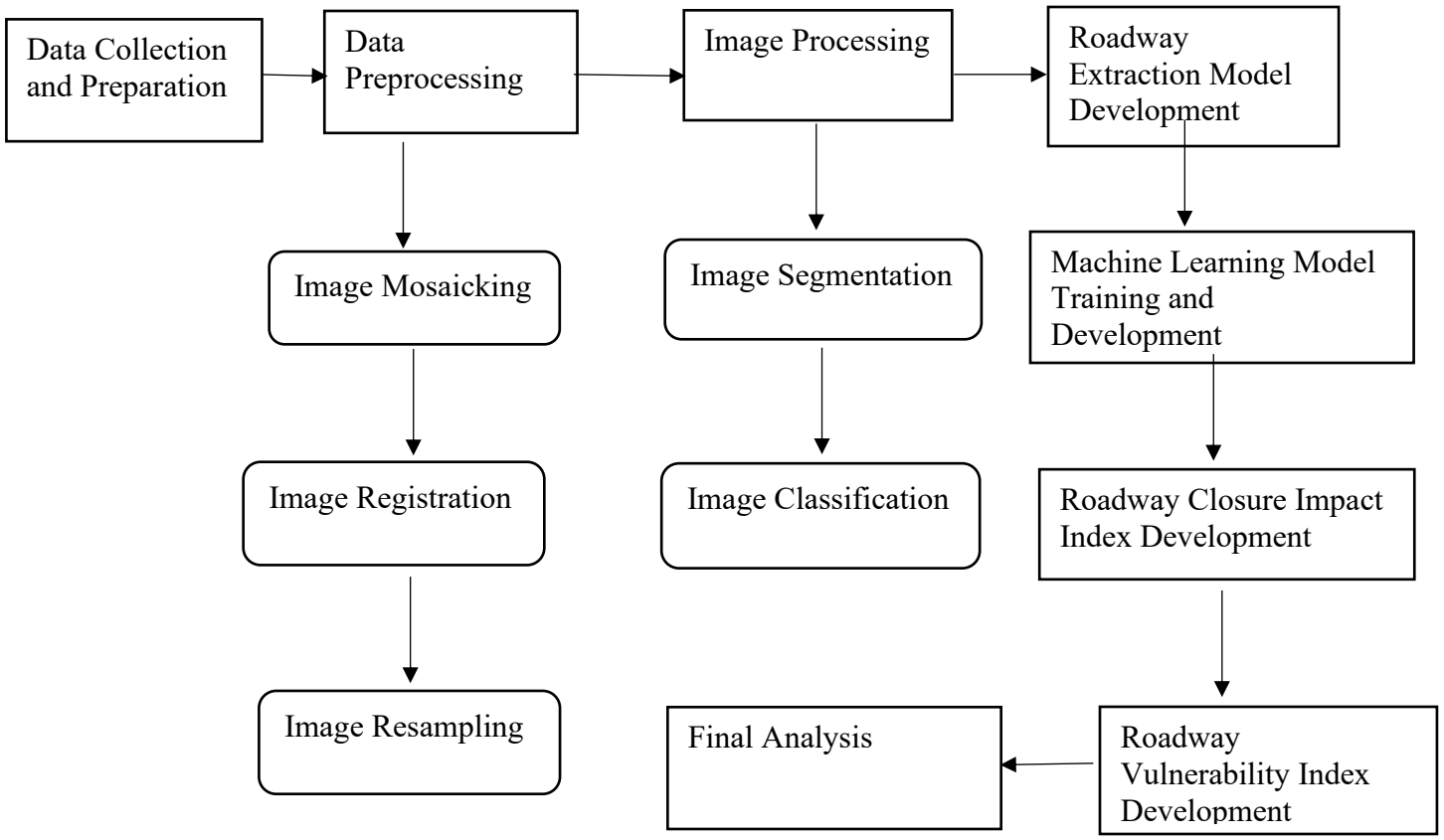

Figure 3:4 Machine Learning-Based Framework for Roadway Vulnerability and Impact Assessment

3.4.1 Data Preprocessing

Before utilizing the aerial imagery for machine learning analysis, several preprocessing steps were necessary to ensure that the data was clean, consistent, and compatible with the models used in this study. The initial step involved image mosaicking, which was essential to create a continuous and comprehensive visual representation of the entire study area. By merging multiple smaller

images into a cohesive mosaic, we ensured that the entire roadway network in Taylor County was included for analysis.

Next, image registration was performed to align the mosaicked images with the roadway shapefiles from FDOT. This step was crucial for ensuring that the imagery matched the spatial coordinates of the roadway network, allowing for accurate overlay and comparison. Georeferencing was also part of this process, enabling precise spatial alignment of the imagery with the coordinate reference system used by the roadway data.

After registration, image resampling was conducted to ensure consistency between images from the two hurricane events. The Hurricane Debby images were resampled to match the pixel resolution of Hurricane Idalia imagery, preserving the spatial extent while standardizing the pixel resolution. In this study, the nearest neighbor method was utilized for the resampling process. This approach allowed for maintaining the integrity of the original pixel values, ensuring that critical features of interest, such as open, partially closed, and fully closed roadways, were accurately detected by the machine learning classification model.

The preprocessed data was then used in conjunction with the roadway shapefiles and evacuation route information to train the machine learning models for roadway damage classification and vulnerability assessment. By combining these datasets, the study aims to provide a comprehensive analysis of roadway network vulnerability and the overall impact of Hurricanes Idalia and Debby on Taylor County's transportation infrastructure.

3.4.2 Image Processing

The preprocessed images underwent image processing techniques to extract relevant features and classify roadway conditions effectively. The first technique employed was image segmentation, which involved partitioning the aerial imagery into smaller segments or regions based on similar characteristics such as color, texture, and intensity. This segmentation process was crucial for isolating roadway areas and distinguishing them from other landscape features such as vegetation, water bodies, and built-up areas. The results of the segmented roadways can be seen in Figure 3.5(b).

Following segmentation, image classification was conducted to categorize the segmented regions into the predefined roadway conditions: open, partially closed, and fully closed. Supervised machine learning models were trained to detect these categories based on the labeled training dataset, which included examples of each roadway condition from both Hurricane Idalia and Hurricane Debby imagery. Advanced classification algorithms were utilized to improve the accuracy and reliability of the detection process, leveraging the spatial and spectral characteristics of the imagery.

By implementing these image processing techniques, the study ensured that critical features of interest were accurately identified and categorized, enabling a robust assessment of roadway damage and vulnerability across the affected regions.

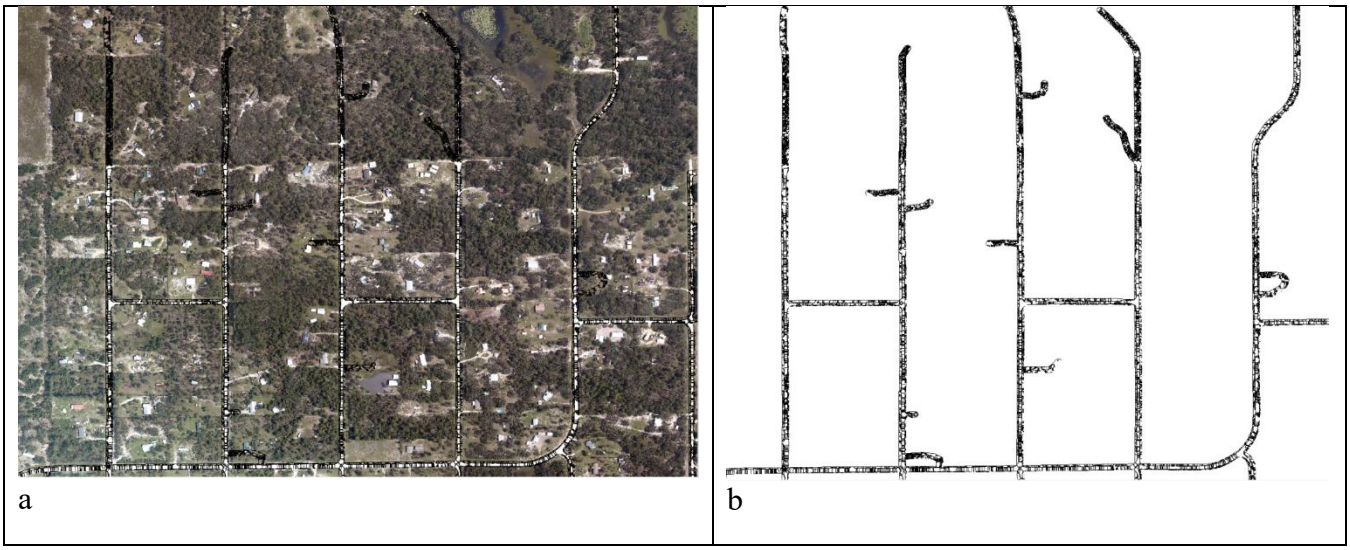

a b

Figure 3:5 (a) Original Hurricane Image, and (b) Segmented Hurricane Image

3.4.3 Roadway Extraction Model

The Multitask Roadway Extraction Model (Lu et al., 2019) is a sophisticated approach designed to enhance the extraction of roadway features from aerial imagery (Figure 3.6). This model integrates multiple tasks during training, allowing it to leverage shared features and improve overall performance. The roadways are then extracted from the entire aerial imagery as shown in Figure 3.8. Below are some key components and functionalities of the model:

i. ***Multilevel Conceptual Characteristics***: The model extracts multilevel conceptual features from the roadway detection network. By convolving these features, the model generates a comprehensive representation of the roadway characteristics. This multilevel approach enhances the model's ability to capture varying scales and complexities of roadway structures, making it effective in diverse environments.

ii. ***ResNet-34 Architecture***: As the backbone of the Multitask Roadway Extraction Model, ResNet-34 leverages skip connections or residual blocks, which facilitate the training of deeper networks by mitigating the vanishing gradient problem. ResNet-34, consisting of 34 layers, is adept at extracting hierarchical features from input images. Its architecture allows it to capture intricate patterns and spatial relationships within the imagery, essential for effective roadway detection (He et al. 2016).

iii. ***Training Strategy***: The model is trained using a multitask learning approach, which optimizes performance across several tasks simultaneously, such as roadway segmentation and centerline extraction. This strategy promotes better feature sharing among tasks, leading to improved accuracy and robustness.

iv. ***Performance Metrics***: Model performance is evaluated using metrics such as Intersection over Union (IoU), precision, recall, and F1 score, which provide a comprehensive assessment of the model's effectiveness in detecting road features. The metrics and loss graph are presented in Figure 3.7 below.

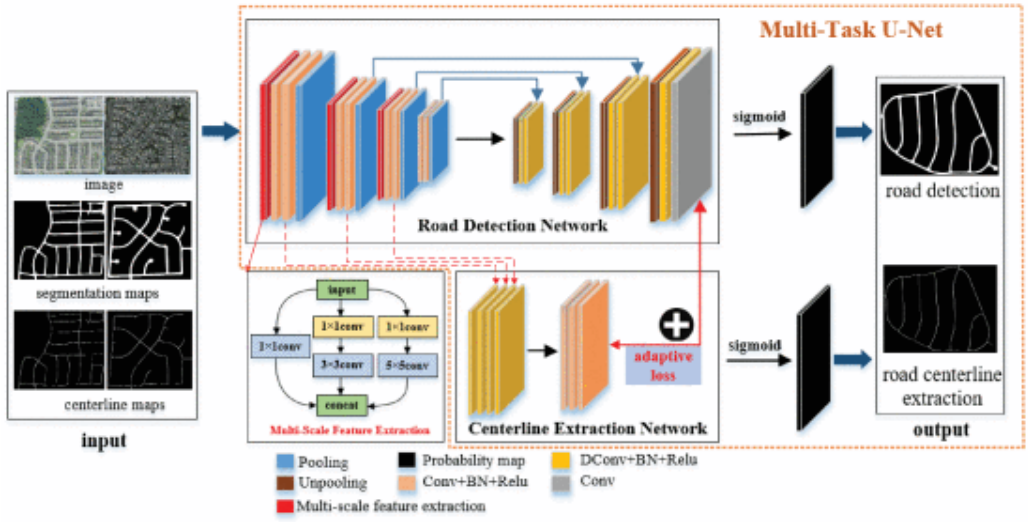

Figure 3:6 Framework of the Multi-Scale and Multi-Task Automatic Roadway Extraction Model (X. Lu et al. 2019)

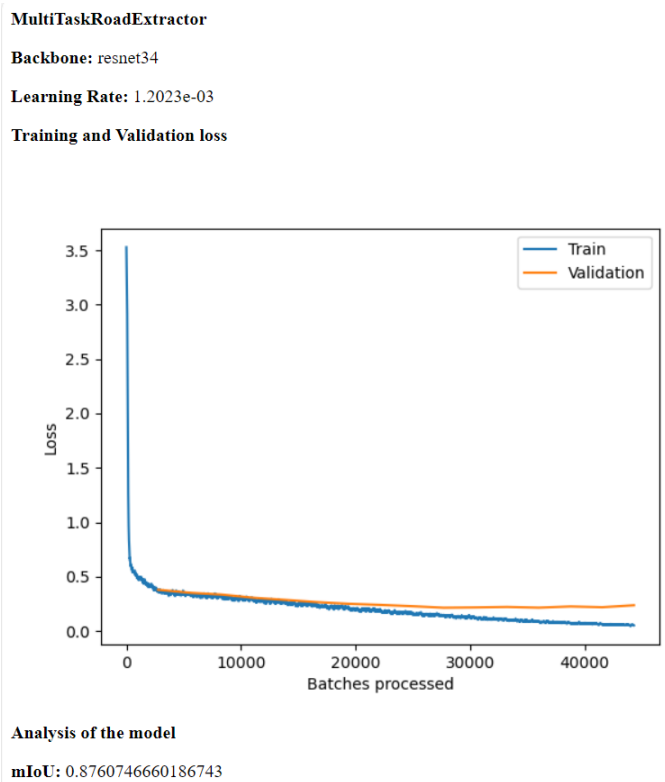

Figure 3:7 Roadway Extractor Model Metrics and Loss Graph

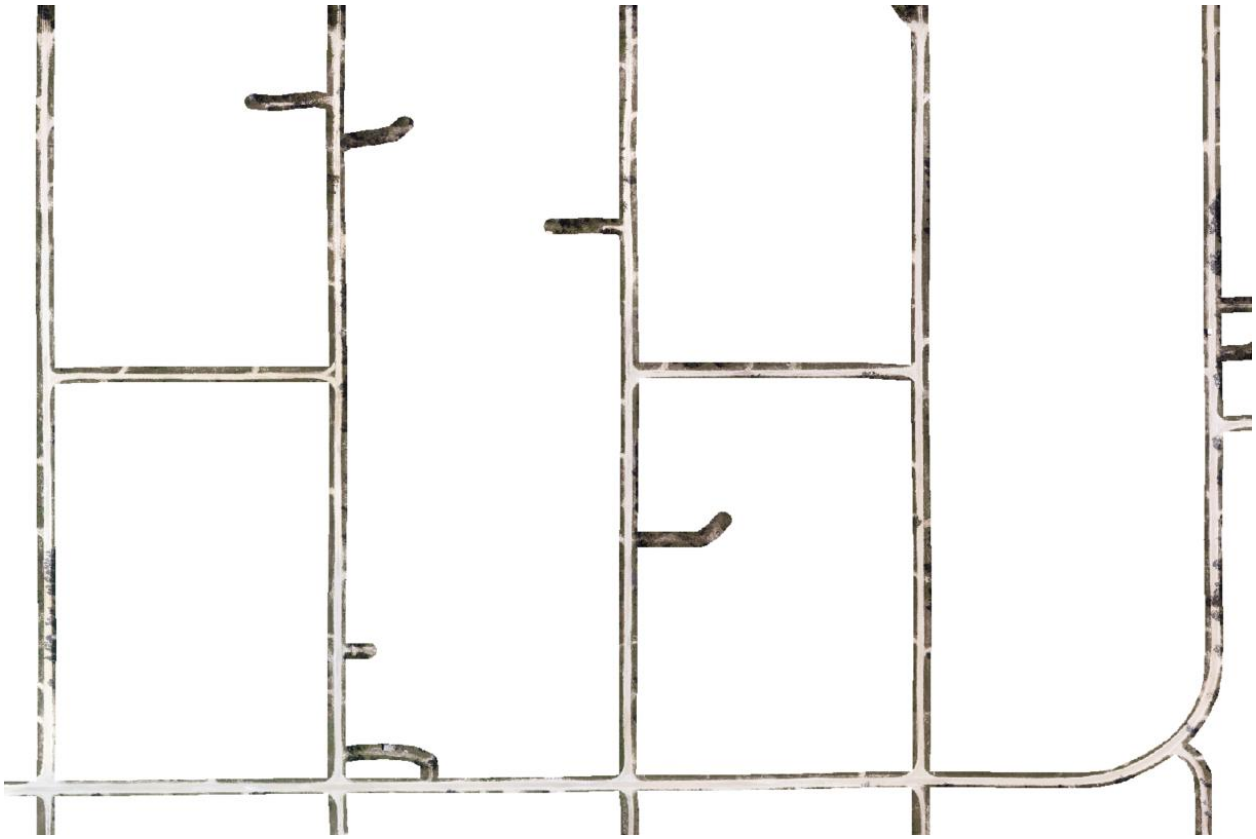

Figure 3:8 Results of the Extracted Roadways

3.4.4 Machine Learning-Based Detection Model

We used a convolutional neural network (CNN) model to classify roadway conditions. The model was trained on labeled data, with features including roadway surface condition, debris presence, and closure extent. The training process involved specific hyperparameters such as Model Architecture: YOLO V3, Learning Rate: 0.001, Number of Epochs: 20, batch size = 4, Image Size: 256x256, Training Split: 80%, Test split: 10%, Validation Split: 100% of the dataset, Non-Max Suppression Threshold: 0.3, Augmentation Techniques: Horizontal and Vertical Flips, Random Rotation.

The model was trained using 600 manually labelled bounding boxes based on the three classes of roadways (i.e., open, partially closed, and fully closed) using the deep learning toolbox in ArcGIS Pro. 40% of the training dataset contained open classes, 30% contained partially closed, and the remaining 30% contained fully closed classes. The partially closed and fully closed data sets were roadway areas that were closed due to a variety of factors such as debris from damages of buildings, trees, and flooding. The learning rate, input image size, number of epochs, batch size, anchor box size and ratios, training and test data percentages are among the configurable parameters and hyperparameters of the object detection model. The validation and training loss graph was used to illustrate the ML model evaluation metrics. Using a suitable loss function, the YOLO v3 model was trained on the provided dataset. On the validation set, which comprises 10%

of the input training dataset, the validation loss and mean average precision were calculated. The batch size, learning rate, and training epoch are the object detection parameters that have the most influence on object detection. To get the best results, the model's hyperparameters were adjusted based on how well it performed on the validation set. The performance of the trained model was assessed on the test set to calculate its accuracy, precision, recall, and F1-score in identifying roadway closures. The data preparation processes were iterated, changing the model design, or gathering new data based on the adequacy of the model's performance. This action helped in improving the outcomes.

3.4.4.1 Training Data Preparation

The success of any machine learning model is heavily dependent on the quality of the training data. In this study, the preparation of training data involved the manual labeling of bounding boxes around roadway features in the aerial imagery. This labeling was performed based on predefined classes: open, partially closed, and fully closed roadways. Each bounding box was carefully annotated to ensure accurate representation of the roadway conditions observed in the images. This meticulous process is essential, as the labeled data serves as the foundation for the model's learning, enabling it to discern different roadway states effectively.

3.4.4.2 Model Training Procedure

Once the training dataset was prepared, the next step involved splitting the data into distinct subsets for model training and evaluation. The dataset was divided into three parts: a training set, a validation set, and a test set. Typically, 80% of the data was allocated to the training set to allow the model to learn the underlying patterns, while 10% was reserved for validation to tune hyperparameters and prevent overfitting. The remaining 10% constituted the test set, which was used to evaluate the model's performance on unseen data after the training was complete.

The model was trained using the prepared dataset, employing techniques such as data augmentation to enhance the variety of data input. Data augmentation involved transformations such as rotation, scaling, and flipping, which helped the model generalize better by exposing it to a wider range of scenarios.

3.4.4.3 Yolo v3 Architecture.

One of the fastest object detection methods available is called "You only look once," or YOLO. YOLO acquires universal representations of items and performs noticeably better than top detection techniques like DPM and R-CNN when trained on actual images. When compared to Fast R-CNN, its background errors are reduced by more than half (Redmon et al. 2016). YOLOv2 uses the Darknet-19 classification network to extract features whereas YOLOv3 uses the far more advanced Darknet-53 network (Tsang 2018). Even though it is no longer the most accurate object detection algorithm due to recent developments, it is still a great option when real-time detection is required without sacrificing too much precision. Therefore, it was preferred in this study.

Initially, YOLO v3 was based on Darknet, a network with 53 layers originally trained on ImageNet. To enhance its detection capabilities, an additional 53 convolutional layers were added, resulting

in a total of 106 layers for the YOLO v3 fully convolutional architecture (Kathuria 2019). This extension contributes to the slower performance of YOLO v3 when compared to YOLO v2. In terms of measured floating-point operations per second, Darknet-53 also performs the best (Redmon, J., & Farhadi 2018). This indicates that the network structure makes better use of the GPU, making evaluation more efficient and faster. The loss graph is shown in Figure 3.9.

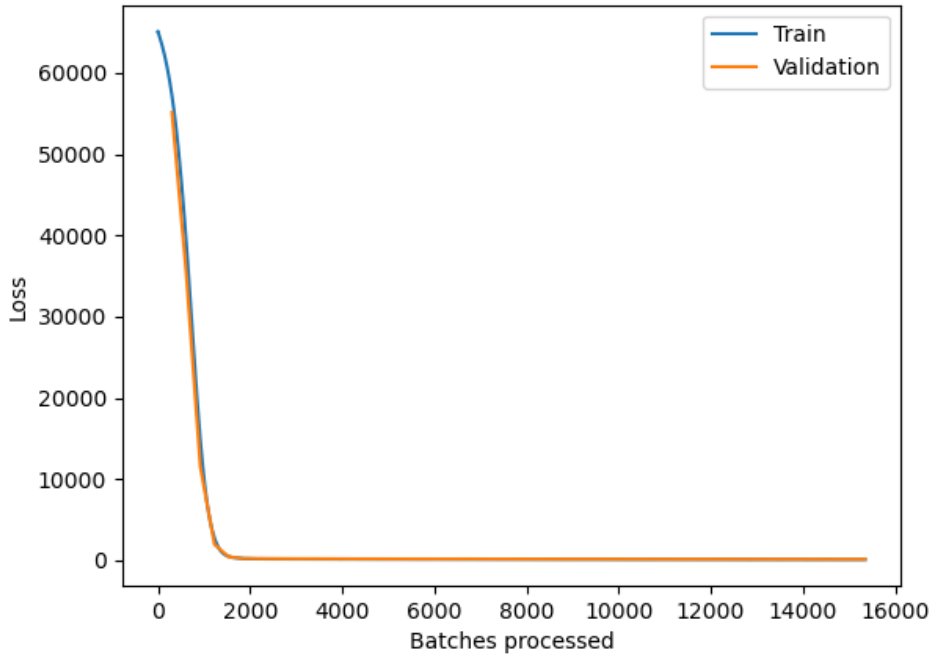

Figure 3:9 Loss Graph for Detection Model

3.4.4.4 Validation

During the training phase, the validation set was used to monitor the model's performance and to make adjustments as necessary. By evaluating the model on the validation set, performance metrics such as loss and accuracy could be observed, allowing for early stopping if the model began overfitting. Hyperparameters, including learning rate and batch size, were tuned based on validation results to optimize model performance.

1. Detection and Classification of Roadways

After the model training and validation phases, the model was deployed for the detection and classification of roads in new aerial images. The trained model processed the test images, generating predictions by identifying and classifying road segments into the three defined classes: open, partially closed, and fully closed. The model utilized techniques such as non-maximum suppression to filter out redundant detections and enhance the quality of the output.

2. Model Performance Evaluation

To assess the model's effectiveness, several performance metrics were employed. Metrics such as Intersection over Union (IoU), precision, recall, and F1 score were calculated to provide a comprehensive evaluation of the model's detection capabilities.

i. Intersection over Union (IoU) measures the overlap between the predicted bounding boxes and the ground truth, indicating the accuracy of the detections.
ii. Precision assesses the proportion of true positive detections among all positive predictions, while recall evaluates the proportion of true positives among actual positive instances.
iii. The F1 score, which combines precision and recall, offers a single metric that captures the model's performance balance, providing a more nuanced view of its effectiveness.

The results from these evaluations guided further refinements of the model, contributing to its overall robustness in detecting and classifying roadway conditions accurately.

3.4.5 Development of Roadway Closure Impact Index (RCII):

The Roadway Closure Impact Index (RCII) is designed to quantify the impact of hurricanes on roadway closures without considering roadway lengths or segments. The RCII is based on the proportion of bounding boxes categorized into three distinct roadway conditions: open, partially closed, and fully closed.

3.4.5.1 Assigning Severity Weights to Each Category

We assign numerical values to represent the severity of impact for each category as follows:

- Open: Weight = 0 (no impact)
- Partially Closed: Weight = 1 (moderate impact)
- Fully Closed: Weight = 2 (high impact)

3.4.5.2 Calculating the Frequency of Bounding Boxes in Each Category

For each hurricane, we count the number of bounding boxes classified in each category:

Let:

- N_{open} be the number of bounding boxes classified as open.
- $N_{partially\_closed}$ be the number of bounding boxes classified as partially closed.
- N_{fully_closed} be the number of bounding boxes classified as fully closed.

3.4.5.3 Calculating the Proportion of Each Category

We determine the proportion of each category relative to the total number of bounding boxes detected:

$$P_{open}=\frac{N_{open}}{N_{total}}$$

$P_{partially\_closed} = \frac{N_{partially\_closed}}{N_{total}}$

$P_{fully\_closed} = \frac{N_{fully\_closed}}{N_{total}}$

where $N_{total} = N_{open} + N_{partially\_closed} + N_{fully\_closed}$

3.4.5.4 Computing the RCII

The RCII can be computed as a weighted sum of the proportions of bounding boxes in each category:

$RCII = (P_{partially\_closed} \times 1) + (P_{fully\_closed} \times 2)$

Since the weight for "Open" is 0, it does not contribute to the index.

3.4.5.5 Normalizing the RCII

To express the RCII on a scale of 0 to 100 for easier interpretation, we multiply it by 100:

$RCII_{normalized} = RCII \times 100$

3.4.5.6 Comparing the RCII for Both Hurricanes

We calculate the RCII for both hurricanes Idalia and Debby using the bounding box data and compare the indices to determine which hurricane had a more severe impact on roadway closures.

3.4.6 Development of Roadway Vulnerability Index (RVI):

The Roadway Vulnerability Index (RVI) quantifies the vulnerability of roads based on their status (open, partially closed, or fully closed) during Hurricanes Idalia and Debby. This index considers the consistency of each roadway's condition across the two events.

3.4.6.1 Assigning Numerical Scores to Closure Categories

We define scores for each closure type to represent their impact level:

- Open (O) = 0 (least vulnerable)
- Partially Closed (PC) = 1 (moderately vulnerable)
- Fully Closed (FC) = 2 (most vulnerable)

3.4.6.2 Determining Roadway Status Consistency Across Hurricanes

For each roadway, we evaluate its status during both hurricanes to compute an average closure score and a consistency factor:

- S_{Idalia} be the closure score for a road during Hurricane Idalia.
- S_{Debby} be the closure score for the same road during Hurricane Debby.

3.4.6.3 Calculating the Average Closure Score (ACS)

The Average Closure Score (ACS) represents the average level of closure for each roadway across both hurricanes:

$$ACS = \frac{S_{Idalia} + S_{Debby}}{2}$$

3.4.6.4 Determining the Consistency Factor (CF)

The CF measures how consistently a roadway is affected by both hurricanes:

$$CF = \begin{cases} 1 & if\ S_{Idalia} = S_{Debby} \\ 0.5 & \text{if } |S_{Idalia} - S_{Debby}| = 1 \\ 0 & \text{if } |S_{Idalia} - S_{Debby}| > 1 \end{cases}$$

3.4.6.5 Computing the Roadway Vulnerability Index (RVI)

The RVI combines both the average closure severity and the consistency of closures:

$$RVI = ACS \times CF$$

The RVI will range from 0 to 2 as shown in Table 1.

Table 3-1 Classification of Roadway Vulnerability Index (RVI) Ranges Based on Hurricane Impact

RVI Range	Vulnerability Level	Interpretation
$0.00 \leq RVI < 0.50$	Low	Minimal to no impact; roadways are resilient.
$0.50 \leq RVI < 1.50$	Moderate	Moderate disruption; may require monitoring.
$1.50 \leq RVI \leq 2.00$	High	Consistent and severe closures; needs prioritization.

Low Vulnerability ($0.00 \leq RVI < 0.50$): Roadways in this range show minimal or no impact from the hurricanes, often being consistently open. These roadways are resilient compared to others and may not require immediate intervention for improvement. Example: Roadways that were open during both hurricanes (RVI = 0.0).

Moderate Vulnerability ($0.50 \leq RVI < 1.50$): Roadways in this range experience some level of disruption, such as a change from open to partially closed or from partially closed to fully closed between the two hurricanes. These roadways indicate moderate vulnerability and may require monitoring and reinforcement to reduce future risk. Example: Roadways that shift between partially and fully closed statuses (RVI = 0.75).

High Vulnerability ($1.50 \leq RVI \leq 2.00$): Roadways in this range are consistently affected by closures, either being fully closed in both hurricanes and/or having severe disruptions. These roadways are highly vulnerable and should be prioritized for maintenance, reinforcement, or redesigning to improve resilience. Example: Roadways that were fully closed during both hurricanes (RVI = 2.0).

The RCII and RVI provide comprehensive metrics for assessing the impact of hurricanes on roadway closures and identifying vulnerable roadways. These indices are valuable for prioritizing roadway maintenance, resilience planning, and resource allocation for future disaster management efforts.

3.5 Results and Discussions

The results indicated that incorporating aerial imagery significantly improved the model's ability to identify damaged roadways and vulnerable road segments. Figure 3.10 shows results of some roadway conditions detected from both hurricanes Idalia and Debby highlighting areas affected by debris. Taylor County's transportation infrastructure, which primarily consists of rural highways and local roadways, is highly susceptible to the effects of hurricanes. Both Hurricane Idalia and Hurricane Debby caused roadway closures, but the nature and extent of the damage varied significantly due to the unique characteristics of each storm. Utilizing the Roadway Closure Impact Index (RCII) and Roadway Vulnerability Index (RVI), this study assesses the varying factors contributing to roadway damage and closures, offering critical insights into the county's response to these natural disasters.

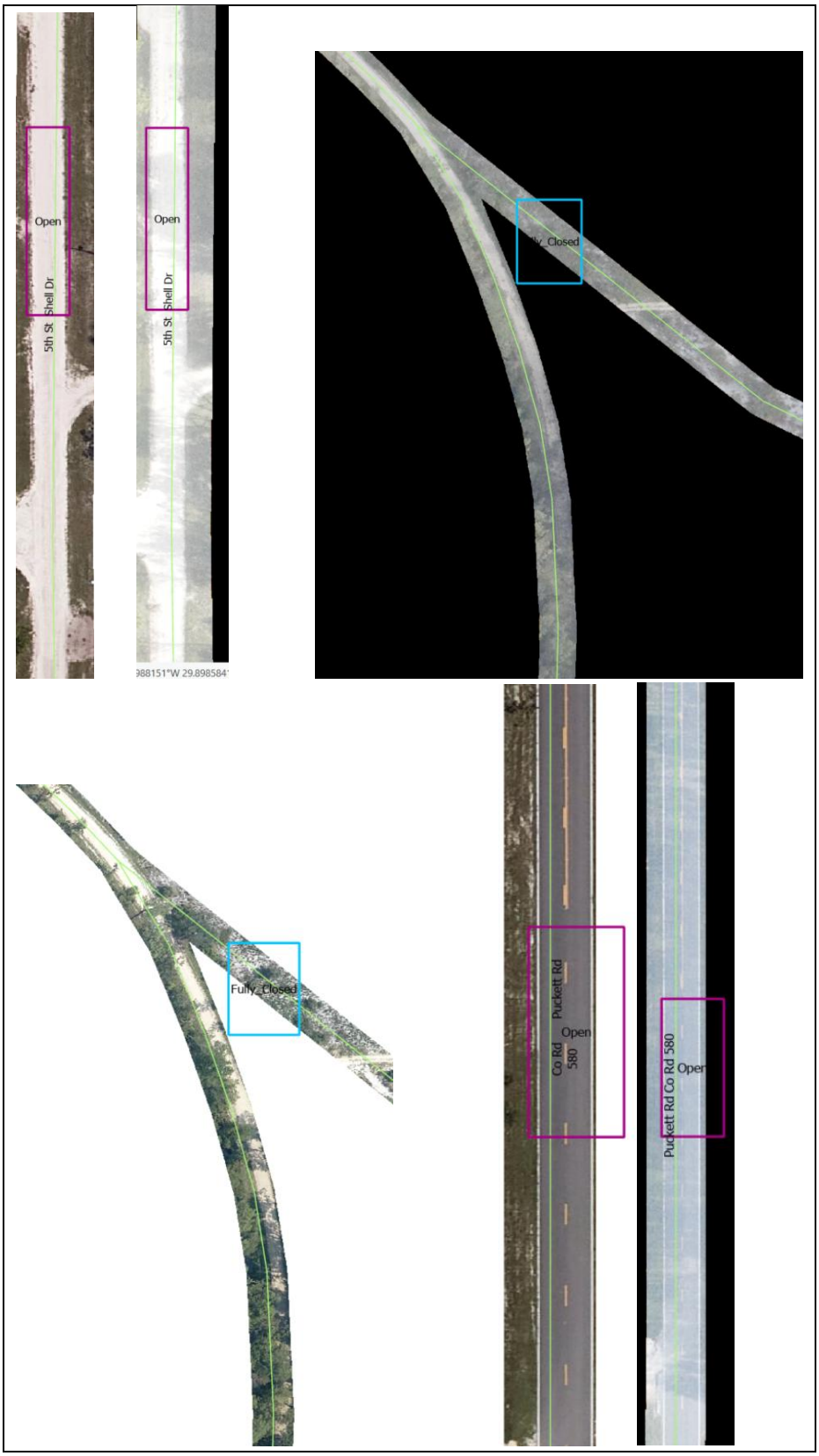

Figure 3:10 Results of Some Roadway Conditions Detected from Both Hurricanes Idalia and Debby

3.5.1 Model Results

In this section, we provide performance evaluations for both hurricanes focusing on detection results given in Table 2, and Table 3. In evaluating the performance of our detection model for categorizing road conditions into "Open," "Partially Closed," and "Fully Closed," three key metrics were utilized: Precision, Recall, and the F1 Score. These metrics provide insights into the accuracy and reliability of the model's predictions and are described in the following subsections.

Table 3-2 Model Performance Evaluations of Hurricane Idalia

Class	Open	Partially Closed	Fully Closed	**Total**
Number of Detections	115	16	38	**169**

	True Positive (TP)	**False Positive (FP)**	**False Negative (FN)**
Open	93	22	
Fully Closed	36	2	7
Partially Closed	15	1	17

	Precision (%)	Recall (%)	F1-Score (%)
Open	81	100	90
Fully Closed	95	84	89
Partially Closed	94	47	63

Table 3-3 Model Performance Evaluations of Hurricane Debby

Class	**Open**	**Partially Closed**	**Fully Closed**	**Total**
Number of Detections	32	12	28	72

	True Positive (TP)	**False Positive (FP)**	**False Negative (FN)**
Open	**27**	**5**	**0**
Fully Closed	**25**	**3**	**6**
Partially Closed	**9**	**3**	**5**

	Precision (%)	**Recall (%)**	**F1-Score (%)**
Open	**84.4**	**100**	**91.6**
Fully Closed	**89.3**	**80.6**	**84.7**
Partially Closed	**75**	**64.3**	**69.2**

3.5.1.1 Precision

Precision (P) measures the accuracy of positive predictions for each class. It indicates the proportion of true positive predictions out of all instances that were predicted as positive (both true positives and false positives). The formula for precision is:

$$P = \frac{TP}{TP+FP}$$

where

TP (True Positives) is the number of instances correctly predicted as positive.

FP (False Positives) is the number of instances incorrectly predicted as positive.

This means that approximately 84.4% of the instances predicted as "Open" were correct.

About 75% of the instances predicted as "Partially Closed" were accurate.

This indicates that roughly 89.3% of the "Fully Closed" predictions were accurate.

Higher precision values indicate that the model has fewer false positives, showing its ability to minimize incorrect predictions.

3.5.1.2 Recall

Recall (R), also known as sensitivity, measures the model's ability to identify all relevant instances of each class. It indicates the proportion of true positive predictions out of all actual instances of the positive class (true positives and false negatives). The formula for recall is:

$$R = \frac{TP}{TP+FN}$$

where

TP (True Positives) is the number of instances correctly predicted as positive.

FN (False Negatives) is the number of instances incorrectly predicted as negative.

A higher recall value indicates that the model effectively detects positive instances, with fewer false negatives. In this case, the "Open" class had a perfect recall, while the other two classes had lower values due to the presence of missed detections.

3.5.1.3 F1 Score

The F1 Score is the harmonic means of precision and recall, providing a balanced measure that considers both false positives and false negatives. It is particularly useful when the class distribution is imbalanced. The formula for F1 Score is:

$$F1 = \frac{2.(P.R)}{P+R}$$

The F1 score shows that the model is generally effective in detecting "Fully Closed" conditions, though some instances were missed.

Overall, the evaluation metrics reveal that the model performs well in identifying "Open" conditions, achieving high precision and perfect recall. However, the performance for "Partially Closed" and "Fully Closed" classes suggests the need for improvements, especially in reducing false negatives. Future enhancements may include refining the model's training process or employing additional data preprocessing techniques to improve the detection rates for these classes.

By understanding and addressing the limitations highlighted by these metrics, the model can be optimized to provide even more accurate and reliable predictions, ultimately enhancing the effectiveness of the evacuation route planning process.

3.5.2 Case Study Application to Taylor County, FL

The RCII values for Hurricanes Idalia and Debby were calculated based on the bounding box data categorized into three roadway conditions: **Open**, **Partially Closed**, and **Fully Closed**. The RCII quantifies the severity of roadway closures without considering road lengths or segments, focusing on the proportion of bounding boxes within each condition as shown in Table 4.

Table 3-4 Results of RCII for Hurricanes Idalia and Debby

Hurricane	**RCII**	**Normalized RCII (%)**
Hurricane Idalia	0.54	54.44%
Hurricane Debby	0.94	94.44%

Hurricane Debby had a significantly higher RCII (0.94) compared to Hurricane Idalia (0.54), with normalized indices of 94.44% and 54.44%, respectively (Figure 3.11). The higher RCII for Hurricane Debby indicates that it had a much more severe impact on roadway closures, with a greater proportion of bounding boxes categorized as partially or fully closed.

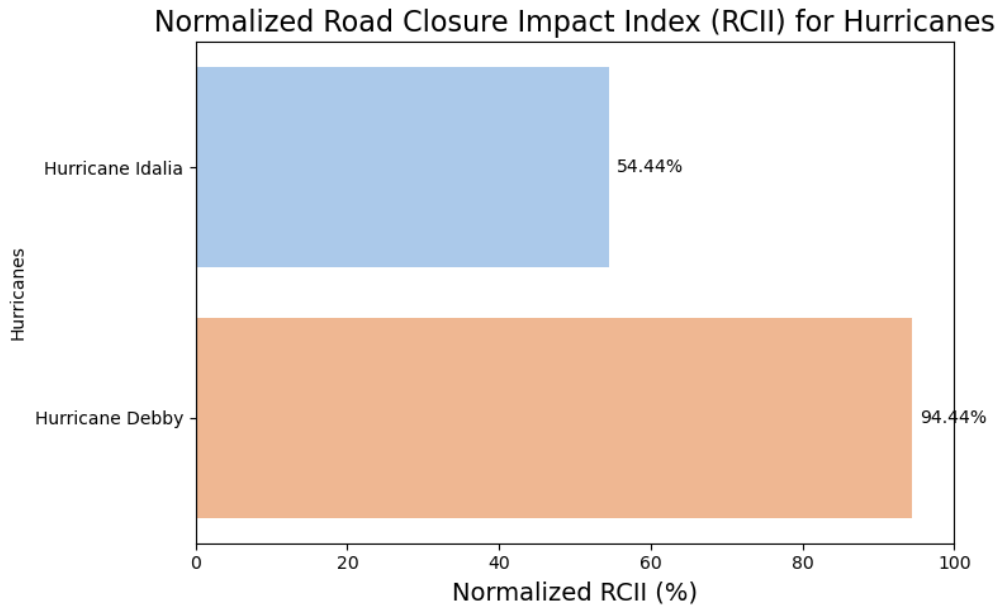

Figure 3:11 Comparison of Normalized Roadway Closure Impact Index (RCII) for Hurricanes Idalia and Debby

In contrast, Hurricane Idalia exhibited a lower RCII, suggesting that a larger proportion of roadways remained open or only partially affected during this event. These results highlight the variability in the impact of hurricanes on roadway closures. Hurricane Debby's higher RCII underscores the need for targeted mitigation strategies and infrastructure resilience enhancements to manage similar events in the future.

On the other hand, Table 5 indicates that CR-38000037 has the highest RVI because it was fully closed in both hurricanes, indicating a consistently high vulnerability. Roadways like SR-38590000, SR-38540001, and SR-38540000 have moderate RVI scores due to their status shifting between partially closed and fully closed, suggesting they are moderately vulnerable but not consistently fully closed. Roadways such as SR-38514001 and others with an RVI of 0 are generally open or show minor variations in their status, indicating low or no vulnerability. These vulnerabilities can also be seen from the visualization in Figure 3.12 with colors red, yellow, and used to symbolize the level of vulnerability.

Table 3-5 Roadway Vulnerability Index Classification for Hurricanes Idalia and Debby

Roadway Vulnerability Index (RVI) for Taylor County Roads

	Road_Number	Hurricane_Idalia_Status	Hurricane_Debby_Status	ACS	CF	RVI	Vulnerability_Level
0	SR-38514000	Open	Open	0.000000	1.000000	0.000000	Low Vulnerability
1	SR-38590000	Partially Closed	Fully Closed	1.500000	0.500000	0.750000	Moderate Vulnerability
2	SR-38655000	Open	Open	0.000000	1.000000	0.000000	Low Vulnerability
3	CR-38000037	Fully Closed	Fully Closed	2.000000	1.000000	2.000000	High Vulnerability
4	SR-38590004	Open	Open	0.000000	1.000000	0.000000	Low Vulnerability
5	SR-38540001	Partially Closed	Fully Closed	1.500000	0.500000	0.750000	Moderate Vulnerability
6	SR-38540000	Fully Closed	Partially Closed	1.500000	0.500000	0.750000	Moderate Vulnerability
7	SR-38590000	Open	Open	0.000000	1.000000	0.000000	Low Vulnerability
8	SR-38514001	Partially Closed	Open	0.500000	0.500000	0.250000	Moderate Vulnerability
9	SR-38580000	Open	Open	0.000000	1.000000	0.000000	Low Vulnerability
10	SR-38509500	Open	Open	0.000000	1.000000	0.000000	Low Vulnerability

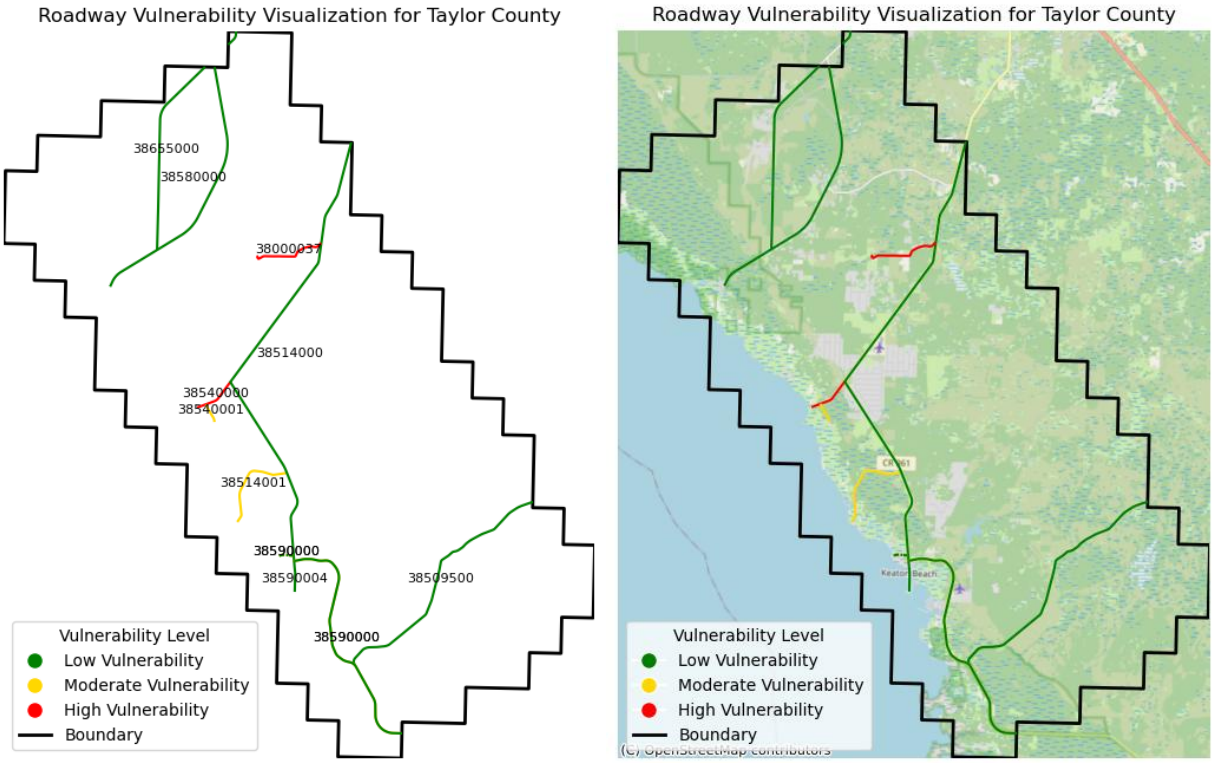

Figure 3:12 Taylor County Road Vulnerability Level for Off System Roads

3.5.3 Discussion

3.5.3.1 Geospatial Analysis and Detection Models

The study employs a detection model that categorizes roadways as either open, partially closed, or fully closed based on remote sensing data and aerial imagery collected before and after the hurricanes. Using advanced geospatial tools like ArcGIS Pro, shapefiles representing the affected roadways are merged to visualize and quantify the impact of both storms. The detection model's accuracy is validated by comparing the results from Hurricane Idalia and Hurricane Debby, allowing for the identification of patterns in roadway closures and recovery times.

This analysis encompasses the entire transportation network in Taylor County, with a particular focus on major evacuation routes, which are critical for effective disaster response and recovery. The merging of shapefiles representing roadway impacts detected from both hurricanes facilitates a comprehensive comparative analysis of the road network's vulnerability. The model's performance in detecting closures is enhanced through machine learning techniques, improving its ability to classify roadway conditions accurately.

By leveraging detection data, the study examines how these two storms affected Taylor County's infrastructure differently. For instance, during Hurricane Idalia, the model detected significant closures immediately after landfall due to high winds and structural damage. In contrast, the detection model captured prolonged closures during Hurricane Debby, primarily attributed to flooding that affected previously damaged roadways. This differentiation is crucial for understanding the dynamics of roadway closures in response to varying storm characteristics.

The integration of detection results provides insights into how long roadways remain closed and the speed of recovery efforts in different areas, allowing for better planning and mitigation strategies in future storms. The ability of the detection model to provide real-time assessments of roadway conditions could enhance decision-making for emergency management and infrastructure planning. The comparison between Hurricanes Idalia and Debby can help refine predictive models for roadway network vulnerability, ultimately improving disaster response and infrastructure planning for future hurricanes in Taylor County and other coastal regions of Florida. By analyzing detection data, the study not only sheds light on immediate impacts but also emphasizes the long-term recovery challenges faced by the transportation network.

Furthermore, the use of machine learning and geospatial analysis contributes to the development of more resilient transportation systems capable of withstanding the varied impacts of extreme weather events. Understanding the effectiveness of detection models in categorizing roadway conditions enhances the capacity of policymakers to create targeted strategies for mitigating future hurricane impacts, ensuring that transportation networks remain accessible during emergencies.

3.5.3.2 Comparison of Impact on the Roadway Network

Hurricane Idalia's stronger winds and broader impact area led to significant structural damage to roadways and bridges. The RVI results indicated that several critical roadways experienced extreme closures due to fallen trees, debris, and blocked access routes, severely impeding emergency response efforts immediately following landfall. The category of Hurricane Idalia (Category 3) played a vital role in the extent of the damage, as its higher wind speeds could cause more severe disruptions than lower-category storms.

In contrast, Hurricane Debby, which struck after Idalia, brought persistent rainfall that resulted in prolonged flooding and roadway submersion. The RCI for Debby reflected a different set of vulnerabilities; while the initial damage from Idalia was severe, many of the roadways had not returned to full operational capacity before Debby made landfall. As a result, the flooding from Debby exacerbated existing vulnerabilities, leading to extended closures that lasted several days, even in inland areas. The cumulative effect of these storms underscores the importance of understanding how successive weather events can compound existing infrastructure challenges.

The nature of flooding associated with Hurricane Debby differed from the wind damage inflicted by Hurricane Idalia. Roadways remained submerged for longer periods, requiring extensive repairs once the waters receded. This highlights a critical aspect of emergency preparedness ensuring that infrastructure can withstand not only the immediate impacts of high winds but also the prolonged effects of flooding, especially in rural regions with limited resources.

By comparing the impacts of these two hurricanes, it is possible to highlight the varying challenges posed by different types of storms and their effects on transportation networks. Understanding how hurricanes with distinct profiles such as wind strength, storm surge, and rainfall intensity affect roadways is crucial for improving future infrastructure resilience. The unique vulnerabilities revealed through the RCII and RVI assessments will aid in developing effective preparation and response strategies for Taylor County, particularly in areas that are prone to the dual threats of high winds and flooding.

Findings from this comparison not only emphasize the need for tailored mitigation strategies that consider the characteristics of individual storms but also advocate for improved resilience measures to address the compounded vulnerabilities posed by successive hurricanes. By fostering a deeper understanding of how such storms impact transportation infrastructure, Taylor County can better equip itself for future challenges.

3.6 Conclusions

This study demonstrated the potential of integrating high-resolution aerial imagery with machine learning models to improve the detection of roadway vulnerabilities in hurricane-prone areas. The use of aerial imagery allowed for more accurate identification of roadway disruptions, thereby enhancing the overall impact assessment framework. It also assesses the impacts of Hurricanes Idalia and Debby on the roadway network in Taylor County, Florida, emphasizing the necessity of understanding how various storm characteristics influence transportation infrastructure. Through

a comparative analysis, it was revealed that Hurricane Idalia's stronger winds resulted in significant structural damage, leading to immediate roadway closures due to possible downed trees and storm surge effects. On the other hand, Hurricane Debby's prolonged rainfall caused extensive flooding, resulting in prolonged roadway closures that lasted even after the storm had passed, particularly affecting evacuation routes critical for disaster response.

The integration of machine learning-based detection models, geospatial analysis, and remote sensing technologies proved essential for accurately assessing vulnerability and understanding the dynamics of road closures. The detection model effectively categorized roadway conditions based on remote sensing data and aerial imagery, allowing for a detailed visualization of the storm impacts. By comparing the aftermath of both hurricanes, this study underscored the importance of tailored emergency response strategies that consider the unique challenges posed by different storm types, such as wind versus flooding.

A key contribution of this research was the identification of the prolonged effects of Hurricane Idalia on road conditions prior to Hurricane Debby's arrival, which exacerbated the closures experienced during the latter event. This aspect highlights the need for continuous monitoring and rapid recovery efforts in regions prone to sequential storms. Furthermore, the study demonstrated that hurricane impacts can vary significantly even within the same geographic area, thus emphasizing the importance of localized data for emergency planning. Findings could serve as a critical foundation for developing more resilient transportation systems in Taylor County and similar rural coastal regions. By leveraging advanced technologies and methodologies, including remote sensing, stakeholders can better prepare for, respond to, and recover from the multifaceted challenges posed by hurricanes and other natural disasters.

Although aerial imagery provided valuable insights into roadway disruptions, its effectiveness was limited by image resolution and weather-related challenges during data acquisition, data availability and quality, as reliance on remote sensing and aerial imagery may result in incomplete or inconsistent datasets. Additionally, the focus on immediate post-hurricane conditions may not capture longer-term impacts and recovery processes of the transportation network. The findings may not be generalizable to other regions, given that Taylor County's specific geographical and infrastructural characteristics could differ from other areas. Furthermore, the machine learning detection model may not account for all variables influencing roadway conditions, leading to potential inaccuracies in vulnerability assessments.

Future work could explore the integration of aerial imagery with other remote sensing sources, such as LiDAR and satellite data, to develop a more robust assessment framework. It could also focus on enhancing the resilience of roadway infrastructure against extreme weather events through improved predictive modeling and the development of adaptive management strategies. Additionally, exploring the role of community engagement in disaster response and recovery could yield valuable insights into effective communication and resource allocation during emergencies.

3.7 References

Barnes, Christopher F., Hermann Fritz, and Jeseon Yoo. 2007. “Hurricane Disaster Assessments with Image-Driven Data Mining in High-Resolution Satellite Imagery.” *IEEE Transactions on Geoscience and Remote Sensing* 45 (6): 1631–40. https://doi.org/10.1109/TGRS.2007.890808.

Buslaev, Alexander, Selim Seferbekov, Vladimir Iglovikov, and Alexey Shvets. 2018. *Fully Convolutional Network for Automatic Road Extraction from Satellite Imagery*. https://doi.org/10.1109/CVPRW.2018.00035.

Cortes, Corinna, Vladimir Vapnik, and Lorenza Saitta. 1995. “Support-Vector Networks Editor.” *Machine Learning* 20:273–97.

Cover, T M, and P E Hart. 1952. “Approximate Formulas for the Information Transmitted Bv a Discrete Communication Channel.” *IEEE TRANSACTIONS ON INFORMATION THEORY* 24 (1): 335–42.

Cristian, Alexandru. 2024. “Post-Disaster Recovery and Environmental Monitoring Using GIS and GeoAI: Building Damage Assessment Insights from McDonough County.” https://doi.org/10.13140/RG.2.2.25657.17760.

Dalal, Navneet, and Bill Triggs. 2005. “Histograms of Oriented Gradients for Human Detection.” In *IEEE Computer Society Conference on Computer Vision and Pattern Recognition (CVPR’05), San Diego, CA, USA,* 886–93. https://doi.org/10.1109/CVPR.2005.177.

Dong, Laigen, and Jie Shan. 2013. “A Comprehensive Review of Earthquake-Induced Building Damage Detection with Remote Sensing Techniques.” *ISPRS Journal of Photogrammetry and Remote Sensing*. Elsevier B.V. https://doi.org/10.1016/j.isprsjprs.2013.06.011.

Drejza, Susan, Pascal Bernatchez, Guillaume Marie, and Stéphanie Friesinger. 2019. “Quantifying Road Vulnerability to Coastal Hazards: Development of a Synthetic Index.” *Ocean and Coastal Management* 181 (November). https://doi.org/10.1016/j.ocecoaman.2019.104894.

Ferguson, Neil, Georgia Boura, Ander Gray, Edoardo Patelli, and Enrico Tubaldi. 2023. “Vulnerability of the Scottish Road Network to Flooding.”

“Florida Department of Transportation. Https://Fdotewp1.Dot.State.Fl.Us/AerialPhotoLookUpSystem/.” 2023. 2023.

Goodfellow, Ian, Yoshua Bengio, and Aaron Courville. 2017. “Deep Learning: The MIT Press, 2016, 800 Pp, ISBN: 0262035618.” *Genetic Programming and Evolvable Machines* 19 (October). https://doi.org/10.1007/s10710-017-9314-z.

Hassan, Sitti Asmah, Hamizah Amalina Amlan, Nor Eliza Alias, Mariyana Aida Ab-Kadir, and Nur Sabahiah Abdul Sukor. 2022. “Vulnerability of Road Transportation Networks under Natural Hazards: A Bibliometric Analysis and Review.” *International Journal of Disaster Risk Reduction* 83 (December). https://doi.org/10.1016/j.ijdrr.2022.103393.

Hauptman, Leanne, Diana Mitsova, and Tiffany Roberts Briggs. 2024. “Hurricane Ian Damage Assessment Using Aerial Imagery and LiDAR: A Case Study of Estero Island, Florida.” *Journal of Marine Science and Engineering* 12 (4). https://doi.org/10.3390/jmse12040668.

He, Kaiming, Georgia Gkioxari, Piotr Dollar, and Ross Girshick. 2017. “Mask R-CNN.” *Proceedings of the IEEE International Conference on Computer Vision* 2017-October (December):2980–88. https://doi.org/10.1109/ICCV.2017.322.

He, Kaiming, Xiangyu Zhang, Shaoqing Ren, and Jian Sun. 2016. “Deep Residual Learning for Image Recognition.” In *Proceedings of the IEEE Conference on Computer Vision and Pattern Recognition (CVPR)*, 770–78. http://image-net.org/challenges/LSVRC/2015/.

Hina Ajmal, Saad Rehman, Umar Farooq, Qurrat U. Ain, Farhan Riaz, and Ali Hassan. 2018. "Convolutional Neural Network Based Image Segmentation: A Review." *Proc.SPIE* 10649 (April). https://doi.org/10.1117/12.2304711.

"Https://Www.Bing.Com/Images/Search?Q=hurricane+ian&qpvt=Hurricane+Ian&form=IGRE &first=1&cw=1473&ch=823." 2023. 2023.

"Https://Www.Tampafp.Com/Hurricane-Debby-Leaves-Severe-Damage-in-Florida-Sen-Rubio-and-Rep-Cammack-Urge-Full-Federal-Assistance/#google_vignette." 2024. 2024.

IEEE Computer Society. n.d. "2015 IEEE Conference on Computer Vision and Pattern Recognition (CVPR) : Date, 7-12 June 2015."

Jeffrey, E. F. 2009. "What-in-the-World-Is-Infrastructure." Infrastructure Investor. 2009. https://corenergy.reit/wp-content/uploads/2018/03/what-in-the-world-is-infrastructure.pdf.

Jena, Ratiranjan, Biswajeet Pradhan, and Ghassan Beydoun. 2020. "Earthquake Vulnerability Assessment in Northern Sumatra Province by Using a Multi-Criteria Decision-Making Model." *International Journal of Disaster Risk Reduction* 46 (June). https://doi.org/10.1016/j.ijdrr.2020.101518.

Ji, Min, Lanfa Liu, Runlin Du, and Manfred F. Buchroithner. 2019. "A Comparative Study of Texture and Convolutional Neural Network Features for Detecting Collapsed Buildings after Earthquakes Using Pre- and Post-Event Satellite Imagery." *Remote Sensing* 11 (10). https://doi.org/10.3390/rs11101202.

Karaer, Alican, Mingyang Chen, Michele Gazzea, Mahyar Ghorbanzadeh, Tarek Abichou, Reza Arghandeh, and Eren Erman Ozguven. 2022. "Remote Sensing-Based Comparative Damage Assessment of Historical Storms and Hurricanes in Northwestern Florida." *International Journal of Disaster Risk Reduction* 72:102857. https://doi.org/https://doi.org/10.1016/j.ijdrr.2022.102857.

Karimiziarani, Mohammadsepehr, and Hamid Moradkhani. 2022. "Social Response and Disaster Management: Insights from Twitter Data Assimilation on Hurricane Ian.," December. https://doi.org/http://dx.doi.org/10.2139/ssrn.4292734.

Kathuria, A. 2019. "What's New in YOLO v3? 2018. Https://Towardsdatascience.Com/Yolo-v3-Object-Detection-53fb7d3bfe6b." https://towardsdatascience.com/yolo-v3-object-detection-53fb7d3bfe6b.

Kerle, N., and R. R. Hoffman. 2013. "Collaborative Damage Mapping for Emergency Response: The Role of Cognitive Systems Engineering." *Natural Hazards and Earth System Science* 13 (1): 97–113. https://doi.org/10.5194/nhess-13-97-2013.

Kim, Jooho, Juhee Bae, and Makarand Hastak. 2018. "Emergency Information Diffusion on Online Social Media during Storm Cindy in U.S." *International Journal of Information Management* 40 (June):153–65. https://doi.org/10.1016/j.ijinfomgt.2018.02.003.

Kourehli, Seyed Sina. 2015. "Damage Assessment in Structures Using Incomplete Modal Data and Artificial Neural Network." *International Journal of Structural Stability and Dynamics* 15 (6). https://doi.org/10.1142/S0219455414500874.

Linardos, Vasileios, Maria Drakaki, Panagiotis Tzionas, and Yannis L. Karnavas. 2022. "Machine Learning in Disaster Management: Recent Developments in Methods and Applications." *Machine Learning and Knowledge Extraction*. MDPI. https://doi.org/10.3390/make4020020.

Loggins, Ryan, and William Wallace. 2015. "Rapid Assessment of Hurricane Damage and Disruption to Interdependent Civil Infrastructure Systems." *Journal of Infrastructure Systems* 21 (October):4015005. https://doi.org/10.1061/(ASCE)IS.1943-555X.0000249.

Lowe, David G. 2004. “Distinctive Image Features from Scale-Invariant Keypoints.” *International Journal of Computer Vision* 60 (2): 91–110.

Lu, Qing-Chang, and Zhong-Ren Peng. 2011. “Vulnerability Analysis of Transportation Network Under Scenarios of Sea Level Rise.” *Transportation Research Record* 2263 (November). https://doi.org/10.3141/2263-19.

Lu, Xiaoyan, Yanfei Zhong, Zhuo Zheng, Yanfei Liu, Ji Zhao, Ailong Ma, and Jie Yang. 2019. “Multi-Scale and Multi-Task Deep Learning Framework for Automatic Road Extraction.” *IEEE Transactions on Geoscience and Remote Sensing* 57 (11): 9362–77. https://doi.org/10.1109/TGRS.2019.2926397.

Ma, Haijian, Nan Lu, Linlin Ge, Qiang Li, Xinzhao You, and Xiaoxuan Li. 2013. “Automatic Road Damage Detection Using High-Resolution Satellite Images and Road Maps.” In *International Geoscience and Remote Sensing Symposium (IGARSS)*, 3718–21. https://doi.org/10.1109/IGARSS.2013.6723638.

Martín, Yago, Susan L. Cutter, Zhenlong Li, Christopher T. Emrich, and Jerry T. Mitchell. 2020. “Using Geotagged Tweets to Track Population Movements to and from Puerto Rico after Hurricane Maria.” *Population and Environment* 42 (1): 4–27. https://doi.org/10.1007/s11111-020-00338-6.

Mathias, Jean Denis, Susan Spierre Clark, Nuri Onat, and Thomas P. Seager. 2018. “An Integrated Dynamical Modeling Perspective for Infrastructure Resilience.” *Infrastructures* 3 (2). https://doi.org/10.3390/infrastructures3020011.

Mauricio Sánchez-Silva, and Libardo García. 2001. “Earthquake Damage Assessment Based on Fuzzy Logic and Neural Networks.” *Earthquake Spectra* 17 (1): 89–112. https://doi.org/https://doi.org/10.1193/1.1586168.

Minaee, Shervin, Yuri Boykov, Fatih Porikli, Antonio Plaza, Nasser Kehtarnavaz, and Demetri Terzopoulos. 2022. “Image Segmentation Using Deep Learning: A Survey.” *IEEE Transactions on Pattern Analysis and Machine Intelligence* 44 (7): 3523–42. https://doi.org/10.1109/TPAMI.2021.3059968.

Mitsova, Diana, Monica Escaleras, Alka Sapat, Ann Margaret Esnard, and Alberto J. Lamadrid. 2019. “The Effects of Infrastructure Service Disruptions and Socio-Economic Vulnerability on Hurricane Recovery.” *Sustainability (Switzerland)* 11 (2). https://doi.org/10.3390/su11020516.

Mostafavi, Ali, Jamie Padgett, Leonardo Dueñas-Osorio, Elaina Sutley, Terri Norton, Henry Lester, Haizhong Wang, et al. 2022. *Hurricane Harvey Infrastructure Resilience Investigation Report*. https://doi.org/10.17603/ds2-gcrf-h607.

Mukherjee, Mahua, Kumar Abhinay, Md Munsur Rahman, Sonam Yangdhen, Subir Sen, Basanta Raj Adhikari, Rekha Nianthi, Sanya Sachdev, and Rajib Shaw. 2023a. “Extent and Evaluation of Critical Infrastructure, the Status of Resilience and Its Future Dimensions in South Asia.” *Progress in Disaster Science* 17 (January). https://doi.org/10.1016/j.pdisas.2023.100275.

———. 2023b. “Extent and Evaluation of Critical Infrastructure, the Status of Resilience and Its Future Dimensions in South Asia.” *Progress in Disaster Science* 17 (January). https://doi.org/10.1016/j.pdisas.2023.100275.

Mustakim, Md Mizanur. 2023. “Road Damage Detection Based on Deep Learning.” https://doi.org/10.13140/RG.2.2.22523.28967.

National Environmental Satellite Data and Information Service. 2022. “Hurricane Ian’s Path of Destruction.” Department of Commerce, National Oceanic and Atmospheric Administration. 2022. https://www.nesdis.noaa.gov/news/hurricane-ians-path-of-destruction.

National Oceanic and Atmospheric Administration. 2023. “Https://Noaa-Eri-Pds.S3.Amazonaws.Com/Index.Html#2023_Hurricane_Idalia/20230902a_RGB/.” 2023.
National Oceanic and Atmospheric Administration (NOAA). n.d. “‘Hurricane Costs.’” Accessed June 26, 2023. https://coast.noaa. gov/states/fast-facts/hurricane-costs.html.
Nguyen, Long, Alexis Slobodzian, Claude Villiers, and Seneshaw Tsegaye. 2022. “Interdependencies of Lifelines: A Case Study of Transportation Infrastructure Under Hurricane Impacts.” In , 1–10. https://doi.org/10.1007/978-981-19-1029-6_1.
Pavur, G., V. Lakshmi, and J.H. Lambert. 2023. “A Hydrological and Socioeconomic Risk Assessment of Tropic Cyclone Disasters by Leveraging Space-Based Earth Observation.” *EGU General Assembly*, April, EGU23-10474. https://doi.org/https://doi.org/10.5194/egusphere-egu23-10474,2023.
Peng, Bo, Zonglin Meng, Qunying Huang, and Caixia Wang. 2019. “Patch Similarity Convolutional Neural Network for Urban Flood Extent Mapping Using Bi-Temporal Satellite Multispectral Imagery.” *Remote Sensing* 11 (21). https://doi.org/10.3390/rs11212492.
Pourebrahim, Nastaran, Selima Sultana, John Edwards, Amanda Gochanour, and Somya Mohanty. 2019. “Understanding Communication Dynamics on Twitter during Natural Disasters: A Case Study of Hurricane Sandy Understanding Communication Dynamics on Twitter During.”
Pouryari, Maghsood, A Ardakani, and Nemat Hassani. 2021. “A Multi-Criteria Vulnerability of Urban Transportation Systems Analysis Against Earthquake Considering Topological and Geographical Method: A Case Study.” *Iranian Journal of Science and Technology, Transactions of Civil Engineering* 46 (July). https://doi.org/10.1007/s40996-021-00699-4.
Redmon, J., & Farhadi, A. 2018. “Yolov3: An Incremental Improvement. Https://Arxiv.Org/Abs/1804.02767. Accessed 12, 2023.”
Redmon, Joseph, Santosh Divvala, Ross Girshick, and Ali Farhadi. 2016. “You Only Look Once: Unified, Real-Time Object Detection.” In *Proc., IEEE Conference on Computer Vision and Pattern Recognition, Las Vegas, NV. IEEE, New York.*, 779–88. http://pjreddie.com/yolo/.
Richard Szeliski. 2022. *Computer Vision: Algorithms and Applications. 10.1007/978-3-030-34372-9*. *Springer*.
Robinson, Anthony C. 2020. *Geographic Information Systems (GIS) for Disaster Management: Second Edition*. https://doi.org/doi.org/10.4324/9781351034869.
Ruseruka, Cuthbert, Judith Mwakalonge, Gurcan Comert, Saidi Siuhi, and Judy Perkins. 2023. “Road Condition Monitoring Using Vehicle Built-in Cameras and GPS Sensors: A Deep Learning Approach.” *Vehicles* 5 (3): 931–48. https://doi.org/10.3390/vehicles5030051.
Shafian, Sultan Al, and Da Hu. 2024. “Integrating Machine Learning and Remote Sensing in Disaster Management: A Decadal Review of Post-Disaster Building Damage Assessment.” *Buildings*. Multidisciplinary Digital Publishing Institute (MDPI). https://doi.org/10.3390/buildings14082344.
Shafique, Ayesha, Guo Cao, Zia Khan, Muhammad Asad, and Muhammad Aslam. 2022. “Deep Learning-Based Change Detection in Remote Sensing Images: A Review.” *Remote Sensing*. MDPI. https://doi.org/10.3390/rs14040871.
Sijia Hu. 2022. “Convolutional Neural Network Combined with Transfer Learning for Damage Assessment with Satellite Imagery.” *CAIBDA 2022; 2nd International Conference on Artificial Intelligence, Big Data and Algorithms*, April, 1–7.
Singh, Prasoon, Vinay Shankar Prasad Sinha, Ayushi Vijhani, and Neha Pahuja. 2018. “Vulnerability Assessment of Urban Road Network from Urban Flood.” *International*

Journal of Disaster Risk Reduction 28:237–50. https://doi.org/https://doi.org/10.1016/j.ijdrr.2018.03.017.

Sodders, Nicole, Kimberly Stockdale, Kayla Baker, Arielle Ghanem, Benjamin Vieth, and Terri Harder. 2023. "Morbidity and Mortality Weekly Report Notes from the Field Vibriosis Cases Associated with Flood Waters During and After Hurricane Ian-Florida, September-October 2022" 72 (18). https://www.

Spekkers, M. H., M. Kok, F. H.L.R. Clemens, and J. A.E. Ten Veldhuis. 2014. "Decision-Tree Analysis of Factors Influencing Rainfall-Related Building Structure and Content Damage." *Natural Hazards and Earth System Sciences* 14 (9): 2531–47. https://doi.org/10.5194/nhess-14-2531-2014.

Tavus, Beste, Sultan Kocaman, and Candan Gokceoglu. 2022. "Flood Damage Assessment with Sentinel-1 and Sentinel-2 Data after Sardoba Dam Break with GLCM Features and Random Forest Method." *Science of the Total Environment* 816 (April). https://doi.org/10.1016/j.scitotenv.2021.151585.

Tsang, S. H. 2018. "Review: Yolov3—You Only Look Once (Object Detection). Https://Towardsdatascience.Com/ Review-Yolov3-You-Only-Look-Once-Object-Detection-Eab75d. Accessed June 25, 2023."

"United States Census Bureau." 2022. 2022. https://data.census.gov/profile/Taylor_County,_Florida?g=050XX00US12123.

Vetrivel, A, N Kerle, M Gerke, F Nex, and G Vosselman. 2016. "Towards Automated Satellite Image Segmentation and Classification for Assessing Disaster Damage Using Data-Specific Features with Incremental Learning." In *GEOBIA*. https://doi.org/10.3990/2.369.

Wang, Yandong, Shisi Ruan, Teng Wang, and Mengling Qiao. 2019. "Rapid Estimation of an Earthquake Impact Area Using a Spatial Logistic Growth Model Based on Social Media Data." *International Journal of Digital Earth* 12 (11): 1265–84. https://doi.org/10.1080/17538947.2018.1497100.

Westen, C. J. Van. 2013. "Remote Sensing and GIS for Natural Hazards Assessment and Disaster Risk Management." In *Treatise on Geomorphology: Volume 1-14*, 1–14:259–98. Elsevier. https://doi.org/10.1016/B978-0-12-374739-6.00051-8.

Yang, Liping, and Guido Cervone. 2019. "Analysis of Remote Sensing Imagery for Disaster Assessment Using Deep Learning: A Case Study of Flooding Event." *Soft Computing* 23 (24): 13393–408. https://doi.org/10.1007/s00500-019-03878-8.

Yuan, Faxi, William Mobley, Hamed Farahmand, and Yuanchang Xu. n.d. "Predicting Road Flooding Risk with Machine Learning Approaches Using Crowdsourced Reports and Fine-Grained Traffic Data." https://doi.org/10.48550/arXiv.2108.13265.

Zapico, J. L., M. P. González, and K. Worden. 2003. "Damage Assessment Using Neural Networks." *Mechanical Systems and Signal Processing* 17 (1): 119–25. https://doi.org/10.1006/mssp.2002.1547.

Zhang, Mingliang, Menghua Xu, Zhaoli Wang, and Chengguang Lai. 2021. "Assessment of the Vulnerability of Road Networks to Urban Waterlogging Based on a Coupled Hydrodynamic Model." *Journal of Hydrology* 603:127105. https://doi.org/https://doi.org/10.1016/j.jhydrol.2021.127105.

Zhong, Hao, and Daan Liang. 2024. "A Study of Road Closure Due to Rainfall and Flood Zone Based on Logistic Regression." *International Journal of Disaster Risk Reduction* 102:104291. https://doi.org/https://doi.org/10.1016/j.ijdrr.2024.104291.

Zhu, Yi Jie, Yujie Hu, and Jennifer M. Collins. 2020. "Estimating Road Network Accessibility during a Hurricane Evacuation: A Case Study of Hurricane Irma in Florida." *Transportation Research Part D: Transport and Environment* 83 (June). https://doi.org/10.1016/j.trd.2020.102334.

Chapter 4 Post-Tornado Roadway Debris Detection from Satellite Images: An Integrated GIS And Image Processing Approach

4.1 Introduction

Tornadoes and other natural hazards claim lives and damage property and infrastructure. Natural hazards are estimated to have cost the United States $1.75 trillion in damages between 1980 and 2019 (NOAA, 2020). Post-disaster debris in the U.S. has disrupted transportation infrastructure financially and operationally over the last decade (Karaer et al., 2021). Every severe weather event

that occurs in the US is recorded in a dataset maintained by the National Oceanic and Atmospheric Administration (NOAA) (NOAA-NCEI, 2024). According to their updated dataset, extreme storms like tornadoes have caused damages worth over $55.5 billion in the US in 2023 (NOAA-NCEI, 2024). Moreover, since 1980, there has been a consistent record of severe weather occurrences, which have been shown to be increasingly destructive every year. Given that buildings, agricultural areas and produce, utility facilities, and transportation infrastructures are among the losses (Motha, 2011; Gossling et al., 2023), it is important to conduct detailed spatial studies of the effects these extreme events have on communities and infrastructure. Severe storms like hurricanes and tornadoes, which frequently cause significant physical damage, occur in a large portion of the U.S. (Koch et al., 2021; Wuebbles et al., 2014; Smith, 2022). For instance, on May 10, 2024, tornadoes devastated Leon County, severely damaging homes, infrastructure, and businesses. When tornadoes occur, they result in road closures, traffic jams, and delays in the rehabilitation of damaged infrastructure (Safapour and Kermanshachi, 2020) which also happened when those tornadoes hit Leon County, Florida. Although evacuations have the potential to reduce loss of life, when employed, post disaster evacuations as well as response and recovery operations still heavily rely on road access. Therefore, in order to make the roads accessible by emergency personnel and the general public, debris needs to be removed (Kocatepe et al., 2019). Consequently, effective debris removal is essential to returning an impacted community's infrastructure to its pre-disaster state (Zhang et al., 2019).

Debris accumulation on roadsides is one of the most important effects of storm disasters, increasing financial losses and making recovery operations more difficult (Axel et al., 2016; Gilliam, 2024), leading to major disruptions in transportation networks. Tornado debris (McEntire, 2006), which can range in composition from man-made objects like cars, buildings, and household items to natural elements like trees and dirt, is one of the primary sources of these disruptions (AP, 2012; Gilliam, 2024). These can be further divided into sediment and non-sediment categories. Demolition, construction, and clean wood are the three categories for non-sediment debris (FEMA, 2007). Conversely, water puddles, downed trees, and tree branches are examples of tornado-induced non-sediment debris that can damage road networks, affecting traffic flow and accessibility. Debris presence has become simpler to report, and to some extent, weather occurrences are more accurately reported as the world grows more interconnected and developed. This is a contributing factor to the decrease in severity of the debris (Butterworth et al., 2010). During the 2004 and 2005 hurricane seasons, 488 cubic yards (cy=~0.76 m^3) of vegetative debris were collected for every mile of roadway segment in Florida. This translates to a cost of $21.50 per cy. (Staudhammer et al., 2009). Extreme tornadoes, with speeds up to 300 mph, can lift and propel debris across great distances. It is possible for obstructions to impede emergency response and cleanup operations on roads, railroads, and waterways. Debris can turn huge objects into projectiles to impact buildings and infrastructure, causing major damage ((Friedson, 2024) and debris in the air or on the ground endanger people. Debris can also cause secondary hazards including gas leaks or fires, contaminating water supplies, and damage ecosystems. Roads may become impassable due to uprooted trees; they must be removed before traffic may continue (Liu

et al., 2021). Debris on major roads and highways can lead to significant traffic delays, rerouting, and disruptions to local businesses and daily commutes (Weisbrod and Fitzroy, 2011). Road surfaces can become slick due to leaves, especially when they're wet, which raises the possibility of cars skidding and collisions. Although smaller branches and leaves may only partially obstruct highways, they still present serious hazards to motorists, increasing the risk of accidents or necessitating detours (Rhee et al., 2021). Thick leaf or branch accumulations can obstruct traffic signs, road markings, and hazards, reducing visibility and raising the chance of collisions. At junctions and curves, piles of leaves or branches can obscure road edges or stop signs, causing confusion which may lead to crashes. Debris-related road closures can have an impact on business traffic, commuting routes, and supply chains (Weisbrod and Fitzroy, 2011; Layne, 2024). Vegetative debris has the potential to choke culverts and storm drains, resulting in water accumulation and possible road flooding (Gilbert, 2023). Restoring damaged road infrastructure and clearing debris can be expensive and time-consuming. Vehicle crashes can result from sudden barriers and unanticipated debris that drivers attempt to avoid or maneuver around. Automobiles that swerve to avoid debris run the risk of running into other cars or objects. Road signs and traffic signals may be damaged or knocked down by debris, causing traffic jams and maybe crashes. Intersection risks can arise from a tornado's ability to shatter or twist traffic lights and signage. Traffic must be rerouted when debris causes road closures or lane limitations, which cause congestion and delays (Parker, 2023). Over $150 million in federal emergency money has been used by the State of Florida for debris removal (Press Release FEMA, 2020). This clearly shows that emergency and transportation authorities are interested in controlling debris since it poses a serious threat to disaster-affected communities' infrastructure.

In addition to researchers studying natural hazards and forestry (Staudhammer et al., 2009; Duryea et al., 2007; Thompson et al., 2011), numerous governmental entities also study disaster debris assessment. The National Flood Insurance Program (NFIP), Property Claim Services (PCS), Federal Emergency Management Agency (FEMA), the United States Department of Agriculture (USDA), the National Agricultural Statistics Service (NASS) & Risk Management Agency (RMA), the National Interagency Fire Center (NIFC), and state agency reporting are just a few of the organizations that provide these damage assessment data. Debris volume estimation models have been developed by public agencies such as the US Army Corps Engineers (U.S. Army Corps of Engineers, 2008), the Federal Emergency Management Agency (FEMA) (FEMA, 2010), and local agencies like the Broward County, FL Emergency Management Office (Umpierre and Margoles, 2005), to support Transportation Departments in their operations during debris removal. These models have limitations in measuring field data, such as tree counts, diameters, and heights, which are inputs for the vegetation cover model, even though they provide reliable information on the creation of hurricane-related vegetative debris (Szantoi et al., 2012). Apart from the safety and accessibility concerns, gathering field data for damage assessment is typically costly and time-consuming (COES, 2005). The inaccessibility of tree data in certain areas is another drawback. Recording and updating tree database creation is expensive and time-consuming (Szantoi et al., 2012; Hoque et al., 2016; Hu and Smith, 2018). Studies have also been done on how natural

disasters affect traffic on roads (Chang et al., 2010; Lee et al., 2011; Zamanifar et al., 2014). These disruptions in traffic patterns were associated with the degree of destruction and frequently resulted in roadblocks that hindered travel.

Remote sensing (RS) provides innovative technologies for assessing tornado debris (Hoque et al., 2017). RS technologies have shown to be effective in damage assessment following disasters, as demonstrated by numerous research (Xie et al., 2016). Aerial images (Schaefer et al., 2020), a form of airborne remote sensing technology, are one important source of data for storm damage assessment. Satellite imagery is continuously acquired every day and is available for usage all year round for assessing damage. Every day, commercial satellite companies offer high-resolution (0.3 to 0.5 pixels/m) images of different portions of the planet. Satellite images are more useful for examining broad areas affected by natural disasters than for studying tiny areas or damage in these communities due to their limited spatial resolution (Reeves and Cho, 2019). It has been possible to accurately evaluate land features such as vegetation health (Metternicht, 2003), water surfaces (Tang et al., 2016), and developed land (Zha et al., 2003), using the spectral indices derived from RS data. As such, they can be used in place of more conventional field data collection techniques when performing an evaluation of debris. Furthermore, recent research on damage assessments from North Florida show that vulnerable and low-income populations are more likely to experience disaster-induced infrastructure disruptions, such as power outages and road closures (Chen et al., 2021). The application of RS technology for post-disaster studies and recovery was enhanced by advancements in machine learning (ML) and the widespread coverage, affordability, and frequency of satellite images (Gazzea et al., 2021a). Consequently, RS offers great potential to develop fast image recognition systems to identify vegetative debris from post-tornado imagery. Reducing the financial burden, environmental concerns, and public health hazards associated with disasters requires effective management of disaster debris. The large costs associated with debris cleanup—$74 million after Hurricane Harvey and $752 million after Hurricane Ike—highlight the significance of precise debris estimation and efficient management techniques (Meads et al., 2021; Amadeo, 2018). There are substantial financial advantages to sustainable debris management techniques, such as recycling and reusing vegetative debris, making assessments necessary for effective management.

Therefore, in order to support rescue and recovery operations as well as disaster planning and management, it is necessary to promptly and effectively provide local governments with information regarding the severity and amount of damage caused by tornado debris. Roadways and other infrastructure are needed in this case to provide the necessary access. This research aims to give an assessment of tornado debris in Leon County, Florida, with a particular focus on the vegetative debris along the roadways using the Normalized Difference Vegetation Index (NDVI) acquired from satellite images taken before and after the disaster. To assess damage at various spatial scales, NDVI analysis is carried out in two ways: a) for the entire county, and b) for the roadway infrastructure alone. The extraction of NDVI values from vegetative areas along roads is of the utmost importance in order to identify the segments of the roadways damaged by the disaster and to detect locations where trees have been struck by tornadoes. The contribution of this research

is the development of an integrated macro-level approach to assess the impact of post-tornado vegetative debris on roadway segments using Geographic Information Systems (GIS) and image processing techniques. This paper then uses GIS and image processing to apply the current NDVI approach to tornado debris evaluation. Population density will be the primary focus of the examination of the conclusions obtained from the NDVI analysis. Additionally, ground truth damage data and the tornado path will be used for validation.

4.2 Literature Review

4.2.1 Remote Sensing Methods for Disaster Debris Damage Assessment

RS technologies—such as satellite images, drone photography, aerial pictures, and LiDAR—are crucial to damage assessment during disasters (Karaer et al., 2022; Jiang and Friedland, 2016; Gazzea et al., 2021b). These technologies are not only appropriate for extreme events like earthquakes and floods, but also for tornadoes. For successful disaster response and recovery operations, accurate and efficient debris estimation and damage assessment are made possible by this innovative technology. Methodologies utilizing high-resolution aerial images, for example, have demonstrated that the use of multivariate texture information reduces confusion with other land cover types, hence improving the accuracy of debris categorization significantly (Jiang and Friedland, 2016). Furthermore, vegetative debris has been successfully identified and quantified using moderate-resolution satellite data and vegetation indices such as the Modified Soil Adjusted Vegetation Index (MSAVI2) and the Normalized Difference Infrared Index (NDII) (Wang et al., 2010).

Researchers (Antwi et al., 2023) used satellite images and GIS tools to evaluate hurricane damage in Calhoun County. After the hurricane, Google Earth Engine (GEE) was utilized to evaluate the number of vegetative debris on the roads in order to pinpoint high-impact locations. Following Hurricane Fran in North Carolina, GIS was utilized to categorize and digitize devastated forest areas (Pickens et al., 2000). Damaged regions were interpolated using the ArcGIS Spatial Analyst Tool from field data. Shedd and Devine ((Shedd et al., 2005) used the Feature Analyst Tool in ArcGIS to map and detect woody debris using leaf area index, NDVI, and classification approaches. Using manually labelled training data, a Convolutional Neural Network (CNN) supervised learning algorithm and satellite images were utilized to detect road closures (Cao and Choe, 2020; Kislov and Korznikov, 2020). In contrast to unsupervised models, supervised models are not scalable (Nex et al., 2019). Most assessments use empirical studies and single-parameter models to estimate debris (Li et al., 2018). In order to undertake multi-spectral analysis and identify changes following a disaster, pre- and post-tornado photos are required (Butenuth et al., 2011) while only post-event imagery requires mono-temporal analysis (Voigt et al., 2011). Rahman and Rashed (Rahman and Rashed (2015) employed Light Detection and Ranging (LiDAR) to evaluate the damage resulting from an ice storm that hit Oklahoma City in 2007. Pre- and post-disaster point clouds were gathered using an airborne laser scanner, and the data was analyzed to produce a digital surface model of the devastation. For in-depth evaluations, LiDAR can produce a three-dimensional representation of the damage. Notably, it is a costly means of acquiring data.

Innovative approaches utilizing unmanned aerial vehicles (UAVs) and aerial photogrammetry allow for the precise estimation of debris volume and detailed disaster impact analysis (Cheng et al., 2024; Gong and Maher, 2014a). By identifying optimal overlapping ratios for aerial imagery, these methods ensure the creation of accurate 3D models, which are essential for comprehensive post-disaster response and recovery planning (DeWitt and Wolf, 2000; Genin, 2019). Integrating advanced remote sensing technologies with sustainable debris management practices enhances the resilience and recovery of disaster-affected communities. Nonetheless, hinderances such as aviation permission for No Flight Zone areas are difficult to attain (US-FAA, 2013; Skrabania, 2021). Aside from these, multiple flights might be required to attain full coverage of the study area (Fadelli and Xplore; Mu˜noz et al., 2021). This although not as much in comparison to traditional methods, is still expensive to acquire in terms of resource allocation. Using Enhanced Vegetation Index (EVI) and Normalized Difference Vegetation Index (NDVI) vegetation indices, Schultz et al. (2016) studied tropical forest zones. The Soil-Adjusted Vegetation Index (SAVI) (Luo et al., 2010) and Advanced Vegetation Index (AVI) (Gobron et al., 2000) are other vegetation indicators. Yeom et al. (2019) used unmanned aerial vehicle (UAV) post-storm data to evaluate damage. For the study, an orthomosaic image and digital elevation model were created. The spectral difference of the debris and changes in building elevation were used to calculate damages. Zhai and Peng (2020) evaluated storm damage in Mexico Beach, Florida, using RS imagery, Google Street photos, and a deep learning algorithm. While the accuracy rate of 70% was satisfactory, the method is limited by time and geography when using Google Street Images. The pros and cons of RS technology are summed up in a comparison of RS technologies for post-disaster damage assessment, which is adapted from Gong and Maher (2014b). Airborne or satellite imaging is less accurate vertically and cannot penetrate vegetative cover, although having a broad coverage area, ease of interpretation, and not requiring ground access. In contrast, unmanned aerial vehicle (UAV)-based photography systems are inexpensive to operate, adaptable, and able to map at low altitudes, however they cannot penetrate dense vegetation. Although airborne LiDAR is less accurate than ground-based LiDAR systems and has a lower resolution, it can distinguish between the ground and canopy, has a vast coverage area, and does not require ground access. Its flight period is brief. Moreover, static terrestrial lidar has a small coverage area but excellent accuracy and resolution. Mobile LiDAR has a wide coverage area, great accuracy, and high resolution, but it needs access to the ground. While these remote sensing techniques improve the overall effectiveness of large-scale post-disaster assessments and present a viable substitute for labor-intensive, risky, and slow traditional human-based investigations, the resolutions of satellite images larger than 10 meters obscure information in the findings (Lipponen, 2017). Furthermore, utility of the photos is not correlated with their availability because of cloud cover and the long returning times of satellite imagery (Li et al., 2022).

4.2.2 Image Processing

Remotely sensed images are significantly utilized in debris assessment and change detection tasks. Using pre-event and post-event images, changes can be assessed in a large scale covering large areas. This approach has been successfully applied in various fields, including forest monitoring,

urban development tracking, coastal erosion assessment and feature change detection (Antwi et al., 2024; Stanturf et al., 2007; Al-Dail, 1998). By leveraging high-resolution satellite data and change detection techniques, it is possible to rapidly and accurately assess roadway debris after a tornado, facilitating timely and efficient disaster response and recovery efforts. The state and health of green vegetation have been depicted by various mathematical computations of spectral bands in satellite images. These indices are discussed in Smith et al. (2014). RS can be used to track the growth of leaves and the point at which a plant dies (Razali et al., 2019). For instance, the Landsat Thematic Mapper (LTM), which is well-known for evaluating changes in land use (Zhang and Zhang, 2007) and forest studies in which mathematical equations are applied to spectral bands, is used to study vegetation stress (Razali et al., 2019). In areas with less vegetation protection or areas with a backdrop of both soil and vegetation, other remote sensing indices, such as the SAVI, are particularly useful for monitoring and assessing the vegetation (Luo et al., 2010). They were developed to lessen the influence of soil background on the vegetation indicator. It uses red and NIR bands, similar to the NDVI, but it also includes a soil adjustment factor that takes variations in soil reflectance into account (Luo et al., 2010).

In order to evaluate plant health by excluding atmospheric effects in locations with large plant densities or high soil reflectance levels, EVI, which was developed to overcome some of NDVI's inadequacies, adds a blue to the red and NIR bands (Schultz et al., 2016). NDVI was developed by Rouse et al. and uses the red (visible) and near-infrared areas (Rouse et al., 1974). The index can detect a drop in biomass because it responds to photosynthetic vegetation and chlorophyll (Razali et al., 2019). Tropical rainforest, herbaceous savannah, crops, and deciduous evergreen broadleaf have all been evaluated using NDVI (Hmimina et al., 2013). The obtained values can be interpreted using the NDVI palette, which has indices ranging from -1 to 1. The palette includes dark brown, orange, yellow, light green, and green. Very low NDVI values (0.1 and lower) correspond to deserted patches of snow, sand, or rock. Shrub and grassland are indicated by values between 0.2 and 0.3, whereas temperate and tropical rainforests are indicated by high values between 0.6 and 1.0 (Weier and Herring, 2000). This paper proposes an integrated GIS and image processing approach to tornado debris assessment employing NDVI retrieved from pre- and post-disaster satellite images, with an emphasis on vegetative debris gathered along roadways during disasters like tornadoes. GIS was used for image processing, findings, and analysis.

4.3 Tornadoes And Study Area

Leon County, which is the home to the capital city of Florida; Tallahassee, has a population of 292,198 and 668 square miles of total area with a population density of 437.1 people per square mile in 2020 (US Census, 2020). It shares a border with other Florida counties like Gadsden, Wakulla, Liberty, and Jefferson as well as Grady and Thomas counties in Georgia (Figure 4.1a). Several tornadoes occurred consecutively on 10th May 2024 with three passing through Leon and Gadsden, while the other three passed through Madison, Jefferson, Taylor, Houston, and Walton Counties, Florida. It is important to mention that meteorologists rate tornadoes using the Enhanced Fujita (EF) scale based on wind speed that is estimated from the damage a tornado produced. EF-

0 wind speeds ranges from 65 - 85 mph, EF-1 ranges from 86 -110 mph, EF-2 is 111 – 135 mph, EF-3 is 135 – 165 mph, EF-4 is 166 – 200 mph, while EF-5 has wind speed over 200 mph. The first tornado with a maximum wind speed of 115 mph and max width of 900 yards classified under an EF-2 rating, touched down in eastern Gadsden County at 6:38am and went on into the western part of Leon County for a total path length of 19.58 mi, destroying buildings and trees in its path before ending at 7:03am. Similarly, the second tornado, which was also an EF-2 rating, passed through the study area having a maximum width of 1,400 yards and wind speed of 115 mph and travelled a path of 27.22 mi starting at 6:50am and ending at 7:14am. The third tornado that passed through the study area, started at 6:50am and ended at 7:13am, and had an EF-1 rating, maximum wind speed of 110 mph, 1,100 yards width and travelled for 31.69 mi. All three tornadoes lasted for a combined duration of 72 minutes. Figure 4.1b illustrates tornadoes' paths with the areas it impacted while the map of Leon County with census population data and roadways is illustrated in Figure 4.1a. Ground truth data for Leon County obtained from NOAA's damage assessment website was used for validating the performance of the framework. The extreme winds from the storm caused massive damages to vegetation and infrastructure producing huge volumes of vegetative debris which disrupted and blocked over 300 roads. The damage scale from these tornadoes exceeded the damage from hurricanes Hermine, Idalia, and Michael combined according to the NOAA (NOAA, 2024a). The event resulted in significant tree damage, roadblocks and extensive power outages totalling over 80,000 affecting more than half of the City of Tallahassee's electric customers.

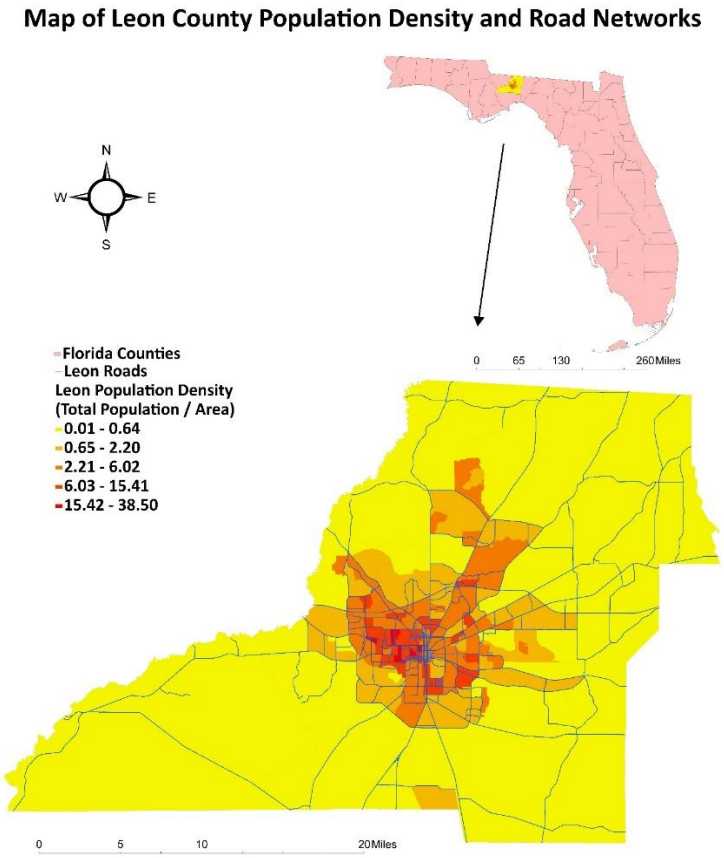

(a)

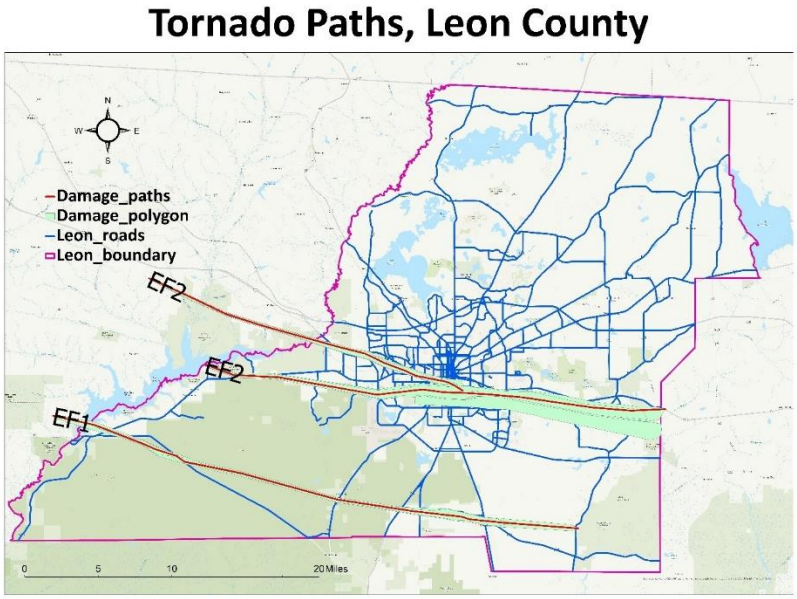

(b)

Figure 4:1 Illustrations of (a) study area with population densities, and (b) Tornadoes' tracks

4.4 Materials And Methodology

In this research, our goal is to create a GIS framework for extracting the NDVI changes to provide a tornado-induced debris assessment for Leon County and identifying and extracting roadway segments that were severely affected. Additionally, the population distribution will be the primary focus of an analysis of the average NDVI values for these road segments. The major assumption is that fallen trees and debris will cause detectable changes in the average NDVI value, reflecting a loss in vegetation greenness and chlorophyll content. Afterwards, NDVI changes will be derived by using an NDVI algorithm to produce an NDVI layer for the study area. In remote sensing applications, NDVI is a commonly used index to detect vegetation greenness and measure chlorophyll content through the infrared band. However, one limitation of NDVI is its inability to distinguish between different types of vegetation, such as bushes, trees, and grass.

The data utilized in this study consists of the Planetscope satellite image collection, tornado tracks, and GIS shapefiles of census data, Leon County boundary, and Leon County roadways. Additionally, ground truth data of damaged areas was used to assess the performance of this methodology. The ground truth data used in this study consists of damage points and tracks/polygons obtained from NOAA following disaster events. These detailed damage assessments are conducted immediately after the event to capture all relevant damage indicators before any cleanup operations commence. Data is collected through on-site inspections, utilizing laptops, GIS software, and handheld GPS devices for precise geolocation. In addition to the field data, geotagged photographs and in-app questionnaires, linked to specific damage indicators, are collected by the field crew as supplementary information about the damage created from the hazard. When available, Civil Air Patrol aerial photography and weather radar observations further enhance the dataset. The collected information is centralized on an ESRI Server where damage points and polygons can be obtained for comprehensive analysis. The analysis concentrated on the county's roadway segments. Images from April 24, 2024, and May 14, 2024, were obtained at a 3-meter resolution and included RGB-NIR channels. Consequently, multiple image collections from before (I_{bfr}) and after (I_{aft}) tornadoes were gathered to cover the entire study area, including the roadway segments (Figure 4.2).

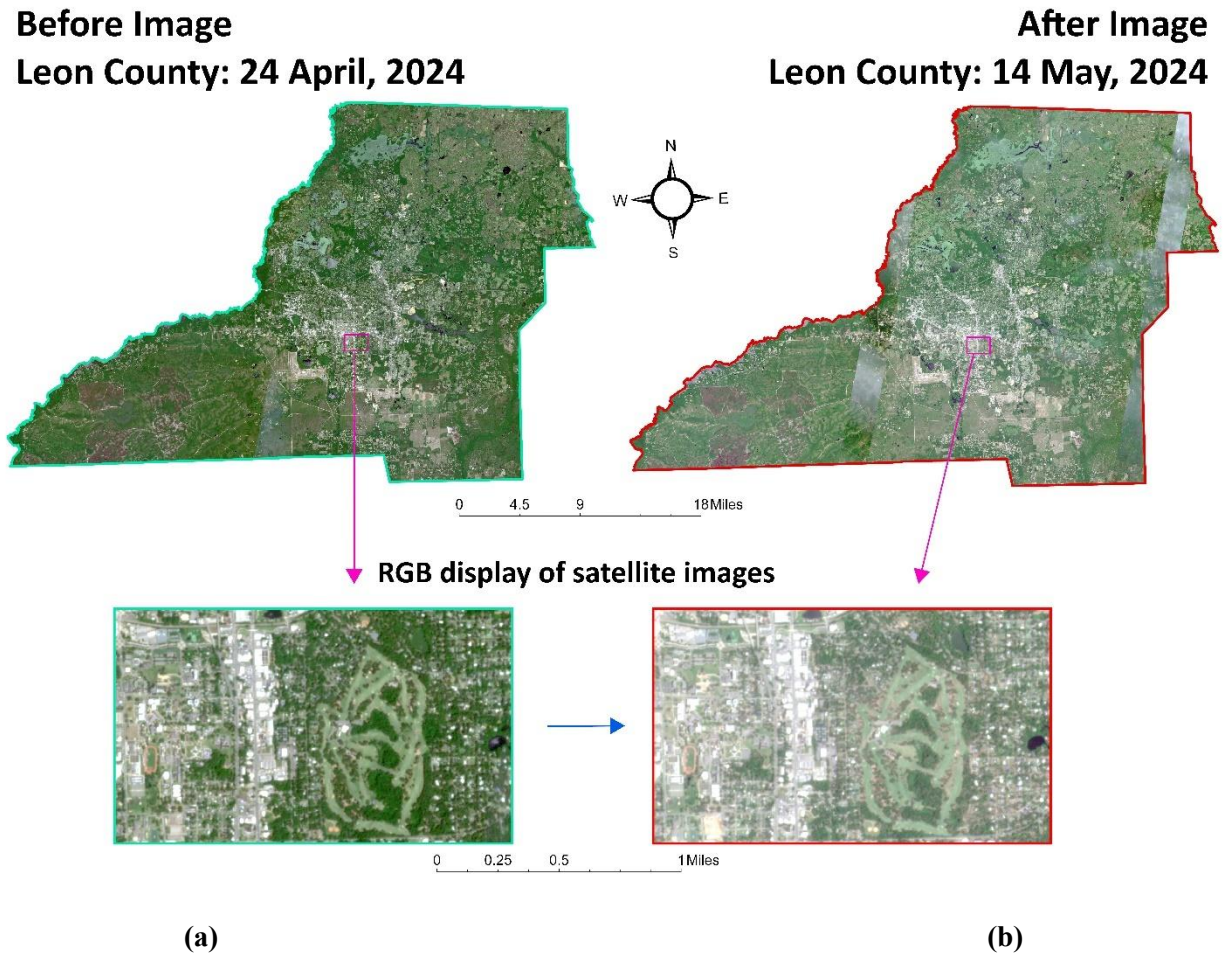

Figure 4:2 Example illustration of: (a) Before, and (b) after image extraction from Planetscope satellite in Leon County RGB: Red-Green-Blue

The research process involved extracting indices from satellite images using remote sensing (RS) algorithms and shapefiles, as well as performing image extraction and filtering, NDVI function creation, applying the NDVI algorithm, extracting NDVI values from the shapefile layer, and creating charts, maps, and descriptive data. The initial stage of data preparation was conducted in the ArcGIS environment. To acquire shapefiles of the study area and polygons, data selection, extraction, and merging were carried out using ArcGIS Pro v3.0. A buffer was created using roadway centerlines and the road widths and then subtracted from a second buffer polygon located 10 feet from the vegetative area along the roadway. This designated area was extracted and zoned for analysis. Since the study objective was to perform a macro level post- disaster roadway vegetative debris assessment, the buffer regions of the larger roadway segments were further divided into smaller segments averaging 0.5 miles each for a more detailed analysis (Figure 4.3). This way, the section of the larger segment that was directly affected can be easily identified for further assessment.

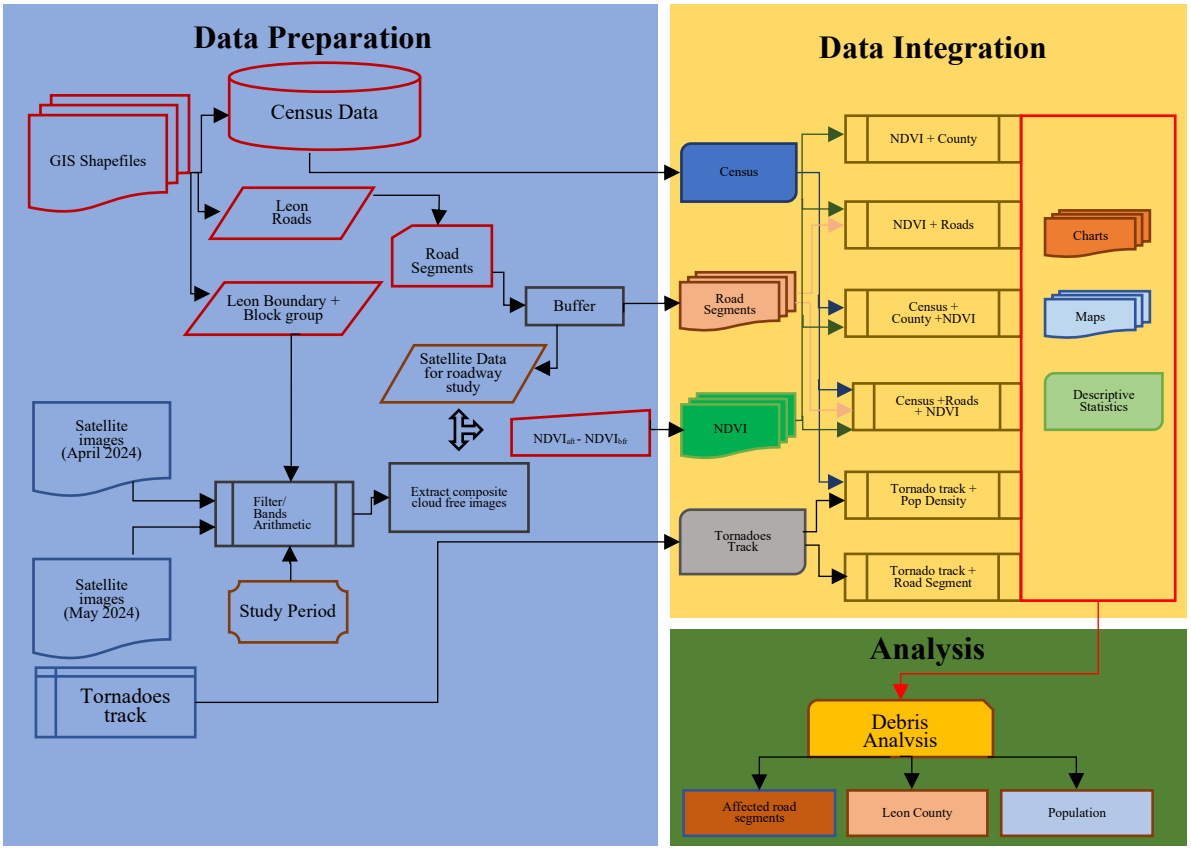

Figure 4:3 Research framework

4.4.1 Satellite Data Acquisition and Processing

The data source for the satellite images used in this research is Norway's International Climate & Forests Initiative (NICFI), hosted by Planet, which provides non-commercial, very high-resolution satellite data. The satellite images have four spectral bands with a sub-decimetre resolution and a temporal resolution or revisit time of 2 days across all constellations. For this study, the RGB (red-green-blue) and NIR (Near-infrared) bands with a 3-meter resolution were utilized, where red is band 3, green is band 2, blue is band 1, and NIR is band 4. This combination offers a cost-free resource to assess roadway debris after a tornado (Planet Labs, 2024). This capability, paired with change detection analysis, enables effective monitoring and quantification of debris extent by comparing satellite images taken before and after a disaster to identify significantly altered areas (Afaq and Manocha, 2021). For this project, satellite images from pre- and post-disaster periods were collected and analyzed. The dataset included images from two dates, spanning from two weeks before the event to one week after the event. This short timeframe was chosen to focus on roadway segments and critically assess the immediate debris created by tornadoes on these segments one week after the disaster.

4.4.2 Dataset Preparation

Satellite images covering a large geographical area with multiple spectral bands were acquired. To ensure optimal analysis, it is necessary to clean pre- and post-event imagery, which are often

affected by haze and cloud cover. While aerial imagery collected below cloud ceilings is ideal, it is limited in coverage, expensive to obtain, and may face controlled airspace restrictions. In contrast, satellite images can cover large areas and may be collected on cloud-free days if revisit time is not a constraint. However, satellite images are susceptible to data losses on very cloudy days. After filtering the image collection to match the study period and required spectral bands, a cloud-free image was selected from the available collections.

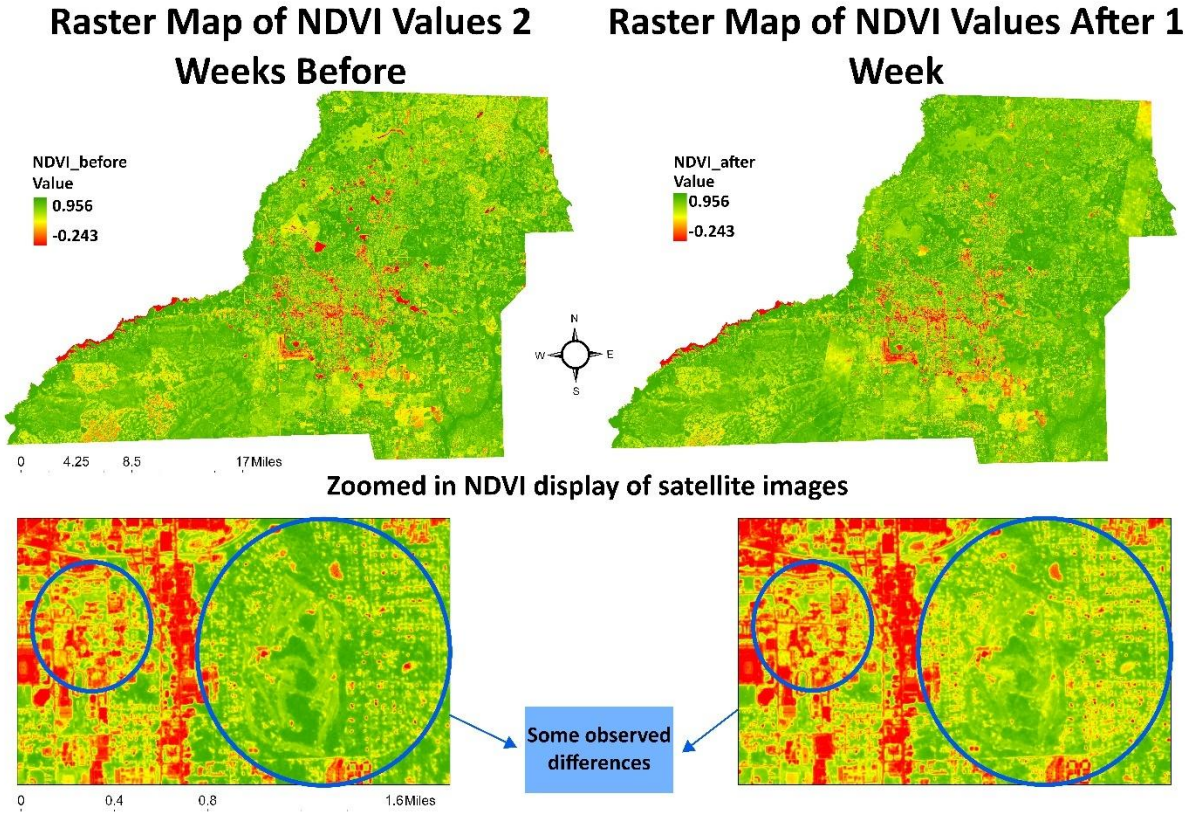

F*igure 4:4 Tornado impacted area observed NDVI changes for roadway segment study.*

4.4.2.1 Normalized Difference Vegetation Index (NDVI) Algorithm

The NDVI is used for determining vegetation greenness and is defined as follows *(Shedd et al., 2005)* (Equation 1):

$$NDVI = \frac{\rho_{nir} - \rho_{red}}{\rho_{nir} + \rho_{red}} \quad \text{..... (1)}$$

where ρ_{red} and ρ_{nir} are the spectral reflectance measurement for red (visible) and near-infrared regions, respectively. Reflectance measurements are included in the satellite images as part of the product. Due to the high reflectance of chlorophyll, green vegetation appears brighter in the near-infrared band. Therefore, a NDVI score (ΔNDVI), representing the percent change in NDVI values, can be calculated by finding the difference between the NDVI values before the tornado ($NDVI_{bfr}$) and after the tornado ($NDVI_{aft}$), and then dividing this difference by the $NDVI_{bfr}$ values (Equation 2).

$$\Delta NDVI = \frac{NDVI_{aft} - NDVI_{bfr}}{NDVI_{bfr}} * 100 \quad \text{..... (2)}$$

The NDVI values were extracted using the NDVI function, which utilizes bands 3 and 4. Band 4 corresponds to the Near-Infrared (NIR) region, while band 3 corresponds to the red (visible) region. After incorporating the NDVI bands into the image collection, a color scheme for NDVI was created and applied to enhance visualization (Figure 4.4). Geographic coordinates of the areas of interest were added to the image collection, allowing for the extraction and visualization of changes in NDVI values over the study area and period using charts.

4.4.2.2 Extracting NDVI Values for County-wide and Roadway Segment Analysis

In ArcGIS Pro, Planetscope image collections, along with boundary and polygon shapefiles, were imported into a variable. NDVI was then generated using bands 3 and 4. The NDVI values for the polygon layers were extracted, and charts were created for analysis. Initially, pre- and post-disaster satellite images, as well as roadway and boundary shapefiles, were imported into ArcGIS. After cropping the images to the desired boundary, the NDVI for the satellite images was extracted (Figure 4.4). The NDVI difference between before (I_{bfr}) and after (I_{aft}) was then computed. The roadway shapefile was segmented and buffered to obtain a 10 feet distance from the roadway edges. To acquire NDVI values for each buffered segment, a zonal statistics method was used to extract average NDVI values. Subsequently, the mean NDVI values of the roadway segments were extracted. The resulting table from the previous step was joined with the roadway shapefile, and NDVI percentages and scores were calculated and symbolized to illustrate NDVI changes.

The analysis of NDVI values was performed for the entire county with a focus roadway segments and population density using the changes in the NDVI values. In this study, population density was incorporated to provide insights into the broader societal and infrastructural impacts of tornado debris. The role of population density was critical in assessing the areas most vulnerable to significant damage. Higher population density typically correlates with a greater concentration of infrastructures—such as buildings, utilities, and road networks—which are more likely to be affected by tornado debris. Additionally, denser areas often experience more roadway activity, further emphasizing the potential for disruption and damage. The analysis of NDVI values, when compared with population density, allowed for a more holistic view of damage by highlighting how highly populated areas might face compounded challenges due to the interaction between debris, infrastructure, and transportation networks. Population density was integrated to assess how debris impact aligns with human settlement patterns, providing a clearer understanding of which communities are at greater risk and might require more resources for recovery and cleanup efforts. In addition, a comparative analysis for the two assessments was also performed to the extracted data for these purposes.

4.5 Results And Discussions

Descriptive statistics of the average NDVI data obtained for the study period is summarized in Table 1. Although, the SW part of the county recorded highest changes in NDVI values, this covered a region with highest population density and these changes were not significantly observed in the county-wide study. As mentioned earlier, extremely small values of NDVI (0.1 and below) relate to deserted areas of rock, sand, or snow. Values of 0.2 to 0.3 signify shrub and grassland,

while high values ranging from 0.6 to 1.0 imply temperate and tropical rainforests (*Weier and Herring, 2000*). High modal values indicate that they represent highly vegetative parts of the county while lower standard deviations show less dispersal of the NDVI values within that area.

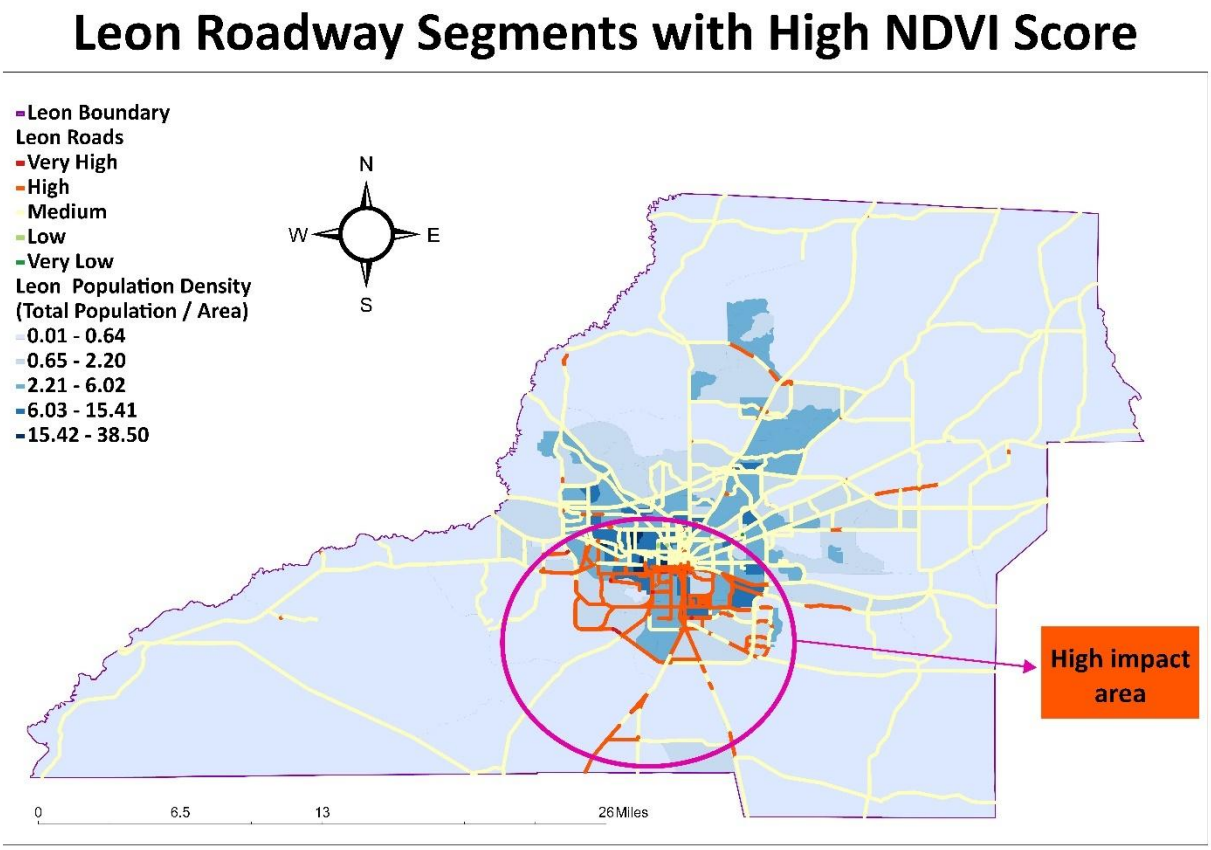

Figure 4:5 A map of Leon County roads showing NDVI values

The NDVI values for the state and local roadways (Figure 4.5), divided into 0.5-mile segments in average (Figure 4.6a), were recorded. The total length of the roadway segments used for analysis was 784.7 mi. The median length of segments was 0.19 mi with a standard deviation of 0.64. The maximum segment length was 2.73 mi and minimum of 0.015 miles. It is important to mention that the study used the existing segments from the roadway data and divided the longer segments into shorter lengths for a more detailed analysis. The total number of segments utilized for analysis was 1,505. Table 1 illustrates the descriptive statistics of roadway segment data. The mean NDVI value before the tornado was 0.578 while the mean after week 1 of the tornado was 0.571. The maximum and minimum NDVI values before the tornado was 0.900 and 0.190. The maximum and minimum NDVI values 1 week after the tornado was 0.900 and 0.176. Negative change values indicate loss in vegetation and creation of vegetative debris, while positive NDVI score value shows gain in vegetation, no creation of vegetative debris. The maximum NDVI change after week 1 was 26.1% and was associated with intersection between South Monroe St. and Tennessee St.

while the minimum of -40.85% was associated with intersection Capital Circle SW and Lake Bradford. Positive values show a gain in vegetation or greenness and negative values show a loss in vegetation but a creation of vegetative debris on affected road segments. The average change of -1.4% was recorded for the entire roadway network after week 1.

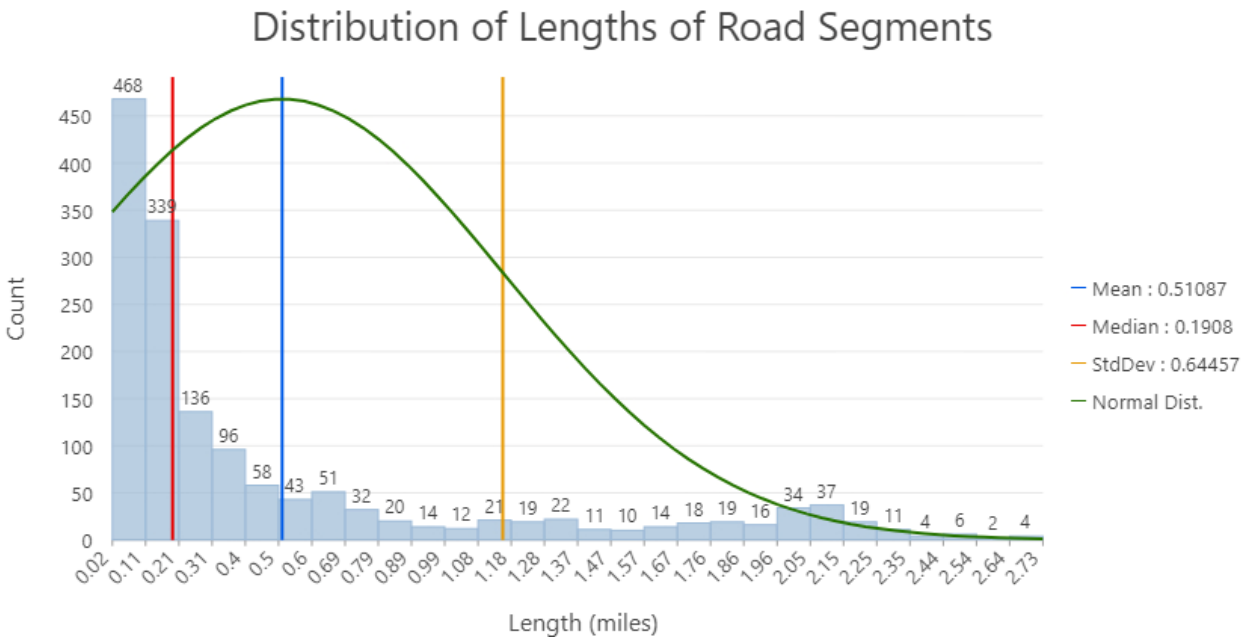

(a)

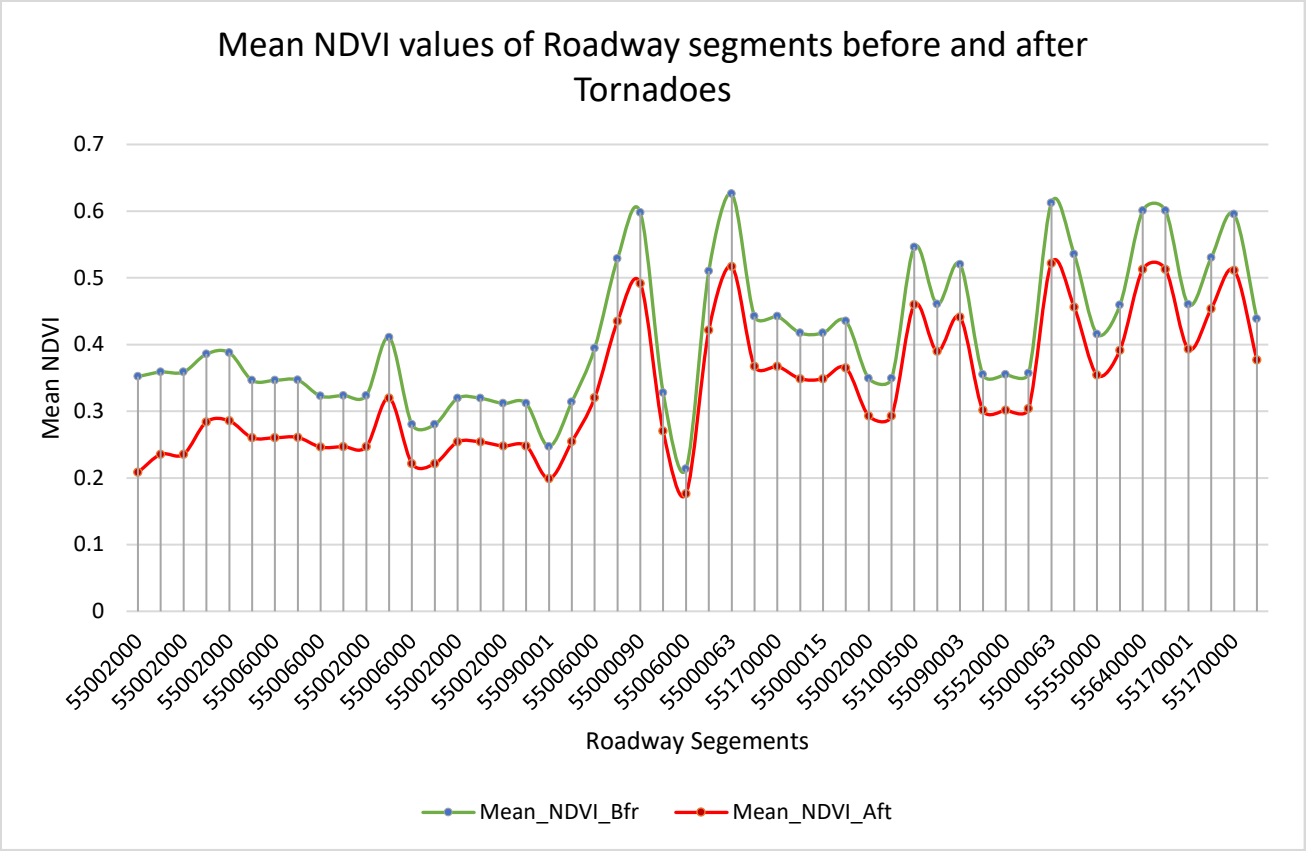
Mean NDVI values of Roadway segments before and after Tornadoes
Mean NDVI
0.7
0.6
0.5
0.4
0.3
0.2
0.1
0
55002000
55002000
55002000
55006000
55006000
55002000
55006000
55002000
55002000
55090001
55006000
55000090
55006000
55000063
55170000
55000015
55002000
55100500
55090003
55520000
55000063
55550000
55640000
55170001
55170000
Roadway Segements
Mean_NDVI_Bfr
Mean_NDVI_Aft

(b)

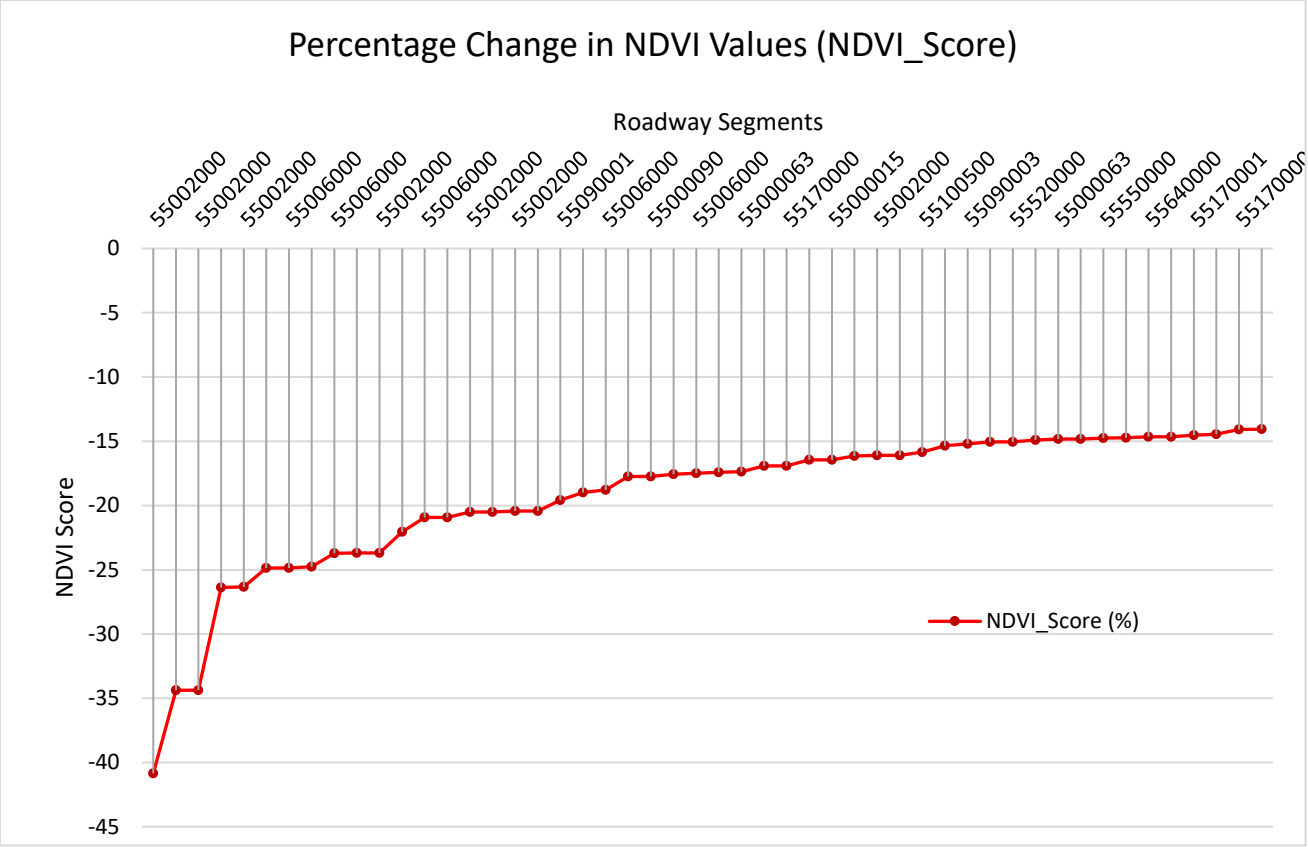

(c)

Figure 4:6 (a) Distribution of roadway segments used for analysis, (b) roadway segments NDVI change before and after tornadoes, and (c) roadway segment NDVI score.

Debris range was classified based on debris change percentage or NDVI score and normalized using the pixel count as follows: Very High: <= -0.155, High: -0.155 to -0.005, Medium: -0.005 to 0.077, Low: 0.007 to 0.554, Very Low: 0.554 to 2.123 (Table 1). Because the number of pixels in each segment was used in determining the average NDVI values for each segment, the debris ranges were normalized using the pixel count to reduce the effect of varying pixel count or length of roadway segments on the mean NDVI values. The NDVI scores can be visualized in Figure 4.7b and were compared with the actual tornado path (Figure 4.7a). Out of the 1,505 roadway segments, 44 fell within very high debris zone, 565 fell within high debris zone, 850 fell within medium debris zone, and 46 low to very low debris zone (Table 1). Another analysis was conducted to examine the lane counts of the affected road segments to understand traffic intensity in those areas. 4 % of the road segments that fell in the very high debris zones were 3 lane roads, 39% were 2 lane roads and the remaining 57% were single lane roads. For those within the high debris zone, less than 1% were 4 lane roads, 3% were 3 lane roads, 37% were 2 lane roads, and 59% were single lane roads.

Table 4-1 50 top affected roadway segments, length, and NDVI changes. Debris range classification based on percent debris: <= -0.155, High: -0.155 to -0.005, Medium: -0.005 to 0.077, Low: 0.007 to 0change. Very High.554, Very Low: 0.554 to 2.123.

Count	ROADWAY	LENGTH (mi)	AREA (sqmi)	Pixel Count (10m*10m)	NDVI (bfr)	NDVI (aft W1)	NDVI_diff_aft _W1	NDVI W1_score (%)	NDVI Score Normalized	Debris Range W1
1	55000125	0.02	0.00007	22	0.43	0.39	-0.05	-10.86	-0.49	Very high
2	55000125	0.02	0.00007	22	0.43	0.39	-0.05	-10.86	-0.49	Very high
3	55100000	0.03	0.00016	48	0.31	0.25	-0.06	-18.98	-0.40	Very high
4	55000031	0.02	0.00014	31	0.42	0.37	-0.05	-11.92	-0.38	Very high
5	55006000	0.07	0.00024	67	0.35	0.26	-0.09	-24.76	-0.37	Very high
6	55006000	0.04	0.00017	51	0.39	0.32	-0.07	-18.78	-0.37	Very high
7	55000097	0.03	0.00008	21	0.35	0.33	-0.03	-7.25	-0.35	Very high
8	55000006	0.04	0.00018	52	0.33	0.27	-0.06	-17.57	-0.34	Very high
9	55000031	0.04	0.00017	48	0.38	0.33	-0.05	-13.57	-0.28	Very high
10	55500000	0.06	0.00022	63	0.51	0.42	-0.09	-17.41	-0.28	Very high
11	55170000	0.04	0.00021	63	0.44	0.37	-0.07	-16.93	-0.27	Very high
12	55170000	0.04	0.00021	63	0.44	0.37	-0.07	-16.93	-0.27	Very high
13	55000032	0.06	0.00028	83	0.41	0.32	-0.09	-22.06	-0.27	Very high
14	55550000	0.06	0.00012	56	0.42	0.35	-0.06	-14.76	-0.26	Very high
15	55002000	0.10	0.00047	131	0.36	0.24	-0.12	-34.39	-0.26	Very high
16	55002000	0.10	0.00047	131	0.36	0.24	-0.12	-34.39	-0.26	Very high
17	55500000	0.06	0.00027	72	0.53	0.43	-0.09	-17.74	-0.25	Very high
18	55000097	0.04	0.00017	53	0.32	0.28	-0.04	-12.33	-0.23	Very high
19	55000090	0.03	0.00011	26	0.44	0.42	-0.03	-5.95	-0.23	Very high
20	55000013	0.05	0.00015	46	0.32	0.28	-0.03	-10.53	-0.23	Very high
21	55000063	0.05	0.00024	65	0.61	0.52	-0.09	-14.82	-0.23	Very high
22	55006000	0.07	0.00037	109	0.32	0.25	-0.08	-23.71	-0.22	Very high
23	55000015	0.07	0.00027	78	0.42	0.35	-0.07	-16.45	-0.21	Very high
24	55000015	0.07	0.00027	78	0.42	0.35	-0.07	-16.45	-0.21	Very high
25	55090003	0.06	0.00026	77	0.52	0.44	-0.08	-15.21	-0.20	Very high
26	55000108	0.03	0.00014	44	0.59	0.54	-0.05	-8.49	-0.19	Very high
27	55000028	0.04	0.00019	59	0.54	0.48	-0.06	-11.04	-0.19	Very high
28	55100500	0.08	0.00030	85	0.55	0.46	-0.09	-15.85	-0.19	Very high
29	55090001	0.07	0.00036	105	0.25	0.20	-0.05	-19.57	-0.19	Very high
30	55160000	0.05	0.00022	66	0.35	0.31	-0.04	-12.06	-0.18	Very high
31	55160000	0.05	0.00022	66	0.35	0.31	-0.04	-12.06	-0.18	Very high
32	55090003	0.08	0.00032	82	0.54	0.46	-0.08	-14.82	-0.18	Very high
33	55000006	0.06	0.00018	52	0.31	0.28	-0.03	-9.05	-0.17	Very high
34	55522500	0.04	0.00026	81	0.44	0.38	-0.06	-14.07	-0.17	Very high
35	55522500	0.04	0.00026	81	0.44	0.38	-0.06	-14.07	-0.17	Very high
36	55006000	0.10	0.00050	148	0.35	0.26	-0.09	-24.87	-0.17	Very high
37	55006000	0.10	0.00050	148	0.35	0.26	-0.09	-24.87	-0.17	Very high
38	55000029	0.06	0.00017	48	0.64	0.59	-0.05	-7.93	-0.17	Very high
39	55000029	0.06	0.00017	48	0.64	0.59	-0.05	-7.93	-0.17	Very high
40	55000027	0.07	0.00030	85	0.64	0.55	-0.09	-13.95	-0.16	Very high
41	55000027	0.07	0.00030	85	0.64	0.55	-0.09	-13.95	-0.16	Very high
42	55000031	0.06	0.00029	80	0.32	0.28	-0.04	-12.89	-0.16	Very high

43	55006000	0.09	0.00039	111	0.21	0.18	-0.04	-17.49	-0.16	Very high
44	55002000	0.20	0.00091	263	0.35	0.21	-0.14	-40.86	-0.16	Very high
45	55000097	0.03	0.00016	46	0.34	0.32	-0.02	-6.83	-0.15	High
46	55120000	0.04	0.00020	59	0.42	0.39	-0.04	-8.73	-0.15	High
47	55120000	0.04	0.00020	59	0.42	0.39	-0.04	-8.73	-0.15	High
48	55550000	0.11	0.00032	87	0.69	0.61	-0.09	-12.43	-0.14	High
9	55000006	0.06	0.00027	74	0.31	0.27	-0.03	-10.49	-0.14	High
50	55002000	0.16	0.00065	187	0.39	0.28	-0.10	-26.39	-0.14	High

	VARIABLES	LENGTH (mi)	AREA (sqmi)	Pixel Count (10m*10m)	NDVI (bfr)	NDVI_(aft W1)	NDVI_diff_aft_W1	NDVI W1 score (%)
	Mean	0.52	0.0023	668.47	0.58	0.57	-0.006	-1.41
	Median	0.19	0.0009	254	0.59	0.58	-0.004	-0.71
	Max	2.73	0.0124	3608	0.90	0.90	0.091	26.14
	Min	0.02	0.000016	4	0.19	0.18	-0.144	-40.86

Leon Roadway Segments, NDVI Score and Tornado Track

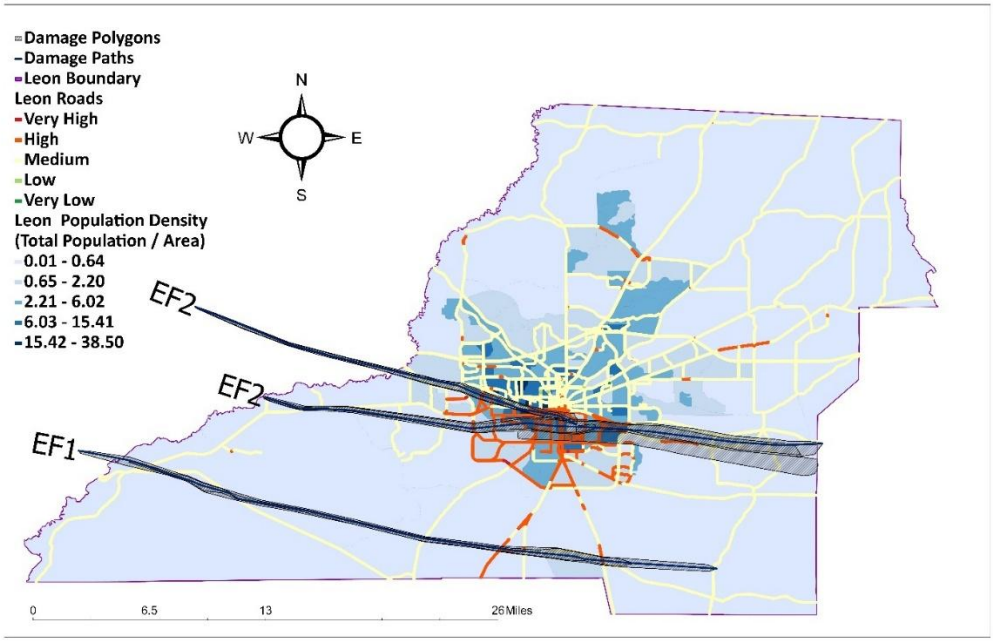

(a)

Leon Roadway Segments, NDVI Score, Tornado Track and Damage Points

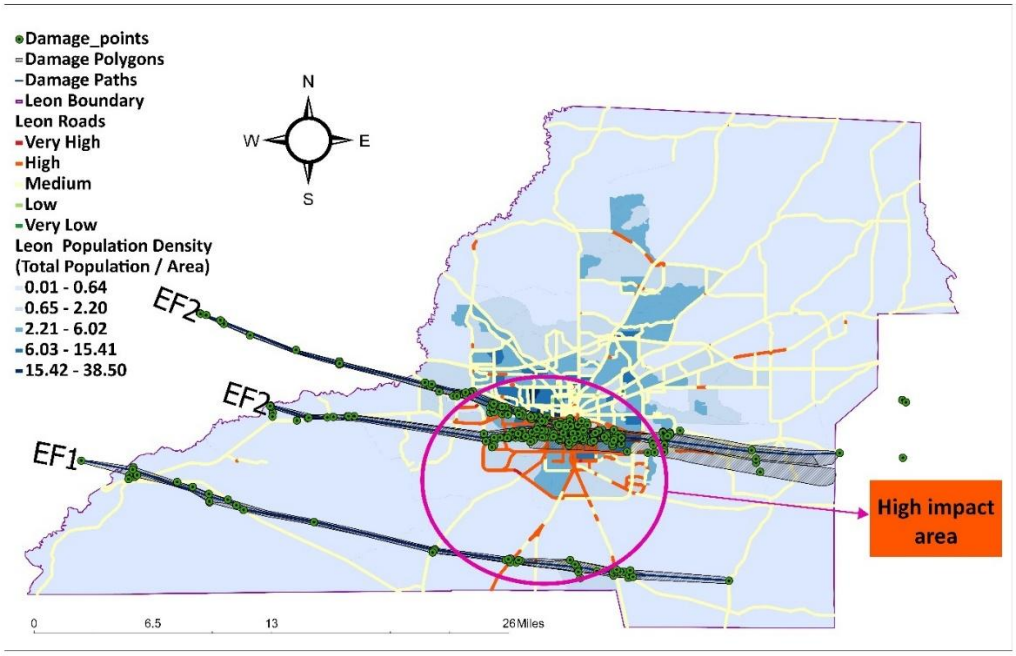

(b)

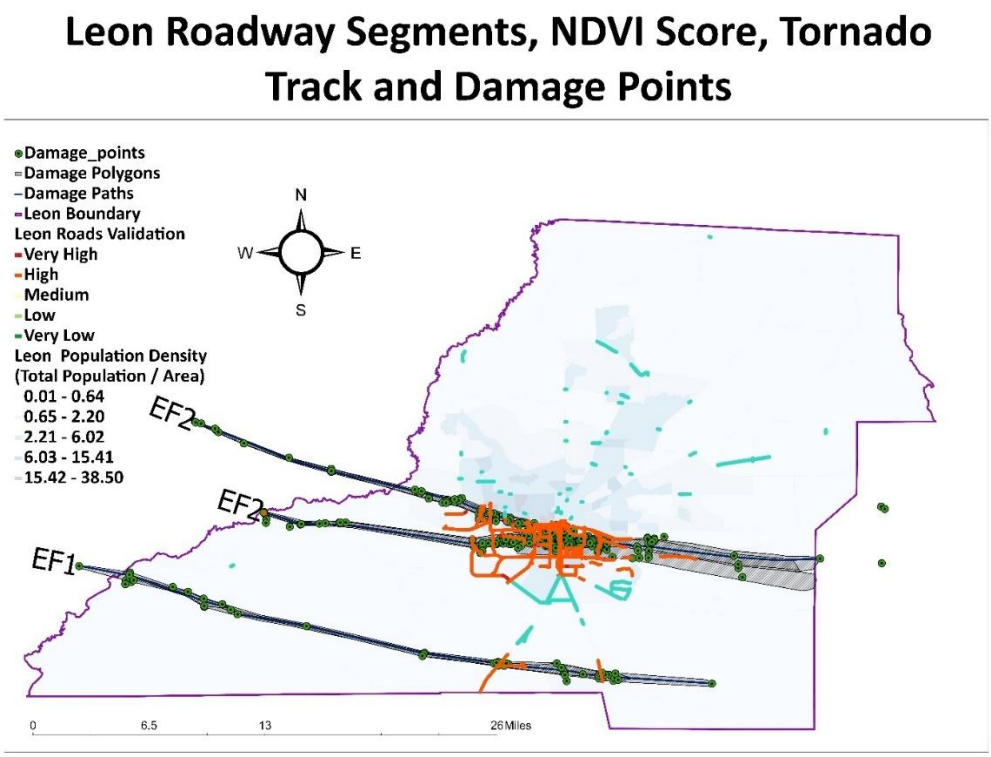

(c)

Figure 4:7 (a) Roadway segments with Week 1 NDVI score, major cities, population density, and damage polygons, (b) roadway segments with tornado track and damage points, and (c) tornado path and detected roadway segment with debris validation using ground truth data

Looking at the graphs in Figures 4.6b and 4.6c, the effects of the tornado on the vegetation in Leon County were very consequential. The entire county experienced loss in NDVI values especially in the SW parts of Leon County. Note that a decrease in NDVI values show a loss of vegetation or greenness, while an increase shows a growth or gain of vegetation. This is also consistent with the actual paths of the tornadoes, which did not directly impact the northern parts of the county.

This indicates the need to show more attention to this area compared to other parts of the county based on the impact of the tornadoes. The NDVI scores from the roadway segments indicate that the roadways within the south-central parts of Leon were massively affected by vegetative debris. This is consistent with the results from the county wide NDVI analysis. Major state roads and local roads in the central parts of the county were affected. These roadway segments recorded the highest changes in NDVI score indicating loss of vegetation and high volume of generated debris (Figure 4.7a). Roadway segments in the northern parts of the county did not record loss in vegetation. This is consistent with the county wide study and tornado path (Figure 4.7a). The EF-2 tornado paths in this study were closely examined to assess the distribution of debris, particularly in relation to population density. The tornadoes primarily affected the south-central region of the county, which is also its most densely populated area. This correlation between tornado path and population density is critical because densely populated areas typically have a higher concentration of

structures, infrastructure, and roadways, all of which contribute to an increased likelihood of debris accumulation.

The central parts of Leon County have the highest population density since the City of Tallahassee is located in that area. Comparative analysis with a focus on population density showed that roadway segments with very high and high debris volumes were found in highly populated areas in the county (Figure 4.7a and 4.7b). Findings indicate that major debris was created at the populated areas in the county after the tornadoes blocking the roadways and interrupting traffic. Some debris was also created in less populated areas such as the western and southern parts of the county. Areas with similar EF ratings showed a relatively uniform distribution of damage and debris. However, the intensity of debris accumulation appeared to increase in highly populated zones, likely due to the concentration of infrastructure and human activity. This comparative analysis highlights the important role that population density plays in understanding the broader impact of tornadoes on communities, as more densely populated regions are more vulnerable to both direct structural damage and indirect disruptions, such as compromised transportation networks. Expanding on this connection further illustrates how tornadoes not only affect physical structures but also create significant challenges for recovery and mobility in densely populated areas. NDVI score and NDVI values were validated by comparing with the actual damage points, damage polygons and tornado path (Figure 4.7b). It was discovered that 609 detected roadway segments had very high to high debris accumulation levels. Comparing this to the ground truth data, 447 roadway segments were true positives whereas 162 were false positives. Therefore, the framework accurately detected 74% of the roadways having high debris accumulation levels (**Figure 4.7c**).

4.6 Conclusions And Future Work

The study presented a detailed satellite-based debris assessment to determine areas and roadway segments within the Leon County with high volumes of debris based on the impact of 2 EF-2 and 1 EF-1 tornadoes. The analysis was conducted on the county's roadway segments using satellite images from April 24, 2024, and May 14, 2024. The first part of the analysis focused on the entire county by performing an extensive study of NDVI value changes before and after the tornadoes. The focus of the second part was directed towards the analysis of NDVI scores of the roadway segments in the county before and after the tornadoes. Both results were assessed with a focus on the population density and roadways. Findings were validated with the tornado track and ground truth damage points obtained from the NOAA damage assessment toolkit (NOAA, 2024b). As mentioned earlier, there are some notable limitations to this methodology which can be addressed in future studies.

First, NDVI is unable to adequately account for seasonal changes, which can significantly impact the observed patterns in vegetation loss. For example, vegetation density, soil moisture, and other environmental factors fluctuate throughout the year, influencing the visibility of key features such as roads and created debris. Failure to incorporate seasonal variability may lead to inaccurate or incomplete findings. To address this limitation, future studies should integrate more detailed and time-sensitive seasonal data, potentially through multi-temporal analyses, to better capture the dynamic nature of the environment. Additionally, vegetation classification was not possible, largely due to limitations in the framework's ability to differentiate between types of vegetation. Vegetation can obscure critical infrastructure, but without precise classification, it is difficult to

model the impact of occlusion on the roads. The complexity of distinguishing between different species or types of vegetation, especially under variable lighting and seasonal conditions, presents a challenge for satellite-based models. Future work could focus on integrating more sophisticated vegetation indices or adopting machine learning techniques specifically designed for vegetation classification.

Transportation networks are susceptible to disruptions and failure after a tornado due to debris accumulation, fallen trees or rising water levels (Horner and Widener, 2011). These disruptions can significantly hinder emergency response efforts, prolong recovery times, and limit the mobility of residents and essential services. This makes post-disaster vegetative assessment very critical to stakeholders to ensure a quick response and recovery after a disaster to facilitate the movement of emergency personnel and resources. To remove debris, the high-risk locations need to be identified in a timely manner. By leveraging this approach, state and local agencies can identify key locations where transportation networks are most vulnerable to blockage or failure. This not only aids in prioritizing debris removal but also allows for more efficient allocation of resources, reducing the time required for recovery and minimizing the broader socio-economic impacts of a transportation network shutdown.

Furthermore, the integration of vegetative debris assessment into disaster response planning could help stakeholders anticipate the areas most likely to experience transportation interruptions. By combining satellite data, on-the-ground observations, and predictive modelling, agencies can establish pre-emptive strategies for addressing debris clearance and roadway repair. This proactive approach can enhance the resilience of transportation infrastructure, ensuring that communities can recover more swiftly from the adverse effects of tornadoes and other natural hazards. There are several directions for future work and study extension. For instance, it would be very promising to develop a GIS model that would automatically identify areas with high amount of debris using pre- and post-tornado images. Post tornado debris can be assessed with a focus on shelter areas, local roadways, socioeconomics, and land characteristics. Also, images from different satellites can be utilized in the study to reduce data loss by cloud cover, cirrus, and long satellite revisit time.

4.7 References

Afaq, Y., Manocha, A., 2021. Analysis on change detection techniques for remote sensing applications: a review. Ecol. Inf. 63, 101310. https://doi.org/10.1016/j.ecoinf.2021.101310.

Al-Dail, M.A., 1998. Change detection in urban areas using satellite data. Journal of King Saud University-Engineering Sciences 10 (2), 217–227. https://doi.org/10.1016/S1018-3639(18)30697-4.

Amadeo, K., 2018. Hurricane Harvey facts, damage and costs. The Balance.

Antwi, R.B., Takyi, S., Ozguven, E.E., Volcy, K., Alam, M.S., Kim, K., et al., 2023. Satellite Imagery-Based Hurricane Debris Assessment: Model Development and Application in Rural Florida.

Antwi, R.B., Takyi, S., Karaer, A., Ozguven, E.E., Kimollo, M., Moses, R., et al., 2024. Automated GIS-based framework for detecting Crosswalk changes from Bitemporal high-resolution aerial images. arXiv preprint arXiv:2406.09731.

Axel, C., van Aardt, J.A., Aros-Vera, F., Holguín-Veras, J., 2016. Remote sensing-based detection and quantification of roadway debris following natural disasters. In: Laser Radar Technology and Applications XXI, vol. 9832. SPIE, pp. 92–103. https://doi.org/10.1117/12.2223073.

Butenuth, M., Frey, D., Nielsen, A.A., Skriver, H., 2011. Infrastructure assessment for disaster management using multi-sensor and multi-temporal RS imagery. International Journal of RS 32 (23), 8575–8594.

Butterworth, R.E., Kloesel, K.A., Veil, S.R., 2010. An assessment of broadcasters' use of new media and radar technology in tv severe weather coverage: benefits, challenges, and a need for training. In: 38th Conference on Broadcast Meteorology.

Cao, Q.D., Choe, Y., 2020. Building damage annotation on post-hurricane satellite imagery based on convolutional neural networks. Nat. Hazards 103 (3), 3357–3376.

Chang, L., Elnashai, A.S., Spencer, B.F., Song, J.H., Quyang, Y., 2010. Transportations Systems Modeling and Applications. Earthquake Engineering, Report. 10-03.

Chen, M., Karaer, A., Ozguven, E.E., Abichou, T., Arghandeh, R., Nienhius, J., 2021. Developing city-wide hurricane impact maps using real-life data on infrastructure, vegetation and weather. Transport. Res. Rec. 2675 (3), 393–404.

Cheng, C.S., Luo, L., Murphy, S., Lee, Y.C., Leite, F., 2024. A framework to enhance disaster debris estimation with AI and aerial photogrammetry. Int. J. Disaster Risk Reduc. 107, 104468. https://doi.org/10.1016/j.ijdrr.2024.104468.

COES (California Office of Emergency Services), 2005. Disaster Debris Management Training Manual. Governor's Office of Emergency Services, State of California. p. 118. http://www.calema.ca.gov/Recovery/Documents/Chapter4.pdf.

DeWitt, B.A., Wolf, P.R., 2000. Elements of Photogrammetry (With Applications in GIS). McGraw-Hill Higher Education.

Duryea, M.L., Kampf, E., Littell, R.C., 2007. Hurricanes and the urban forest: I. Effects on southeastern United States coastal plain tree species. Arboric. Urban For. 33 (2), 83.

Fadelli, I., Xplore, T. A method to enhance the planning of missions completed by multiple UAVs. https://techxplore.com/news/2024-03-method-missions-multipleuavs. html. (Accessed 31 July 2024).

Federal Emergency Management Agency (FEMA), 2010. Debris Estimating Field Guide, vol. 329. FEMA, Washington, D.C. Publication FEMA.

FEMA, 2007. Debris Management Guide, vol. 325. FEMA Publication. 06 June 2008. http://www.fema.gov/government/grant/pa/demagde.shtm.

Gazzea, M., Pacevicius, M., Dammann, D.O., Sapronova, A., Lunde, T.M., Arghandeh, R., 2021a. Automated power lines vegetation monitoring using high-resolution satellite imagery. IEEE Trans. Power Deliv. 37 (1), 308–316.

Gazzea, M., Karaer, A., Ghorbanzadeh, M., Balafkan, N., Abichou, T., Ozguven, E.E., Arghandeh, R., 2021b. Automated satellite-based assessment of hurricane impacts on roadways. IEEE Trans. Ind. Inf. 18 (3), 2110–2119. https://doi.org/10.1109/TII.2021.3082906.

Genin, S.M., 2019. Photogrammetry: methods of survey and applications on restoration works. Int. Arch. Photogram. Rem. Sens. Spatial Inf. Sci. 42, 557–564. https://doi.org/10.5194/isprs-archives-XLII-2-W11-557-2019.

Gilbert, N., 2023. Tornados and Their Impact on the Environment: Unleashing Nature's Fury. Environmental Pollution and Climate Change 7, 346. Available: https://www.omicsonline.org/open-access-pdfs/tornados-and-their-impact-on-the-environment-unleashing-natures-fury.pdf.

Gilliam, T., 2024. Leon County Nears End of Tornado Debris Pickup. WTXL ABC 27 Tallahassee News [Online]. Available: https://www.wtxl.com/southwest- tallahassee/leon-county-nears-end-of-tornado-debris-pickup. (Accessed 1 July 2024).

Gobron, N., Pinty, B., Verstraete, M.M., Widlowski, J.L., 2000. Advanced vegetation indices optimized for up-coming sensors: design, performance, and applications. IEEE Transactions on Geoscience and RS 38 (6), 2489–2505.

Gong, J., Maher, A., 2014a. Use of mobile lidar data to assess hurricane damage and visualize community vulnerability. Transport. Res. Rec. 2459 (1), 119–126. https://doi.org/10.3141/2459-14.

Gössling, S., Neger, C., Steiger, R., Bell, R., 2023. Weather, climate change, and transport: a review. Nat. Hazards 118 (2), 1341–1360. https://doi.org/10.1007/s11069-023-06054-2. Sep. 2023.

Hmimina, G., Dufrêne, E., Pontailler, J.Y., Delpierre, N., Aubinet, M., Caquet, B., et al., 2013. Evaluation of the potential of MODIS satellite data to predict vegetation phenology in different biomes: an investigation using ground-based NDVI measurements. RS of environment 132, 145–158.

Hoque, M.A.A., Phinn, S., Roelfsema, C., Childs, I., 2016. Assessing tropical cyclone impacts using object-based moderate spatial resolution image analysis: a case study in Bangladesh. International Journal of RS 37 (22), 5320–5343.

Hoque, M.A.A., Phinn, S., Roelfsema, C., Childs, I., 2017. Tropical cyclone disaster management using RS and spatial analysis: a review. Int. J. Disaster Risk Reduc. 22, 345–354.

Horner, M.W., Widener, M.J., 2011. The effects of transportation network failure on people's accessibility to hurricane disaster relief goods: a modeling approach and application to a Florida case study. Nat. Hazards 59 (3), 1619–1634.

Hu, T., Smith, R.B., 2018. The Impact of Hurricane Maria on the Vegetation of Dominica and Puerto Rico Using Multispectral RS. RS, vol. 10. p. 827. 6.

James S., 'Tornados and their impact on the environment: Unleashing Nature's Fury', vol. 7, no. 4.

Jiang, S., Friedland, C.J., 2016. Automatic urban debris zone extraction from post-hurricane very high-resolution satellite and aerial imagery. Geomatics, Nat. Hazards Risk 7 (3), 933–952. https://doi.org/10.1080/19475705.2014.1003417.

Karaer, A., Ulak, M.B., Abichou, T., Arghandeh, R., Ozguven, E.E., 2021. Post-hurricane vegetative debris assessment using spectral indices derived from satellite imagery. Transport. Res. Rec. 2675 (12), 504–523.

Karaer, A., Chen, M., Gazzea, M., Ghorbanzadeh, M., Abichou, T., Arghandeh, R., Ozguven, E.E., 2022. Remote sensing-based comparative damage assessment of historical storms and hurricanes in Northwestern Florida. Int. J. Disaster Risk Reduc. 72, 102857. https://doi.org/10.1016/j.ijdrr.2022.102857.

Kislov, D.E., Korznikov, K.A., 2020. Automatic Windthrow Detection Using Very-High-Resolution Satellite Imagery and Deep Learning. RS, vol. 12. p. 1145. 7.

Kocatepe, A., Ulak, M.B., Kakareko, G., Ozguven, E.E., Jung, S., Arghandeh, R., 2019. Measuring the accessibility of critical facilities in the presence of hurricane-related roadway closures and an approach for predicting future roadway disruptions. Nat. Hazards 95 (3), 615–635.

Koch, E., Koh, J., Davison, A.C., Lepore, C., Tippett, M.K., 2021. Trends in the extremes of environments associated with severe US thunderstorms. J. Clim. 34 (4), 1259–1272.

Layne, R. Tornado Alley may be moving east, placing billions in business and supply chains at risk - CBS News. https://www.cbsnews.com/news/tornado-alley-may-bemoving-east-threatening-businesses-supply-chains/. (Accessed 31 July 2024).

Lee, Y.J., Song, J., Gardoni, P., Lim, H.W., 2011. Post-hazard flow capacity of bridge transportation network considering structural deterioration of bridges. Structure and Infrastructure Engineering 7 (7–8), 509–521.

Li, Y., Ye, S., Bartoli, I., 2018. Semisupervised classification of hurricane damage from postevent aerial imagery using deep learning. Journal of Applied RS 12 (4), 045008.

Li, Z., Shen, H., Weng, Q., Zhang, Y., Dou, P., Zhang, L., 2022. Cloud and cloud shadow detection for optical satellite imagery: features, algorithms, validation, and prospects. ISPRS J. Photogrammetry Remote Sens. 188, 89–108. https://doi.org/10.1016/j.isprsjprs.2022.03.020.

Lipponen A., 'Comparison of Spatial Resolutions in Satellite Images', Medium. Accessed: July. 31, 2024. [Online]. Available https://medium.com/@anttilip/comparison-of-spatial-resolutions-in-satellite-images-3185963a2e96.

Liu, Z., Cao, Y., Wang, Y., Cao, S., Yang, Q., 2021. Study of turbulence effects on flying compact debris in tornadoes at different stages. J. Wind Eng. Ind. Aerod. 218, 104777. https://doi.org/10.1016/j.jweia.2021.104777. . Nov. 2021.

Luo, Z., Sun, O.J., Wang, E., Ren, H., Xu, H., 2010. Modeling productivity in mangrove forests as impacted by effective soil water availability and its sensitivity to climate change using Biome-BGC. Ecosystems 13 (7), 949–965.

McEntire, D.A., 2006. Managing debris successfully after disasters: Considerations and recommendations for emergency managers. Journal of Emergency Management 4 (4), 23–28.

Meads, M., Gonzalez-Duenas, C., HighField, W., Padgett, J., 2021. Understanding and deriving land Use and land cover variables as a predictor of debris from coastal storm events. AGU Fall Meeting Abstracts 2021, A35I–A35IA1756.

Metternicht, G., 2003. Vegetation indices derived from high-resolution airborne videography for precision crop management. International Journal of RS 24 (14), 2855–2877.

Motha, R.P., 2011. The impact of extreme weather events on agriculture in the United States, Challenges and Opportunities in Agrometeorology. pp. 397–407. https://doi.org/10.1007/978-3-642-19360-6_30.

Muñoz, J., López, B., Quevedo, F., Monje, C.A., Garrido, S., Moreno, L.E., 2021. Multi UAV coverage path planning in urban environments. Sensors 21 (21), 7365. https://doi.org/10.3390/s21217365.

N. C. for E. Information (NCEI), 'U.S. Billion-dollar Weather and Climate Disasters, 1980 - present (NCEI Accession 0209268)'. Accessed: July. 1, 2024. [Online]. Available https://www.ncei.noaa.gov/access/metadata/landing-page/bin/iso?id=gov.noaa.nodc:0209268.

National Oceanic and Atmospheric Administration (NOAA), 2020. Hurricane costs. https://coast.noaa.gov/states/fast-facts/hurricane-costs.html. (Accessed 11 July 2024).

National Oceanic and Atmospheric Administration (NOAA), 2024a. Tornadoes. May 10, 2024. [Online]. Available: https://www.weather.gov/tae/2024_05_Tornadoes (Accessed 30 July 2024).

National Oceanic and Atmospheric Administration (NOAA), 2024b. Damage assessment toolkit. https://apps.dat.noaa.gov/stormdamage/damageviewer/.

Nex, F., Duarte, D., Tonolo, F.G., Kerle, N., 2019. Structural Building Damage Detection with Deep Learning: Assessment of a State-Of-The-Art CNN in Operational Conditions. RS, vol. 11. p. 2765. 23.

Pickens, L.M., Cheshire, H.M., Devine, H.A., 2000. Use of geographic information systems and photogrammetric techniques to improve the NC division of forest resources pre-suppression fire planning and forest management. In: IGARSS 2000. IEEE 2000 International Geoscience and RS Symposium. Taking the Pulse of the Planet: the Role of RS in Managing the Environment. Proceedings (Cat. No. 00CH37120), vol. 6. IEEE, pp. 2712–2714.

Press Release, FEMA. Approves Additional $46.8 Million for FDOT Hurricane Michael Debris Removal Expenses. https://www.fema.gov/press-release/20210318/fema-approves-additional-468-million-fdot-hurricane-michael-debris-removal.

Press Release, 2020, FEMA. FEMA Approves Additional $46.8 Million for FDOT Hurricane Michael Debris Removal Expenses. https://www.fema.gov/press-release/20210318/fema-approves-additional-468-million-fdot-hurricane-michael-debris-removal.

Rahman, M.T., Rashed, T., 2015. Urban tree damage estimation using airborne laser scanner data and geographic information systems: an example from 2007 Oklahoma ice storm. Urban For. Urban Green. 14 (3), 562–572.

Razali, S.M., Nuruddin, A.A., Lion, M., 2019. Mangrove vegetation health assessment based on RS indices for Tanjung Piai, Malay Peninsular. Journal of Landscape Ecology 12 (2), 26–40.

Reeves, Z., Cho, H., 2019. Hurricane Michael Damage Assessment.

Rhee, D.M., Lombardo, F.T., Kadowaki, J., 2021. Semi-automated tree-fall pattern identification using image processing technique: application to Alonsa, MB tornado.

J. Wind Eng. Ind. Aerod. 208, 104399. https://doi.org/10.1016/j.jweia.2020.104399.

Rouse, J.W., Haas, R.H., Schell, J.A., Deering, D.W., 1974. Monitoring vegetation systems in the great Plains with ERTS in Proc. In: ERTS-1 Symposium 3rd. Greenbelt, Washington, NASA.

Safapour, E., Kermanshachi, S., 2020. Identification and categorization of factors affecting duration of post-disaster reconstruction of interdependent transportation systems. In: Construction Research Congress 2020: Computer Applications. American Society of Civil Engineers, Reston, VA, pp. 1290–1299.

Schaefer, M., Teeuw, R., Day, S., Zekkos, D., Weber, P., Meredith, T., Van Westen, C.J., 2020. Low-cost UAV surveys of hurricane damage in Dominica: automated processing with co-registration of pre-hurricane imagery for change analysis. Nat. Hazards 101 (3), 755–784.

Schultz, M., Clevers, J.G., Carter, S., Verbesselt, J., Avitabile, V., Quang, H.V., Herold, M., 2016. Performance of vegetation indices from Landsat time series in deforestation monitoring. International journal of applied earth observation and geoinformation 52, 318–327.

Shedd, J., Millinor, B., Devine, H., 2005. Updating Fuel Fire Loads and Vegetation Datasets after a Natural Disaster [thesis]. Raleigh (NC). North Carolina State University.

Skrabania, L. ‘Interview: how Problematic are satellites and drones in terms of data protection?’, digital for Good | RESET.ORG. https://en.reset.org/interview-howproblematic-are-satellites-and-drones-terms-data-protection-03072021/. (Accessed 31 July 2024).

Smith, A.B., 2022. US Billion-dollar weather and climate disasters. http://doi.org/10.25921/stkw-7w73.

Smith, A.M., Kolden, C.A., Tinkham, W.T., Talhelm, A.F., Marshall, J.D., Hudak, A.T., et al., 2014. RS the vulnerability of vegetation in natural terrestrial ecosystems. RS of environment 154, 322–337.

Stanturf, J.A., Goodrick, S.L., Outcalt, K.W., 2007. Disturbance and coastal forests: a strategic approach to forest management in hurricane impact zones. For. Ecol. Manag. 250 (1–2), 119–135. https://doi.org/10.1016/j.foreco.2007.03.015.

Staudhammer, C.L., Escobedo, F., Luley, C., Bond, J., 2009. Patterns of urban forest debris from the 2004 and 2005 Florida hurricane seasons. South. J. Appl. For. 33 (4), 193–196.

Szantoi, Z., Malone, S., Escobedo, F., Misas, O., Smith, S., Dewitt, B., 2012. A tool for rapid post-hurricane urban tree debris estimates using high resolution aerial imagery. Int. J. Appl. Earth Obs. Geoinf. 18, 548–556.

Tang, Z., Li, Y., Gu, Y., Jiang, W., Xue, Y., Hu, Q., et al., 2016. Assessing Nebraska playa wetland inundation status during 1985–2015 using Landsat data and Google Earth Engine. Environ. Monit. Assess. 188 (12), 1–14.

Thompson, B.K., Escobedo, F.J., Staudhammer, C.L., Matyas, C.J., Qiu, Y., 2011. Modeling hurricane-caused urban forest debris in Houston, Texas. Landsc. Urban Plann. 101 (3), 286–297.

Umpierre, D., Margoles, G., 2005. Broward county's web-based Hurricane debris estimation tool (HurDET). In: 2005 ESRI International User Conference Proceedings.

U.S. Army Corps of Engineers, 2008. Debris Management Guide, APPENDIX A: Hurricane Debris Estimation Model. USACE, Washington, D.C.

Voigt, S., Schneiderhan, T., Twele, A., Gähler, M., Stein, E., Mehl, H., 2011. Rapid damage assessment and situation mapping: learning from the 2010 Haiti earthquake. Photogrammetric Engineering and RS (PE&RS) 77 (9), 923–931.

Wang,W., Qu, J.J., Hao, X., Liu, Y., Stanturf, J.A., 2010. Post-hurricane forest damage assessment using satellite remote sensing. Agric. For. Meteorol. 150 (1), 122–132. https://doi.org/10.1016/j.agrformet.2009.09.009.

Weier, J., Herring, D., 2000. Measuring vegetation (ndvi & evi). NASA Earth Observatory 20, 2.

Weisbrod, G., Fitzroy, S., 2011. Traffic congestion effects on supply chains: Accounting for behavioral elements in planning and economic impact models. In: Supply Chain Management-New Perspectives. IntechOpen. https://doi.org/10.5772/23057. Ch. 16.

Wuebbles, D.J., Kunkel, K., Wehner, M., Zobel, Z., 2014. Severe weather in United States under a changing climate. Eos, Transactions American Geophysical Union 95 (18), 149–150.

Xie, S., Duan, J., Liu, S., Dai, Q., Liu, W., Ma, Y., et al., 2016. Crowdsourcing Rapid Assessment of Collapsed Buildings Early after the Earthquake Based on Aerial RS Image: A Case Study of Yushu Earthquake. RS, vol. 8. p. 759. 9.

Yeom, J., Han, Y., Chang, A., Jung, J., 2019. Hurricane building damage assessment using post-disaster UAV data. In: IGARSS 2019-2019 IEEE International Geoscience and RS Symposium. IEEE, pp. 9867–9870.

Zamanifar, M., Pooryari, M., Ahadi, M.R., 2014. Estimation of reconstruction cost and traffic functionality relating to roadway transportation lifelines after natural disasters. International Journal of Transportation Engineering 2 (1), 67–80.

Zha, Y., Gao, J., Ni, S., 2003. Use of normalized difference built-up index in automatically mapping urban areas from TM imagery. International journal of RS 24 (3), 583–594.

Zhai, W., Peng, Z.R., 2020. Damage assessment using google street view: evidence from hurricane michael in Mexico beach, Florida. Appl. Geogr. 123, 102252.

Zhang, J., Zhang, Y., 2007. RS research issues of the national land use change program of China. ISPRS Journal of Photogrammetry and RS 62 (6), 461–472.

Zhang, F., Cao, C., Li, C., Liu, Y., Huisingh, D., 2019. A systematic review of recent developments in disaster waste management. J. Clean. Prod. 235, 822–840. https://www.census.gov/quickfacts/leoncountyflorida

(Accessed 20 June 2023).

United States Census Bureau (US Census), 2020. Population estimates. https://www.census.gov/quickfacts/leoncountyflorida. (Accessed 20 June 2023).

United States - Federal Aviation Administration (US-FAA). 2013 ‘No Drone Zone | Federal Aviation Administration’. Accessed: Jul. 31, 2024. [Online]. Available: https://www.faa.gov/uas/resources/community_engagement/no_drone_zone‘No Drone Zone | Federal Aviation Administration’. Accessed: July. 31, 2024. [Online]. Available https://www.faa.gov/uas/resources/community_engagement/no_drone_zone.

Chapter 5 Conclusions

This study presented a machine learning-based methodology to assess the impact of hurricanes and tornadoes on roadway infrastructure, with a focus on roadway closures, debris accumulation, and accessibility challenges. By integrating high-resolution aerial imagery, satellite data, and advanced classification techniques, we categorized roadway conditions into open, totally closed, and partially closed classes. Our comparative analysis of Hurricanes Ian, Idalia, and Debby highlighted the varying impacts of wind intensity, storm surge, and prolonged rainfall on roadway networks. Additionally, a debris assessment framework was employed to evaluate the effects of EF-2 and EF-1 tornadoes on Leon County's roadways, using NDVI-based analysis and ground-truth validation. Based on these applications, our findings provide valuable insights into disaster response, emergency management, and infrastructure resilience, enabling better decision-making for transportation agencies and first responders.

The results demonstrate that the proposed methodology can provide accurate and timely data on roadway closures, which is essential for disaster response and planning. Emergency responders and disaster management agencies can utilize this technique to evaluate roadway conditions immediately after hurricanes and tornadoes, facilitating optimal route planning for emergency vehicles and efficient resource allocation. Furthermore, engineers and urban planners can leverage this information to assess infrastructure resilience, identify vulnerabilities, and prioritize future investments in roadway improvements. By understanding the spatial distribution of damage and debris, government agencies can streamline post-disaster recovery efforts, ensuring the effective allocation of resources for reconstruction and restoration.

Despite the effectiveness of this methodology, several limitations must be acknowledged. One key challenge is occlusion in aerial and satellite imagery caused by debris, vegetation, and other obstructions, which can hinder the accurate identification of roadway conditions. Differentiating between fully and partially closed roadways is also complicated by debris accumulation, leading to misclassifications. Additionally, environmental factors such as shadows, reflections, and terrain variations can introduce noise into the imagery, resulting in false positives. The dynamic nature of roadway conditions, including changes over time due to debris removal and flooding, is difficult to capture using static imagery. The absence of timestamped data further limits our ability to assess the temporal evolution of road accessibility.

The NDVI-based assessment of tornado impacts also has notable limitations. Seasonal vegetation changes can significantly affect NDVI values, leading to potential inaccuracies in debris detection. Additionally, the framework's inability to distinguish between different vegetation types complicates the analysis of infrastructure occlusion. The reliance on remote sensing and aerial imagery may result in incomplete datasets due to cloud cover, varying resolutions, and satellite revisit times. Moreover, the study's findings may not be entirely generalizable to other regions due to differences in geographical and infrastructural characteristics.

To address these limitations, future research should explore the integration of multi-temporal data sources to enhance the accuracy of roadway condition assessments. Incorporating real-time temporal data and advanced image-processing techniques could mitigate occlusion effects and

improve classification accuracy. Additionally, the use of LiDAR, synthetic aperture radar (SAR), and hyperspectral imagery could provide more robust assessments by capturing terrain variations and structural damage more effectively. Enhancing machine learning models to account for debris accumulation patterns and environmental variations could further refine the classification process.

Future work should also focus on developing automated GIS-based models for detecting high-risk areas with significant debris accumulation. By leveraging pre- and post-disaster imagery, such models could aid in prioritizing debris removal efforts and optimizing emergency response strategies. Integrating on-the-ground observations with remote sensing data could improve predictive modeling for disaster preparedness and recovery. Furthermore, incorporating community engagement into disaster response planning could enhance communication strategies and resource distribution, ensuring that impacted populations receive timely assistance.

This study underscores the critical role of remote sensing and machine learning in disaster management, demonstrating their potential for improving infrastructure resilience in hurricane- and tornado-prone regions. By advancing these methodologies, stakeholders can develop more effective strategies for mitigating transportation disruptions, enhancing emergency response, and fostering long-term recovery efforts in impacted communities.